WAVELENGTH-SPECIFIC EFFECTS OF ULTRAVIOLET LIGHT ON MICROORGANISMS AND VIRUSES FOR IMPROVING WATER DISINFECTION

by

SARA ELIZABETH BECK

B. S., B. A. University of Colorado, 2003

M. S. Georgia Institute of Technology, 2009

A dissertation submitted to the

Faculty of the Graduate School of the

University of Colorado in partial fulfillment

Of the requirement for the degree of

Doctor of Philosophy

Department of Civil, Environmental, and Architectural Engineering

2015

This dissertation entitled:
Wavelength-Specific Effects of Ultraviolet Light on Microorganisms and Viruses for Improving Water Disinfection

written by Sara Elizabeth Beck
has been approved for the
Department of Civil, Environmental and Architectural Engineering

_____
Dr. Karl G. Linden, University of Colorado, Boulder
(Chair)

_____
Dr. Mark Hernandez, University of Colorado Boulder

_____
Dr. JoAnn Silverstein, University of Colorado Boulder

_____
Oliver R. Lawal, Aquionics, Inc.

_____
Dr. James P. Malley Jr., University of New Hampshire

_____
Dr. Roberto A. Rodriguez, University of Texas
-Health Sciences Center at Houston

Date:_____

The final copy of this thesis has been examined by the signatories, and we find that both the content and the form meet acceptable presentation standards of scholarly work in the above mentioned discipline.

Beck, Sara Elizabeth (Ph. D. Civil and Environmental Engineering)

Wavelength-Specific Effects of UV Light on Microorganisms and Viruses for Improving Water Disinfection

Dissertation directed by Professor Karl G. Linden, Ph.D.

This research assessed the wavelength-specific effects of germicidal ultraviolet (UV) irradiation on viruses and microorganisms. Every organism has a unique spectral sensitivity to UV irradiation, called its action spectrum. In many cases, the action spectra of bacteria strongly correlate with their DNA or RNA absorbance. For many viruses, however, the action spectra deviate from the UV absorbance of their DNA or RNA, suggesting that mechanisms other than nucleic acid damage are contributing to their UV inactivation.

This research determined the UV spectral sensitivity of *Cryptosporidium parvum*, adenovirus 2 and coliphage MS2, T1UV, Q Beta, T7, and T7m. Two viruses, MS2 coliphage and adenovirus were studied more thoroughly to investigate whether UV damage to their genomes contributed alone to virus inactivation or whether UV damage to other viral components was also a contributing factor. The results indicated that polychromatic UV inactivation of MS2 coliphage is dominated by damage to its viral RNA across the germicidal wavelength range. However, for adenovirus, UV-induced damage to viral proteins also contributed to loss of infectivity, primarily at wavelengths below 240 nm. This finding provides insight into why UV irradiation from polychromatic, medium-pressure UV sources has been shown to be more effective than monochromatic (254 nm), low-pressure UV irradiation at inactivating adenovirus.

The research informed the design of a tailored, multiple-wavelength UVC LED unit that combines LEDs emitting at 260 nm and 280 nm with the goal of optimizing pathogen inactivation at a lower energy cost. The unit was tested with *E. coli*, MS2 coliphage, adenovirus

2, and *Bacillus pumilus* spores. Although the UVC LEDs are competitive with LPUV and MPUV lamps for water disinfection, they currently require more energy per log reduction of MS2, adenovirus 2, and *B. pumilus* spores. The 280 nm UV LED was more efficient (per log reduction) for inactivating *E. coli.* The UVC LED unit was also evaluated for potential synergistic effects. No dual-wavelength synergy was detected in bacterial or viral inactivation or in damage to the DNA or RNA.

Ultimately, the research adds fundamental insight into the mechanisms of inactivation of polychromatic germicidal UV irradiation for improving ultraviolet water disinfection.

DEDICATION

To Ed.

When I decided to go to grad school, Ed jumped right in alongside me. We spent Thanksgiving, 2005, in my townhome, studying for the GRE together, taking practice tests in between cooking a massive turkey dinner for two and camping overnight by the fireplace. It was one of my favorite Thanksgiving memories. Ed already had a Master's degree, but thought he might get another, or else maybe a Ph.D. in medical physics or mechanical engineering. Why not?! Driving home for the holidays that year, we missed a turn somewhere in West Texas, distracted by my vocabulary cards. It gave us an extra hour to cram. Three days before Christmas, we sat side by side at the GRE testing facility. The questions were getting harder and harder and eventually easier, which meant we were getting them wrong. We both seemed to be squirming in our seats, tempted to decline our scores. Ultimately, we did just fine. We tied in math. Ed beat me in verbal and I beat him in the writing.

Georgia Tech

Two weeks later, Jan 2006, I started my Master's through a Distance Learning Program at Georgia Tech. I'd watch recorded lectures after work and submit my homework by fax. Come exam time, my bosses would proctor my tests and fax them from wherever I happened to be at the time: Johnson Space Center in Houston or the Mission Control Center near Moscow.

Balancing school with work was challenging, especially during Space Shuttle missions. School interfered with our evenings, too, but Ed had his own evening schedule: ice hockey on Sunday nights, Crossfit and climbing on Tuesdays and Thursdays, sailing and ultimate on Wednesdays. School interfered with our weekends, as well, and I skipped plenty of climbing trips to Austin or Potrero Chico, Mexico to stay home and study or catch up.

Environmental engineering was also challenging! I had an aerospace and art background so I lacked knowledge in biology and chemistry and had to teach myself concepts I had either forgotten from high school or never learned in college. When I was struggling in my Biological Processes class, in particular, Ed tutored me given what he happened to remember from AP

Biology, 17 years earlier. “Ed. How do you know this stuff?” “Eh. I don’t know,” he shrugged “I just remember it.” His knowledge retention was incredible.

After 3 years of grad school at the slow pace of one class a semester, I took a leave of absence from work to finish. We packed my Toyota Carolla full with a futon mattress, a papasan chair, a bike, and some clothes, and drove to Atlanta where I spent the summer taking my last 4 classes. My backpack was falling apart at the time so Ed cleaned out his and gave it to me the night before we left; I still use it daily. We Skyped almost every weeknight. He flew out to visit over 4th of July and we met halfway in Alabama for a climbing trip. Three months later, he flew out again and we made the long drive home together.

I didn’t attend my commencement ceremony so when my diploma arrived in the mail, I asked Ed to hand it to me. He downloaded Pomp and Circumstance on his iphone and called my name out loud; I walked across the ‘stage’ that was our living room, in between the couch and the TV, shook his hand, accepted my diploma, and smiled for invisible photographers. I told Ed he had to repeat the ceremony and mispronounce my name in the process. He was wearing boxers at the time, or nothing at all; I honestly cannot remember, but I do remember laughing and thinking “I love this.” I could not imagine a more perfect commencement ceremony.

CU Boulder

The following January, 2010, Ed and I were once again on a road trip, this time to move me to Boulder for my doctorate. He planned to join me after the Space Shuttle program ended ten months later. Unfortunately, the final three Shuttle missions were delayed. Ten months became almost two years. His coworkers left the group; he stayed. His coworker had a baby and worked part-time; he stayed a few extra months to make up for her absence.

To keep the long distance relationship going, we Skyped or talked almost daily and visited often. Six weeks was too long, so we made the effort to see each other every 5 weeks, splitting time between Colorado and Houston, or meeting for other events in Orlando, San Francisco, L.A., Germany, or Spain. I watched other grad students lose their long distance relationships, but we managed to make ours work. It was an investment. “Ok, how long do we have in the bank?” he asked after a particularly perfect weekend together. “What do you mean?” “When should I come visit you before we lose this?”

Ed worked the Space Shuttle program through until its end; we watched the final landing together, side by side, from the bleachers at Kennedy Space Center. A few weeks later, he left NASA and a career he had held for 15 years to join me in Colorado.

In Boulder, Ed supported me even more. He was genuinely interested in my research. Since I study ultraviolet disinfection, he started ordering us UV gadgets for the house: a UV water purifier, UV toothbrush sterilizers he found on sale. When I bought a deuterium lamp for some of my experiments, Ed constructed a wooden lamp housing for it as a fun side project to keep him busy. Occasionally he'd join me in the lab to help count colonies. He suggested gifts for our lab's white elephant gift exchange (soaps in the form of Petri dishes with glow-in-the dark bacterial colonies). He proofread some of my grant proposals and scholarship cover letters. He listened to me rehearse my conference presentations and, not only that, but he was able to ask intelligent questions about a subject completely outside of his specialty. Before long, he was also doing work for my advisor, redoing our lab webpage.

I biked or walked the two miles to campus and Ed often picked me up from the lab late at night or when it was raining or snowing. We always had the same conversation: "Thanks for getting me," I'd say. "I didn't for-get you!" he'd respond. Every. Single. Time. The few times I walked home with a flat tire late at night, he'd surprise me by meeting me halfway to walk me home. He protected me.

Ed also doubled as my IT specialist. He'd fix computer problems before I even had them. "Where's your laptop? I'm upgrading your RAM." "Hey, I'm gonna upgrade your operating system." "Hey- I got you a new hard drive" "Look! I got you a trackball mouse to help with your carpal tunnel." When my computer screen shattered three days before my preliminary exam, Ed replaced it in a 4-5 hour procedure on the kitchen table. When I thanked him, genuinely, he said "Babe. These are the moments guys live for! To be the hero for the girl."

"We're a team!" we would say, and we meant it, but I often think I got the better deal.

As a grad student, I brought my work home in a way that Ed never did. So many times, he listened to my frustrations and reminded me why I was pursuing this degree. He cheered me on – quite literally – with phrases like "Ra! Ra! Sa! Ra!" or "The future of water everywhere depends on you!" or, my personal favorite: "You're gonna do great! And don't let Sara tell you any differently."

When my friend graduated, we watched her commencement ceremony at Macky Auditorium one December. Ed mocked the announcer who repeated over and over in a strange accent: “Doctor of PHEElosuPHEE Civilengineering.” “Doctor of PHEElosuPHEE Civilengineering.”

During 8 years of grad school, Ed supported me, without hesitation, in more ways than I could ever imagine or describe. I don’t think I ever adequately thanked him enough nor came close to returning the favor.

Ed died in September of 2013 in a fall at Grand Teton National Park.

Finishing my doctorate without him by my side proved to be tremendously, tremendously difficult. I had to battle an enormous amount of lethargy and apathy. Who cares about work when your life has been turned upside down with zero warning at the happiest time of your life? Who cares about research when you’ve lost your past, your present, and your future, overnight, in the span of 3 seconds? Who cares about water disinfection when your best friend and life partner was reduced to a ceramic on the kitchen counter? Who cares about DNA and protein damage when you feel like someone carved out your heart with a butcher knife, shoved it still beating into a blender, and pureed it before repackaging it back in back in your chest cavity? What do you begin to work on when your dining room table is covered in stacks of estate paperwork and decisions you never imagined were possible? How do you write a dissertation when your brain is wound up in one giant knot and simply will not let you concentrate? How do you prioritize something that has fallen several notches on your newfound spectrum of significance? How do you work toward a finish line when every time you envision that finish line without your partner, teammate, and number one supporter, you sob?

I went back to work in November, revised a manuscript, and then got slammed by the holidays and Ed’s birthday. I went back to work in February, conducted an experiment, and then got slammed by the 6-month anniversary of his death, my birthday, and the arrival of Spring. I went back to work in April and then got slammed by the triggers that inevitably came when I had to repeat in the lab every single thing I was doing in the lab the week before he died. I was living in an alternate reality where nothing made sense and nothing was right. And I was forcing myself to work in that alternate reality that everyone else pretended was normal, oblivious to the fact that the world was actually upside down and my pureed heart was actively dripping out of my chest cavity. It was bizarre. And maddening.

I went back to work in May and then got slammed by the arrival of summer. I went back to work in June, finished a manuscript, and then got slammed by the date of the wedding we had planned for our 10-year anniversary. I went back to work in August and then got slammed by the one-year anniversary of his death and a visit to the site of his accident. I went back to work in September, set a defense date, did some experiments, revised a manuscript, escaped to Siberia, wrote non-stop, and defended to a caring committee, an incredibly supportive advisor and a group of colleagues, friends and family.

Nine years after Ed and I sat side-by-side taking the GRE together and squirming in our seats, I participated in another December commencement ceremony at Macky Auditorium. This time, the man with the strange accent announced "Doctor of PHEElosuPHEE Civilengineering" and pronounced my name – correctly – as I walked across a stage larger than our living room and received my diploma from a fully-clothed man. My advisor, Karl, hooded me, catching my chin in the process, and after eight years of unwavering support, Ed was not there to watch it.

Ed, this degree is as much yours as it is mine. We're a team! You helped make every single part of it possible and I am indebted to your encouragement, your selflessness, your patience, and your sacrifice as you put your career on hold and moved to another state to support mine. I hate so much that you're not here to close out this chapter that we started together, to cross the finish line with me, and to start writing the next chapter, as always, side by side. You liked to read books out of order so that you would always know the ending. I wonder if you read your book out of order and if you already knew the ending, and, if so, whether you would have wanted to rewrite any of this chapter. I miss you, my love.

Ra! Ra! Sa! Ra! The future of water everywhere depends on me.

ACKNOWLEDGMENTS

I was working in Moscow in Feb of 2009 when **Dr. Karl Linden** let me know I was accepted to CU and invited me to work with his lab group. Months later, he informed me about upcoming fellowship deadlines and offered to write a recommendation letter on my behalf even though we had only met once. We worked together, taking advantage of the time zone difference, emailing back and forth across the Atlantic a fellowship proposal to the EPA that would ultimately fund 3 years of my research - all of this before I even set foot on campus. I was impressed then at Karl's accessibility and willingness to work with and support his students. That accessibility and support continued for the next 5 years, coming full circle as we wrote or reviewed this dissertation, passing sections of it back and forth across the ocean, once again taking advantage of the time difference between the US and Russia. Karl, your dedication to the fields of ultraviolet treatment and water reuse are inspiring. Thank you for your guidance, patience, and continual support, particularly in this last year, and thank you for investing in me.

To my doctoral dissertation committee, **JoAnn Silverstein, Mark Hernandez, Roberto Rodriguez, Oliver Lawal,** and **Jim Malley**, thank you for your contributions to this work, for your time, your valuable comments, your expertise, and your professional insight. To **Roberto Rodriguez**, thank you for your help with microbiology assays and for your mentorship during and long after your time as a post-doc at CU. It was a pleasure working alongside you and I sincerely appreciate your patience, guidance, and sense of humor. **Chris Poepping**, thank you for your brilliant sense of humor and for making the challenges of lab work fun and enjoyable. **Michael Hawkins**, thank you for your work; you are a natural born scientist and I look forward to seeing how you apply your skills and knowledge. **Kaitlyn Jeanis**, thank you for contributing your time and expertise at a time when I genuinely needed both. Your passion is inspiring and empowering. You are driven to positively impact all those you encounter and I look forward to watching you continue to make your mark. To my fellow CU graduate students and colleagues in Civil and Environmental Engineering, thank you for sharing the journey.

To my parents and siblings, **Charles Beck, Elizabeth Beck, Kateri Drexler, Will Drexler, Regina Drexler, Jane Drexler, Kristi Drexler, Tim Drexler, Matt Drexler**, **Paul Drexler,** and **Pete Drexler**, and to my second family, **Alfred Tom, Billie Tom, Anna Tom,** and **Judy Klima**: thank you, sincerely, for your unwavering love, support, and encouragement.

Thank you for showing me the importance of education, instilling in me a strong work ethic, and showing me that the world is full of limitless opportunities. To my love and partner in life, **Edward Tom**, thank you for your endless love, support and encouragement and for joining me on this journey, as always, side by side. Thank you for the lessons you continue to teach, for inspiring me with your insatiable curiosity, for demonstrating that learning doesn't stop with a diploma, and for your unique and witty perspective.

I am fortunate to have been financially supported by the United States Environmental Protection Agency (EPA) Science to Achieve Results (STAR) Fellowship (FP91709801), a PEO Scholar Award, a Civil Engineering Outstanding Graduate Research Assistantship (RA), Water Research Foundation Project 4376, a doctoral assistantship for completion of dissertation from the CEAE Department, a Graduate School Summer Fellowship, the Mortenson Center Dean's Outstanding Merit Award, and the Malcolm Pirnie Award from the American Water Works Association (AWWA). Thank you for financially investing in me and in this important research.

For work involving the NIST tunable laser, I thank **Harold Wright** and **Karl Linden** for coordinating its use. I thank **Tom Hargy** for performing the UV irradiations with the technical expertise of **Tom Larason**. I acknowledge **Randi McCuin** of Corona Environmental Consulting and **Jeff Budzik** of Tetra Tech, for their microbiological expertise and work on the *Cryptosporidium* and adenovirus cell culture assays and MS2 plaque infectivity assays. I also acknowledge Harold Wright for his work on the statistical analysis.

The action spectra research discussed in Chapter 2 was funded by Water Research Foundation Project 4376 and several organizations that provided cash or in-kind contributions including: Los Angeles Department of Water and Power, Aquionics, Calgon Carbon Corporation, Atlantium Technologies, ITT Wedeco, ETS, Trojan Technologies, Tetra Tech Clancy Environmental Consultants, Hydroqual/HDR, CDM, Black & Veatch, CH2M Hill, Metropolitan Water District of Southern California, NY State Department of Health, CA DHS, WA DOH, and US Environmental Protection Agency (EPA).

For the MS2 and adenovirus genome work discussed in Chapters 3 and 4, I thank **Roberto Rodriguez** for his training on the RT-qPCR and LR-qPCR methods and **Michael Hawkins** and **Kaitlyn Jeanis** for their contributions to data collection.

The adenovirus protein work in Chapter 5 was possible thanks to the trailblazing efforts of **Chris Poepping** and the microbiological expertise of **Natalie Hull**.

The UV LED work discussed in Chapter 6 would not have been possible without the collaboration of the US EPA, specifically the work of **Hodon Ryu** on ICC-qPCR, **Laura Boczek** on *B. pumilus* membrane filtration, and **Jennifer Cashdollar** on the adenovirus 2 quantal assay. I thank **James Rosenblum** for his work on the MS2 double agar layer method and the *E. coli* spread plate method. I thank **Sydney Ulliman** for her work on irradiance and power draw measurements. I thank **Kaitlyn Jeanis** for her work with the MS2 RT-qPCR, adenovirus 2 LR-qPCR, and *E. coli* qPCR procedures.

Disclaimer: The mention of certain commercial products in this dissertation is for information purposes only and does not constitute an endorsement by the authors or their institutions. This dissertation has not been subjected to any EPA or NIST review and therefore does not necessarily reflect the views of the agencies.

"From your vantage point, your education and imagination will carry you to places which we won't believe possible. Make your life count and the world will be a better place because you tried."

-Elison Onizuka, NASA Astronaut, Space Shuttle Challenger

TABLE OF CONTENTS

LIST OF TABLES

LIST OF FIGURES

CHAPTER 1

INTRODUCTION

Ultraviolet light is an accepted technology for water and wastewater treatment as an alternative to chlorine or ozone (USEPA 1999). UV effectively inactivates viruses, bacteria, and protozoan oocysts without chemical addition or the formation of known disinfection byproducts (Hijnen, et al. 2006). Use of UV technology has grown considerably in recent years due to its demonstrated efficacy against *Cryptosporidium parvum*, a protozoan parasite responsible for multiple disease outbreaks, that is highly resistant to chemical disinfection with chlorine (Fayer, et al. 2000; Mackenzie et al., 1994; Bukhari et al., 1999).

UV technology continues to evolve. Polychromatic, medium-pressure mercury vapor lamps are becoming more common in part because they have been shown to be more effective than monochromatic, low-pressure mercury vapor lamps at inactivating adenovirus, the virus that drives the UV disinfection requirements. Increased viral inactivation under polychromatic UV light as well as the impact of low wavelengths on medium-pressure UV system validation have revealed a need to fully understand the fundamentals of polychromatic UV inactivation. It has also revealed an opportunity to gain insight into disinfection by wavelength-specific UV light-emitting diodes (LEDs), which are advancing as a low-energy consumption alternative UV technology. The objective of this research project was to gain insight into the mechanisms of polychromatic UV inactivation by studying loss of infectivity of several pathogens and surrogates as well as genomic damage in viruses. The results were incorporated into the design of a UV LED reactor, with a combination of UV wavelengths with the goal of optimizing pathogen inactivation at low energy cost.

1.1 BACKGROUND: VALIDATING POLYCHROMATIC UV REACTORS

The UV dose-response of microorganisms and viruses varies across the UV spectrum. The spectral sensitivity of an organism or virus is called its action spectrum, which is a measurement of UV inactivation as a function of wavelength for a given UV dose (USEPA, 2003). Understanding the action spectra of a target microorganism and its surrogate is necessary for validating medium-pressure UV reactors. Unlike low-pressure UV lamps, which emit monochromatic light primarily at 253.7 nm, medium-pressure lamps emit polychromatic light across the UV spectrum, playing a significant role in UV inactivation in the 200-300 nm wavelength range. Medium-pressure UV lamps not only damage DNA, but they also cause photochemical reactions in proteins and enzymes as described below (Harm, 1980).

In the United States, the US Environmental Protection Agency's Ultraviolet Disinfection Guidance Manual (UVDGM) provides a framework for ultraviolet disinfection and validation practices. Written to familiarize state and federal regulatory agencies and public water systems with the design, operation and maintenance of UV disinfection systems, the UVDGM supplements the UV disinfection requirements listed in the Long Term 2 Enhanced Surface Water Treatment Rule (LT2ESWTR) to regulate UV dose, reactor validation methods, monitoring and reporting requirements (USEPA, 2006c). UV reactors in the United States are currently validated using biodosimetry in which the log inactivation of a surrogate is measured through a UV disinfection chamber and the corresponding average UV fluence is back-calculated using a reference dose-response curve. When surrogates or challenge microorganisms are used, an action spectrum correction factor must be applied in order to account for differences between the action spectrum of the surrogate and that of the regulated pathogen requiring disinfection.

A surrogate is characterized by, among other things, its ability to mimic the response of a

target pathogen. For UV reactor validation with lamps emitting polychromatic irradiation, surrogates should have similar UV inactivation kinetics or action spectra as the pathogens they are representing. Surrogates such as MS2 and *Bacillus subtilis* are often used in order to obtain a particular reactor validation credit for pathogens including *Cryptosporidium*, *Giardia lamblia,* and viruses. Looking at their action spectra, however, MS2 and *Bacillus subtilis* are much more sensitive at lower wavelengths (below 240 nm) than *Cryptosporidium* (Linden et al., 2001, Cabaj et al., 2002, Mamane-Gravetz et al., 2005). Advances in UV technology, specifically with MP UV lamp output and quartz sleeve transmission, have resulted in transmission of those lower wavelengths (Wright et al., 2009). Using MS2 to validate polychromatic UV systems can underpredict the dose delivered to target pathogens by a factor of 2 or more (Wright et al., 2007). The result is a potential regulatory credit concern surrounding the UV system validation, demonstrating the need for more research into UV disinfection below 240 nm. The water treatment community must reevaluate which surrogates are used for validation testing as well as the action spectra correction factors applied to relate them to target pathogens.

1.2 BACKGROUND: UV DISINFECTION OF ADENOVIRUS

In recent years, there has been a growing interest in the inactivation of adenovirus due to its relative resistance to UV irradiation and its impact on UV treatment regulations. Adenovirus is an enteric virus primarily responsible for respiratory and gastrointestinal illness in humans. Although immunocompromised individuals, infants, and children are the most at risk of adenovirus infection, it has historically caused acute respiratory illness in military recruits as well (Russell, 2006). As a known public health risk subject to future regulation, adenovirus is one of the microbial contaminants listed on the US Environmental Protection Agency's

Contaminant Candidate List (CCL 3). Relative to other pathogens, adenovirus has a strong resistance to UV light. When disinfecting with low-pressure (LP) UV light, 4-log inactivation of adenovirus type 2 requires a dose between 120-168 mJ/cm^2, four times greater than that required for inactivating other enteric viruses, including echovirus, coxsackievirus, and poliovirus (Gerba et al., 2002; Linden et al., 2009; Shin et al., 2005; Thompson et al., 2003). Given this resistance, adenovirus governs the US Environmental Protection Agency regulations for virus inactivation. The Surface Water Treatment Rule, which requires 4-log inactivation of viruses, requires a minimum UV dose of 186 mJ/cm^2, based on empirical results of adenovirus by low-pressure UV light (USEPA, 2003; USEPA, 2006a). For groundwater treatment, the US EPA stipulated that UV is not sufficient standalone treatment for viruses unless adequate inactivation is demonstrated through a field-scale challenge test (USEPA, 2006b).

Although adenovirus has demonstrated a resistance to monochromatic, low-pressure UV light, polychromatic UV light from a medium-pressure (MP) mercury vapor lamp was two to four times more effective (Linden et al., 2009; Linden et al., 2007). A MP UV dose of 40-80 mJ/cm^2 was necessary for 4-log inactivation. The experiments described above measured adenovirus inactivation using cell culture infectivity assays; however, researchers believed that repair enzymes in host cells were repairing damage to double stranded DNA following UV exposure, thereby affecting the inactivation results. This theory was confirmed by a recent study in which adenovirus was assayed using a cell line without repair capability (XP17BE) where LP and MP UV doses as low as 57 and 42 mJ/cm^2 respectively resulted in 4-log inactivation (Guo et al., 2010). Additionally, when direct DNA damage was measured with a PCR assay, low- and medium-pressure UV light were equally effective at damaging DNA, causing the same amount of DNA lesions per kilobase (Eischeid et al., 2009). These studies highlight the need to

understand how the polychromatic light was contributing to adenovirus inactivation as measured by cell culture infectivity.

Studies comparing monochromatic and polychromatic inactivation of viruses are limited. According to a previous AWWA (American Water Works Association) Research Foundation report, polychromatic light has been considered more effective than monochromatic light for inactivating other viruses in addition to adenovirus. For rotavirus, calicivirus, and MS2 bacteriophage, medium-pressure lamps were a factor of 2 times more effective than monochromatic, low-pressure UV (Malley, 2004). The difference in dose response of these viruses to monochromatic and polychromatic UV light could be due to the dose calculation for MP lamps, which may have been weighted incorrectly (Malley, 2004; Hijnen, 2010). When the MP dose calculation is weighted correctly, dose response of an organism to polychromatic light should match its response to monochromatic light (Cabaj et al., 2001; Guo et al., 2009). Current practice, as in the Malley study, is to determine the polychromatic UV dose by weighting the average irradiance in the water sample germicidally, based on the absorbance of DNA (Linden and Darby, 1997; USEPA, 2006a). However, the difference in dose response may be due to the sensitivity of viral components other than nucleic acid; the polychromatic UV light may be more effective than monochromatic light at damaging viral proteins, impacting the ability of the viruses to infect. It's important to consider the unique spectral sensitivity of organisms, including viruses, and account for that sensitivity in the dose calculations for medium-pressure UV.

1.3 BACKGROUND: SPECTRAL SENSITIVITY

The first wavelength-sensitivity experiments were conducted in the early 1890s using a series of colored glass screens to filter natural or simulated sunlight entering a Petri dish. Ward

demonstrated that the blue, violet, and ultraviolet portions of the light spectrum were responsible for inhibiting bacterial growth (Ward, 1893). In experiments with *Bacillus anthracis*, Ward highlighted the importance of separating wavelengths into monochromatic emissions when determining bactericidal action. According to the First Law of Photochemistry, the Grotthuss-Draper law, light must be absorbed by molecular compounds in order to cause photochemical effects. In 1930, Gates connected bactericidal action to UV absorbance. Using a quartz monochromator, to measure the spectral sensitivity of *Staphylococcus aureus* and *Bacillus coli* (*E. coli*), Gates revealed a clear maximum of bactericidal effectiveness occurring near 265 nm, as well as an increase in action at wavelengths below 240 nm, which correlated with the UV absorbance of the bacteria at those same wavelengths (Gates, 1930). Gates suggested that absorbance by "a single vital and sensitive structural and chemical unit" led to bacterial inactivation (Gates, 1930). Each organism and virus has a unique action spectrum. The following is a collection of action spectra data for pathogens commonly found in the water treatment industry as well as surrogates frequently used for validating medium-pressure UV reactors.

1.3.1 Pathogens of Interest

Escherichia coli

Escherichia coli (*E. coli*) are Gram-negative, rod-shaped bacteria ubiquitous in the human intestines, which frequently serve as indicator organisms for fecal contamination. *E. coli* is highly susceptible to UV light. Low-pressure UV doses as low as 8.4 mJ/cm^2 have resulted in 4-log reduction (Chang et al., 1985). Non-pathogenic *E. coli* has occasionally been used for validation testing (USEPA, 2006c). Guo compared low-pressure and medium-pressure inactivation of *E. coli*. When germicidal doses of MP UV lamps were applied correctly, the LP

UV and MP UV exhibited the same dose-response in *E. coli*; however, differences in photoreactivation occurred depending on the irradiation source. The percentage of photoreactivation was considerably less for MP UV than for LPUV (20% vs 50%) after the same germicidal UV dose. At a higher dose of 15 mJ/cm^2, no photoreactivation was detected (Guo, et al., 2009).

As described earlier, the action spectrum for *E. coli* (previously called *B. coli*) was first developed in 1930 (Appendix A, Figure 1). It directly correlated to the absorption of a thin layer of *E. coli* bacteria on an agar surface (Gates, 1930). More recently, an action spectrum was determined for *E. coli* using a pulsed xenon flashlamp emitting 30 ms pulses in a broadband spectrum across the UV to infrared regions. The wavelengths were dispersed with a monochromator with bandwidths of approximately 8 nm in 10 nm increments between 220 nm and 300 nm (Wang et al., 2005). The results (Appendix A, Figure 2) show an apparent maximum inactivation at a wavelength of 270 nm. When irradiated with pulsed UV, *E coli* bactericidal action was significantly lower at 230 nm and 240 nm. No inactivation was detected at 300 nm.

Cryptosporidium

Cryptosporidium is a protozoan parasite that infects the cell lining of the digestive tract, causing the diarrheal disease, cryptosporidiosis. The pathogen's resistant oocysts, 4-6 μm in size, can infect humans through multiple transmission pathways and have been associated with numerous waterborne disease outbreaks (Fayer, 2000), including one that affected the lives of 400,000 people in Milwaukee in 1993 (Mackenzie et al., 1994). The two *Cryptosporidium* species most frequently responsible for infection in humans are *C. parvum* and *C. hominis* (Xiao and Ryan, 2004). *Cryptosporidium* is important to the water treatment industry due to its

resistance to chemical disinfection with chlorine. Initial studies found it to be resistant to UV disinfection as well (Campbell et al., 1995); however, those studies incorporated vital dye and in vitro excystation assays, which significantly underestimated UV inactivation. When animal infectivity assays with neonatal mice were used for detection, medium pressure UV light caused 3.9 log reduction at a UV dose of 19 mJ/cm^2 (Bukhari et al., 1999). Later studies correlated tissue and cell culture assays with animal infectivity for UV disinfection (Rochelle et al., 2002; Shin et al., 2001, Slifko et al., 2002). Low-pressure light was shown to be effective with cell culture assays; a dose as small as 3 mJ/cm^2 reached the detection limit of ~3-log inactivation (Shin et al., 2001). The regulated dose for 4-log inactivation of *Cryptosporidium* is 22 mJ/cm^2 (USEPA, 2006a).

An action spectrum was developed for *Cryptosporidium parvum* in 2001 using bandpass filters with a medium-pressure mercury vapor lamp (Linden et al., 2001). The filters provided half-peak bandwidths of 9-11 nm with peaks at 216, 230, 242, 255, 263, 271, 281, and 291 nm. Inactivation was assayed with Madin-Darby canine kidney (MDCK) cell cultures and the MPN method. Log inactivation of *Cryptosporidium* was determined at UV doses of 2 mJ/cm^2. Wavelengths between 250 nm and 270 nm were the most sensitive to the UV light (Appendix A, Figure 3). These results clearly demonstrated that inactivation of *Cryptosporidium* oocysts is wavelength-dependent. However, since bandpass filters allowed the transmission of specific wavelengths native to the light source in each given range, the results did not quantify precise inactivation efficiencies of specific individual wavelengths. Determining action spectra with a UV light source with a more precise and narrow bandwidth would give more precise data on wavelength-dependent inactivation.

Giardia lamblia

Giardia lamblia is a flagellate protozoan that infects the small intestines, causing giardiasis. *Giardia*'s highly resistant oocysts are prevalent in surface water sources (Marshall et al., 1997) and have been responsible for several waterborne outbreaks (Gibson et al., 1998). Like *Cryptosporidium*, *Giardia* cysts were also thought to be highly resistant to UV disinfection. When measured using in vitro excystation assays, *Giardia lamblia* was highly resistant to conventional doses of LP UV light (Rice and Hoff, 1981). Studies assaying LP UV inactivation with animal infectivity models using Mongolian gerbils reported high sensitivity to LP UV light, both reaching their detection limits, indicating >2-log inactivation at a dose of 3 mJ/cm^2 and >3-log inactivation at a UV dose of 20 mJ/cm^2 (Campbell and Wallis, 2002). A subsequent study with medium-pressure UV light, also using animal infectivity with gerbils, reported reaching the ~4-log detection limit at a dose of 1 mJ/cm^2 (Mofidi et al., 2002; Shin et al., 2009). The regulated dose for 4-log inactivation of *Giardia* is 22 mJ/cm^2 (USEPA, 2006a). No references are available with an action spectrum for *Giardia lamblia*.

Salmonella

Salmonella is a Gram-negative, rod-shaped, flagellate bacterium, 1 μm in diameter, responsible for causing salmonellosis, a diarrheal disease, in humans. *Salmonella* is primarily a foodborne pathogen; however, it can also be transmitted through water and waterborne outbreaks of *Salmonella* have been documented (King et al., 2011). *Salmonella typhimurium,* the less-virulent strain of *Salmonella*, is often used as a surrogate for laboratory testing of *Salmonella spp. Salmonella* is similar in structure to *E. coli* and has a similar susceptibility to UV light. LP

UV inactivation of *S. typhimurium* requires close to 7 mJ/cm^2 for 4-log inactivation (Chang et al., 1985).

The action spectrum for *Salmonella typhimurium* was determined using medium-pressure UV light and bandpass filters of varying bandwidth (3 nm–13 nm). Data points were collected at 10 wavelengths between 200 and 300 nm (214, 220, 228, 239, 248, 260, 270, 280, 290, 300). The result (Appendix A, Figure 4) showed a strong correlation between the action spectrum of *S. typhimurium* and the relative absorbance spectrum of its DNA, extracted from vegetative cells at wavelengths above 240 nm (Chen et al., 2009).

Pseudomonas aeruginosa

Pseudomonas aeruginosa is a Gram-negative bacterium commonly found in graywater, rainwater, and untreated wastewater. Responsible for skin, eye, and lung infections as well as gastroenteritis, it is considered an opportunistic pathogen and often serves as an indicator organism. Due to its presence in biofilms, *P. aeruginosa* is frequently used for studying biofilm formation. Low-pressure light is effective at inactivating *P. aeruginosa*, but higher levels of inactivation are obtained when using a polychromatic spectrum obtained with a medium-pressure UV light. An MP UV dose of approximately 12 mJ/cm^2 is capable of delivering 4-log reduction (Lakretz et al., 2010).

An action spectrum was developed for *Pseudomonas aeruginosa* in an effort to evaluate UV irradiation as a biofouling control technology (Lakretz et al., 2010). Medium-pressure UV light was used with bandpass filters, generating transmission curves with an average full width at half maximum of 20-27.5 nm at peaks of 220, 239, 254, 270, and 280 nm. The polychromatic

spectrum of bacterial inactivation (Appendix A, Figure 5) matched the absorbance of its DNA at the most effective germicidal wavelengths between 254 and 270 nm.

Adenovirus

Adenovirus is responsible for respiratory and gastrointestinal illness in humans, primarily affecting immunocompromised individuals including infants and the elderly. It has been associated with waterborne disease outbreaks (Kukkula et al., 1997) and has been detected in treated drinking water (Lee and Kim, 2002). Adenovirus is a non-enveloped virus with a double stranded DNA of 30-40 kilobase pairs packaged within an icosahedral protein capsid, 70-110 nm in diameter. Fifty-two serotypes have been identified and classified into six species (Jones et al., 2007). An action spectrum was developed for adenovirus type 2 using medium-pressure UV light with bandpass filters (Linden et al., 2007). The filters provided half-peak bandwidths of approximately 10 nm wide with peaks at 222, 228, 239, 260, 280, and 289 nm. The virus inactivation was assayed using the A549 cell line with the 50% tissue culture infective dose method. The results showed a significantly greater sensitivity to UV light at the lower, 222 and 228 wavelengths, which displayed four to six times greater inactivation than at 254 nm (Appendix A, Figure 6). MP UV is more effective than LP UV light when assayed using cell culture most likely because the polychromatic light causes widespread protein damage to the virus in addition to the significant DNA damage caused at peak germicidal wavelengths. The adenovirus type 2 action spectrum indicates the importance of wavelengths below 240 nm in causing this widespread damage. When those lower wavelengths were blocked out with a 240 nm cutoff filter, inactivation of adenovirus type 2 was approximately one log less than with the full MP UV spectrum (Linden et al., 2007).

Rotavirus

Rotavirus causes gastroenteritis, particularly in young children and has been implicated in numerous outbreaks in developed and developing countries, not necessarily related to drinking water (Kirkwood et al., 2004; Skaza et al., 2011). The rotavirus genome is comprised of 11 segments of double-stranded RNA located within a double-layer protein structure, 60-80 nm in diameter; 18 serotypes have been identified and classified into seven groups, A-G.

Low-pressure inactivation (253.7 nm) of Simian Rotavirus (SA-11) requires a dose between 40-60 mJ/cm^2 for 4-log reduction (Battigelli et al., 1993; Hijnen et al., 2006; Malley et al., 2004); the rotavirus strain was propagated and assayed in MA104 cells. For inactivation with polychromatic medium-pressure UV lamps, the inactivation rate constants were significantly higher than for monochromatic inactivation with 26 mJ/cm^2 required for 4-log reduction (Hijnen et al., 2006). An action spectrum was developed for Rotavirus using medium-pressure UV light and bandpass filters with peaks of 220, 228, 239, 260, 280, and 289 nm (Malley et al., 2004). With the exception of an increase in sensitivity at 260 nm, the sensitivity of Rotavirus to UV light increased as the UV wavelength decreased (Appendix A, Figure 7).

1.3.2 Surrogates of Interest

Surrogates or challenge microorganisms used for validating UV systems are characterized by their non-pathogenicity, stability, ease of assay in the laboratory, and especially their ability to mimic UV inactivation of the target pathogen. The following pathogen surrogates are either currently in use or being researched for use in UV reactor validation.

MS2 Coliphage

Male-specific 2 (MS2) coliphage is a single-stranded RNA virus of the Liviviridae family that infects *E. coli* and serves as an indicator of fecal contamination. MS2 is an F+ coliphage, meaning that it infects the F pilus of male-specific strains of *E. coli*. Frequently used for reactor validation in North America, MS2 is similar in size and shape to other viruses, such as poliovirus, enteroviruses, Coksackievirus, Norovirus, and Hepatitis A virus, yet it is often more resistant, making it an ideal surrogate for testing. UV inactivation of MS2 is very straightforward with 65-70 mJ/cm^2 of LP UV light required for 4-log inactivation (Meng and Gerba, 1996; Park et al., 2011).

The MS2 action spectrum was first determined in 1965 using a large diffraction grating monochromator that dispersed monochromatic UV light into approximately 1.2 nm in bandwidth. MS2 was found to have an action spectrum identical (within experimental error) to three other phages of similar size and shape. The action spectra for these and other viruses are shown in Appendix A (Figure 8). The sensitivity of MS2 to UV light peaked near 260 nm; it also increased with decreasing wavelength below 240 nm. The spectrum was again measured in 2005 with a monochromator at wavelengths of 214, 230, 240, 254, 265, 280, and 293 with a maximum bandwidth of 10 nm (Mamane-Gravetz et al., 2005). In that spectrum, MS2 exhibited a small peak near 259 nm; however, the spectral sensitivity was considerably higher at lower wavelengths. At 214 nm, MS2 was three times more sensitive than at 254 nm. Appendix A (Figure 9) shows the variation in action spectra measurements with data from three different research studies normalized to their sensitivity at 254 nm. The same general trends were observed, but the extent of MS2 sensitivity at germicidal wavelengths near 260 and at wavelengths below 240 nm differs.

Bacillus subtilis

Bacillus subtilis is a Gram-positive, rod-shaped bacterium able to form resistant endospores, which are frequently used for biodosimetry in UV reactor validation in Europe. It has been shown that the culture method used to grow *B. subtilis* affects its LP UV inactivation. LPUV doses for 4-log inactivation varied between 30-60 mJ/cm^2 (Sommer and Cabaj, 1993). The accepted LP UV dose for 4-log inactivation of *B. subtilis* cultured in a liquid enrichment medium is 62 mJ/cm^2 (Sommer and Cabaj, 1993; Sommer et al., 1998; USEPA, 2006c).

The action spectrum of *B. subtilis* spores cultured in a liquid enrichment medium was measured using a Xenon lamp and monchromator, emitting at 20 nm bandwidths at central wavelengths of 214, 251, 254, and 293 nm (Cabaj et al., 2002). The resulting spectrum (Appendix A, Figure 10) is shown relative to 253.7 nm with additional input from the literature. The relative spectral sensitivity function, $k_{rel}(l)$, which peaks near 265 nm, was adopted by the Austrian National Standards Institute for medium-pressure UV disinfection systems, ÖNORM (Österreichisches Normungsinstitut) (ONORM, 2003). An additional action spectrum for *B. subtilis* cultured on agar plates was developed using a monochromator at dispersed wavelengths of 217, 231, 241, 254, 266, 281, and 294 (Mamane-Gravetz et al., 2005). Those results were comparable to the previous study, with the spectral sensitivity of *B. subtilis* peaking near 265 nm. Appendix A (Figure 11) compares the spectral sensitivities of *B. subtilis* and MS2 (relative to that at 253.7 nm) with DNA absorbance. The sensitivity increases at wavelengths below 240 nm; however, *B. subtilis* is not nearly as sensitive to these lower wavelengths as the viruses described above. Chen compared the action spectrum of *B. subtilis* spores with the absorbance spectrum of their DNA as well the absorbance spectrum of decoated *B. subtilis* spores (Chen et al., 2009). The spore action spectrum (Appendix A, Figure 12) differed from the two mentioned above; it

displayed a higher sensitivity to wavelengths below 240 nm and a higher sensitivity at its peak of 270 nm. Nevertheless, the Chen spectrum closely matched the absorbance spectrum of the spores themselves, more so than the absorbance spectrum of their DNA. Munakata created an action spectrum for *B. subtilis* spores under vacuum UV and far UV. The wild-type spores exhibited strong resistance to 190 nm light, but were sensitive to 220 nm, 250 nm, 150, and 165 nm (Munakata et al., 1996).

T1 Coliphage

T1 coliphage is a double-stranded DNA virus that infects bacteria, specifically *E. coli*. As a somatic coliphage, T1 infects host *E. coli* cells through their outer cell membrane. T1 is stable in liquid suspensions and has been applied as a biological dosimeter for measuring UV-B sunlight (Furusawa et al., 1990). T1UV, an organism with DNA similar to T1 was isolated from swine manure by GAP Microbial Services. Like T1, T1UV is also a double-stranded DNA virus with a non-contractile tail (Stefan et al., 2007). T1UV has similar sensitivity to low-pressure UV light as *Cryptosporidium* and *Giardia* and has been suggested as a surrogate microorganism for reactor validation. An LP UV dose of ~18 mJ/cm^2 is capable of 4-log reduction of T1UV.

An action spectrum of dry T1 was developed in vacuo at wavelengths between 150 and 254 nm (Maezawa et al., 1984). Synchrotron radiation was applied from an electron storage ring at the Synchrotron Radiation Laboratory in Tokyo with a full width at half maximum (FWHM) bandwidth of 8.7 nm (Ito et al., 1984). Results shown in Appendix A (Figure 13) indicated that inactivation efficiency was lowest at 230 nm. At the wavelength decreased below 230 nm, the inactivation efficiency increased, with the highest reported at the boundary of 150 nm. At 150

nm, the inactivation sensitivity was four times as high as at 230 nm. At the low-pressure emission of 254 nm, T1 coliphage was twice as high as at 230 nm.

An action spectrum was developed for T1UV using a medium-pressure mercury arc-lamp with six bandpass filters between 9-11 nm in bandwidth (220, 228, 239, 254, 265, and 280 nm) (Stefan et al., 2007). The spectrum is shown in Appendix A (Figure 14) along with that of Q-beta. The spectrum was similar in shape to that of MS2, with an apparent peak sensitivity occurring at 265 nm; however T1UV was more sensitive at 280 nm. T1UV has similar inactivation kinetics as *Cryptosporidium parvum* and *Giardia lamblia*. As such, it has been suggested as a surrogate organism for those pathogens in MPUV reactor validation. It is important to note, however, that T1UV is more sensitive than *Cryptosporidium* (and potentially *Giardia*) at wavelengths below 240 nm.

T7 Coliphage

T7 coliphage is a double-stranded DNA virus in the Podoviridae family that infects *E. coli.* It is commonly applied as a biological dosimeter for solar UV radiation (Ronto et al., 1994) and also used for calibration of chemical actinometry (Kuhn et al., 2004). The T7 coliphage genome was one of the first to be fully sequenced (Dunn and Studier, 1983). Like T1UV, T7 coliphage exhibits inactivation kinetics similar to *Cryptosporidium* and *Giardia* and has been considered for reactor validation. For 4-log inactivation of T1UV, 16.6 mJ/cm^2 of LP UV is required (USEPA, 2006c). MP UV light is considerably more effective than LP UV. For 3-log reduction, a MP UV dose of 9.2 mJ/cm^2 was required compared to a required LP UV dose of 10.9 mJ/cm^2. Pulsed UV was significantly more effective with 3-log reduction at 3.4 mJ/cm^2 (Bohrerova et al., 2008).

An action spectrum was developed for T7 coliphage using a xenon lamp and a monochromator with ~4 nm dispersion (Ronto et al., 1992). Inactivation dose curves were measured every 10 nm from 240 nm to 340 nm. The spectrum is given in Appendix A (Figure 15). The apparent maximum occurred at a wavelength of 260 nm. For LP UV, T7 exhibits similar inactivation kinetics as *Cryptosporidium parvum* and *Giardia lamblia*; however, the spectral sensitivity of T7 at wavelengths below 240 nm is unknown.

Q beta Coliphage

Similar to MS2, Qβ (Q beta) coliphage is a virus of the Liviviridae family that infects *E. coli* through the F pilus of male-specific strains. The coliphage is sometimes used as a biological indicator to detect the state of host *E. coli* cells and determine if they are active viable but non culturable (VBNC) bacteria (Ben Said, 2010). Q beta has been used in the past for UV reactor validation (USEPA, 2006c). It is more sensitive to UV light than MS2. The accepted dose required for 4-log inactivation of Q beta, is 48 mJ/cm^2 (USEPA, 2006c).

An action spectrum was developed for Q beta in the same study as for T1UV (Stefan et al., 2007). The Q beta spectrum, shown in Appendix A (Figure 14), was similar in shape to that of MS2, with an apparent peak sensitivity occurring at 265 nm.

1.4 BACKGROUND: DNA/RNA AND PROTEIN DAMAGE

In many action spectra studies, the spectral sensitivity held a direct correlation to the absorbance spectrum of the DNA or RNA of the pathogen or surrogate tested. This proved true for *E coli* and *Salmonella* (Chen et al., 2009; Gates, 1930). For *Pseudomonas aeruginosa*, the sensitivity matched the DNA absorbance spectrum at wavelengths between 240-270 nm (Lakretz

et al., 2010). Similarly, the MS2 spectral sensitivity matched the absorbance of DNA at wavelengths above 240 nm (Mamane-Gravetz et al., 2005). The action spectrum of *Bacillus subtilis* did not match its DNA absorbance, but it did match the absorbance of spores themselves (Chen et al., 2009).

Many studies describe the wavelength dependence of DNA or RNA damage caused by UV light. Absorption of photons by nucleotides leads to the formation of photoproducts. The most prevalent photoproduct is the pyrimidine dimer, in which adjacent pyrimidine thymine (T) and cytosine (C) nucleotides, are bonded together or to each other (Adams, 1986). A recent study (Besaratinia et al., 2011) shows a direct correlation between UV light generated by a Ti:sapphire laser (FWHM of 2-4 nm) and the formation of cyclobutane pyrimidine dimers and other photodimeric lesions. Other methods of DNA damage include 6-4 photoproducts, single and double strand breaks, and DNA-DNA or DNA-protein crosslinks. RNA differs from DNA in composition primarily with the presence of uracil nucleotides instead of thymine. UV irradiation forms several RNA photoproducts, primarily from adjacent pyrimidine nucleotides, such as uracil dimers (Miller and Plagemann, 1974; Smith, 1963), as well as RNA-protein crosslinks (Wurtmann and Wolin, 2009), and 6-4 photoproducts (Petit-Frere et al., 1996). UV-induced photodimeric lesions prevent synthesis, transcription, and replication and ultimately lead to inactivation of the microorganism or virus (Wellinger and Thoma, 1996; Smith et al., 1998, Petit-Frere et al., 1996). DNA and RNA absorbance varies with each organism and virus. Slight variations may be due to differences in the composition of nucleotides. The absorbance spectrum of nucleotide bases in an aqueous solution (Blatchley and Peel, 2001) is shown in Appendix A (Figure 17). The absorbances of adenine, thymine, and uracil peak near 260 nm. Guanine has two peaks near 245 and 275 nm.

Direct UV damage to nucleic acids occurs at the wavelengths absorbed by DNA and RNA, in the germicidal UV region between 200 and 300 nm (Besaratinia et al., 2011; Rosenstein, 1987). In this wavelength range, however, UV light also damages other cellular and viral components, causing, for example, photochemical reactions in proteins and enzymes, specifically near 280 nm or below 240 nm (Jagger, 1967; Harm, 1980). Absorption of UV light by proteins was once thought to be most significant for large microorganisms like fungi, protozoa, and algae (Kalisvaart, 2001), but recent research suggests it may be important for viruses as well (Eischeid and Linden, 2011). In viruses where proteins form a higher percent of the total viral material, protein absorbance may play a larger role (Rauth, 1965; Mamane-Gravetz, et al. 2005). In general, protein absorbance has a relative peak near 280 nm due to the absorbance of the tryptophan and tyrosine amino acids. At that wavelength, however, the absorbance of the amino acids is an order of magnitude lower than DNA absorbance as shown in Figure 1.1 (Harm, 1980). At wavelengths below 240 nm, protein absorbance roughly equals that of DNA, primarily because of the higher absorbance of peptide bond (Jagger, 1967). Peptide bonds in amino acids absorb at 205 nm. Peptide bonds are prevalent in protein structures as the link between amino acids. Therefore, they are a major contributor to UV absorbance. Figure 18 in Appendix A shows the absorption spectra of many amino acids used to construct proteins, including tryptophan, tyrosine, phenylalanine, cystine, and cysteine (Blatchley and Peel, 2001).

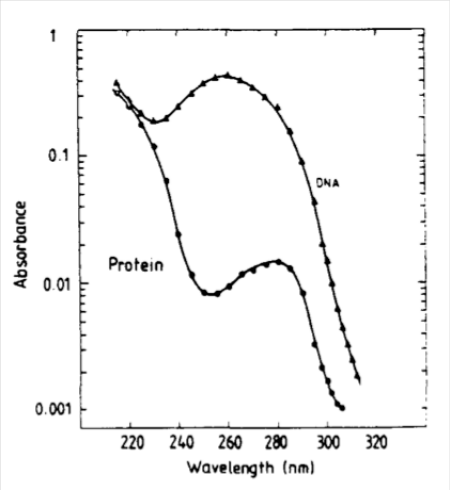

Figure 1.1. Absorbance of proteins and DNA in equal concentrations (Harm, 1980).

In part because of this absorbance of proteins across the UV spectrum, sources that emit polychromatic light, across the germicidal UV spectrum, are considered more effective at inactivating certain pathogens than sources that emit monochromatic light at 253.7 nm (Hijnen et al., 2006; Eischeid and Linden, 2011; Linden, et al., 2007).

1.5 BACKGROUND: UV LIGHT EMITTING DIODES (LEDS)

As polychromatic sources become more common, more research is being undertaken to understand the mechanisms of inactivation occurring in pathogens exposed to polychromatic UV irradiation. Emerging UV technology, such as UV light emitting diodes (LEDs), is also rapidly advancing without fundamental understanding of the disinfection impacts. LEDs are semiconductors activated with a voltage, which release that energy in the form of light. When manufactured with materials such as gallium nitride, aluminum nitride, aluminum gallium nitride, indium gallium nitride, boron nitride, and diamond, the wide bandgaps enable high-energy emission in the UV-C range to wavelengths as low as 210 nm.

UVC LEDs have significant potential since they are smaller and lighter, and consume less power than traditional mercury vapor lamps (Vilhunen 2010). They also provide the capability to be turned on or off instantaneously, and often have a longer lifetime than mercury vapor lamps (Crawford et al., 2005). Additionally, research has shown that graywater treated by UVC LEDs may be less affected by the presence of particles than traditional UV sources given the small size of the UV LEDs, which emit from multiple diodes at different angles compared to traditional UV collimated beam sources (Crook et al, 2014). As an emerging technology, LEDs are constantly improving in energy efficiency, lifespan, and affordability, all of which will make them more practical for widespread use (Ibrahim, 2014). A recent (2014) analysis on the economic viability of UV LEDs predicts "water disinfection systems employing UVC LEDs should start to appreciably penetrate the residential and industrial market within the next 5 years" (Ibrahim et al., 2014). Given rapid research and development in UVC LED technology, broad potential exists for its use for sustainable, point-of-use disinfection in drinking waters through, for example, a photovoltaic (PV) powered system like that detailed previously (Lui, G.Y. et al., 2014).

Deep UV LEDs emitting UV-C light at wavelengths between 260 and 300 nm have proven effective in inactivating bacterial, viral and protozoan pathogen surrogates (Bowker, 2011) and have been demonstrated for point-of-use water disinfection (Chatterley and Linden 2010). Several studies have evaluated the efficacy of germicidal irradiation from UVC LEDs emitting in relatively narrow bandwidths at or near 255 nm, 265 nm, 269 nm, 275 nm, and 282 nm for inactivating *E. coli* (Oguma et al., 2013; Bowker et al, 2011; Chatterley and Linden, 2010; Vilhunen, 2009), *Bacillus subtilis* spores (Wurtele et al., 2011), and/or coliphage such as MS2 and T7 (Bowker et al., 2011).

A few studies have evaluated the combination of multiple wavelengths. Chevremont et al. (2012) combined LEDs emitting in the UVA and UVC range to combine microbial disinfection and chemical degradation for wastewater treatment. Oguma et al. (2013) combined LEDs emitting in the germicidal range, measuring their combined inactivation of *E. coli*. However, more research is necessary to combine multiple UV LEDs in the germicidal range and test them against other pathogens and surrogates to attempt to optimize pathogen inactivation and understand potential synergistic effects that occur when combining LEDs of different wavelength emissions.

1.6 RESEARCH OBJECTIVES AND HYPOTHESES

The primary research objective was to add fundamental insight into the mechanisms of inactivation of polychromatic UV-C light. The research required measuring action spectra of pathogens and surrogates of interest to the water industry. MS2 bacteriophage and adenovirus were analyzed more thoroughly. UV damage to MS2 and adenovirus nucleic acids at wavelength intervals between 200 and 300 nm were compared to infectivity spectra to gain insight into the role DNA damage played in viral inactivation and to understand which wavelengths might cause damage to viral components (other than DNA) that were also responsible for loss of infectivity. Ultimately, the research findings culminated in the design of a UVC LED system that tailors multiple wavelengths to optimize inactivation of target pathogens at low energy cost. The following hypotheses were developed in order to better understand polychromatic UV inactivation:

1) **Weighting polychromatic UV dose calculations by their action spectra would be more accurate, i.e. yield dose response results that are more equivalent to the LP**

UV dose response, than weighting by DNA absorbance.

2) **For MS2, loss of viral infectivity from polychromatic UV irradiation is due primarily to genomic damage.**
3) **For adenovirus, loss of infectivity from polychromatic UV irradiation is due to damage to other viral components, i.e. proteins, in addition to genomic damage.**
4) **A UVC LED system that combines 260 and 280 nm would be as effective as a polychromatic, medium-pressure mercury vapor lamp but at a lower energy cost.**
5) **A UVC LED system combining 260 and 280 nm wavelengths would be more effective at inactivating bacterial and viral pathogens than the sum of efficacy from the 260 nm and 280 nm LEDs separately.**

1.7 RESEARCH OVERVIEW

The research discussed in **Chapter 2** measured the UV spectral sensitivity, called action spectra, of *Cryptosporidium parvum*, adenovirus 2, and MS2, T1UV, Q Beta, T7, and T7m Coliphage, as well as *Bacillus pumilus* spores. A tunable laser from the National Institute of Standards and Technology was used to isolate single UV wavelengths at 10 nm intervals between 210 and 290 nm. Above 240 nm, all bacteria and viruses tested exhibited relative peak sensitivities between 260 and 270 nm. Of the coliphage, MS2 exhibited the highest relative sensitivity below 240 nm, relative to its sensitivity at 254 nm, followed by Q Beta, T1UV, T7m and T7 coliphage. *B. pumilus* spores were more sensitive to UV light at 220 nm than any of the coliphage. Adenovirus 2 was also significantly more sensitive at the lower wavelengths of 210-230 nm and least sensitive at 290 nm. These spectra are required for calculating action spectra correction factors for MP UV system validation, for matching appropriate challenge

microorganisms to pathogens, and for improving UV dose monitoring. When using the adenovirus and MS2 action spectra to calculate the UV dose for medium-pressure UV light, in place of the DNA absorbance, the dose response of adenovirus and MS2 was statistically more similar (less statistical significance) to the dose response to LP UV light than when the calculation was weighted by DNA absorbance. This confirms Hypothesis 1 for these two viruses.

As discussed in Chapters 1 and 2, every organism has a unique sensitivity to ultraviolet (UV) light, called its action spectra. In many cases, the action spectra of bacteria strongly correlate with the absorbance of their DNA. For many viruses, however, the action spectra deviate from the DNA or RNA absorbance, suggesting that mechanisms other than nucleic acid damage are contributing to their UV inactivation. The research presented in **Chapter 3** and **Chapter 4** examined the spectral sensitivity of the MS2 and adenovirus 2 genomes for comparison with the spectral sensitivities, or action spectra, of both viruses as measured by their loss of viral infectivity. MS2 and adenovirus experiments were conducted using the same tunable laser described in Chapter 2 at 10 nm wavelength intervals between 210 and 290 nm.

Damage to the MS2 viral genome was assessed with a reverse transcription (RT) polymerase chain reaction (PCR) assay. The relative genome sensitivity followed the same trend as the action spectra; both exhibited a relative peak near 260 nm, decreased to 240 and then increased below 240. The susceptibility of the MS2 genome to UV light was statistically similar to the susceptibility of the MS2 virus to UV light at 210 nm, 220 nm, 253.7 nm, 260 nm, 270 nm, 280 nm, and 290 nm. This indicates that inactivation of the RNA bacteriophage MS2 is dominated by damage to the nucleic acids throughout the germicidal wavelength range, confirming Hypothesis 2.

Damage to the adenovirus 2 viral genome was assessed with a long range and quantitative polymerase chain reaction (LR-qPCR) assay. The inactivation rate corresponding to adenoviral genome damage matched the inactivation rate of adenovirus infectivity at 253.7 nm, 270 nm, 280 nm, and 290 nm, suggesting that damage to the viral DNA was primarily responsible for loss of infectivity at those wavelengths. At 260 nm, more damage to the nucleic acid was observed than reduction in viral infectivity. At 240 nm and below, the reduction of viral infectivity was significantly greater than the reduction of DNA amplification, suggesting that UV damage to a viral component other than DNA contributed to the loss of infectivity at those wavelengths.

In **Chapter 5**, this work was taken one step further. A deuterium lamp with bandpass filters (214 nm, 220 nm, 227 nm, 240 nm, 268 nm), a low-pressure mercury vapor lamp (254 nm nm), and UVC LEDs (261 nm, 278 nm) were used to measure protein damage across the UVC spectrum. Samples of concentrated adenovirus were exposed to the UV sources and then assayed using SDS-PAGE (sodium dodecyl sulphate polyacrylamide gel electrophoresis). The hexon, penton, minor capsid, fiber, and core proteins were analyzed for UV-induced damage. The SDS-PAGE gel clearly showed damage to the adenoviral proteins, primarily at the low wavelengths, below 240 nm. When analyzed in detail, the 220 nm wavelength was significantly more effective at inducing protein damage. Just 10 mJ/cm^2 decreased the protein quantity by approximately 60% for all five proteins analyzed, compared to little to no damage from 254 nm at doses as high as 400 mJ/cm^2.

These findings confirm Hypothesis 3 and provide insight into why medium-pressure (MP) UV irradiation has been shown to be more effective than 254 nm at inactivating adenovirus 2. This research has significant implications for the UV treatment industry, particularly because

adenovirus is regarded as the most resistant pathogen to UV disinfection and it drives the UV dose requirements for all viruses in regulations set by the United States Environmental Protection Agency.

This wavelength-specific research can help predict the effects of emerging UV disinfection technology, such as deep UV light emitting diodes (LEDs), on viruses and other microorganisms. The research discussed in Chapters 2 through 4 informed the design of a UVC LED unit to optimize, and evaluate possible synergistic effects that may occur in common water-borne pathogens and surrogates when illuminating with two wavelengths, 260 nm and 280 nm, simultaneously. **Chapter 6** evaluated the UVC LED unit for its efficacy in inactivating the common water-borne pathogens, fecal indicators, and surrogates *E. coli*, MS2 Coliphage, adenovirus 2, and *Bacillus pumilus* spores. Inactivation by 260 nm and 280 nm LEDs separately and simultaneously was compared with the efficacy of another common polychromatic UV source, the medium-pressure (MP) UV lamp as well as with low-pressure (LP) UV irradiation.

For *E. coli*, the results showed similar inactivation rates among all five UV sources. For MS2 coliphage, the 260 nm LED was most effective, followed by the equally effective 260|280 nm combination and MPUV, and subsequently the 280 nm and LP UV sources. For adenovirus 2, the MP UV was significantly more effective than the other four UV sources. For *B. pumilus* spores, the MP UV was most effective, followed by the equally effective 260 nm and 260|280 nm LEDs with the 280 nm LED and LPUV irradiation the least effective. When comparing electrical energy per order of log reduction, E_{EO}, the LP UV lamp was consistently the most energy efficient. For MS2, *B pumilus* spores, and adenovirus, the MP UV lamp required less energy per log reduction than the LEDs emitting, in order, at 280 nm, 260|280 nm, and 260 nm.

For *E coli*, the 280 nm LED required less energy per order reduction than the MP UV. This disproves Hypothesis 4 for the current state of UV LED disinfection technology.

The combination of UVC LEDs was also evaluated for potential synergistic effects. For all four microorganisms and viruses tested, no dual-wavelength synergy was detected at both the inactivation and the DNA and RNA damage level. This disproves Hypothesis 5. Although UVC LEDs require more energy per log reduction at the present time, they are competitive with common mercury vapor lamps at inactivating microorganisms and viruses important to the water treatment industry.

Ultimately, this body of work helps broaden our understanding of the dose response of many organisms across the germicidal UV spectrum for improving ultraviolet water disinfection.

CHAPTER 2

ACTION SPECTRA FOR VALIDATION OF PATHOGEN DISINFECTION IN MEDIUM-PRESSURE ULTRAVIOLET (UV) SYSTEMS

This chapter discusses determination of the UV spectral sensitivity or action spectra of *Cryptosporidium parvum,* Adenovirus, and MS2, T1UV, Q Beta, T7, and T7m Coliphage as well as *Bacillus pumilus* spores. These action spectra are required for calculating action spectra correction factors for MP UV system validation, for matching appropriate challenge microorganisms to pathogens, and for improving UV dose monitoring. Additionally, understanding the dose response of these organisms at multiple wavelengths can improve polychromatic UV dose calculations and enable us to predict pathogen inactivation from wavelength-specific disinfection technologies such as UV light emitting diodes (LEDs).

The work described in this chapter has been published (Beck, S.E., Wright, H.B., Hargy, T.M., Larason, T.C., Linden, K.G. 2015. Action Spectra for Validation of Pathogen Disinfection in Medium-Pressure Ultraviolet (UV) Systems. *Water Res.* 70, 27-37. and Beck, S.E., Rodriguez, R.A., Linden, K.G., Hargy, T.M., Larason, T.L., Wright, H.B. 2013. Wavelength-Dependent UV Inactivation of Adenovirus as Measured by Cell Culture Infectivity and Quantitative PCR. *Environ. Sci. Technol*. 48, 591-8.

2.1 INTRODUCTION

Ultraviolet (UV) disinfection is common for pathogen inactivation in drinking water and wastewater sources. UV systems generally use either low-pressure (LP) or medium-pressure (MP) mercury vapor lamps. In the germicidal spectrum, between 200 and 300 nm, LP lamps emit monochromatic light at 253.7 nm. Photons at this wavelength primarily form lesions in nucleic acids (DNA and RNA), due to their relative peak absorbance at 260 nm. MP lamps emit polychromatic light across the electromagnetic spectrum. The broader wavelength range is responsible not only for damaging nucleic acids, but also for causing photochemical reactions in proteins and enzymes. Most protein damage occurs below 240 nm, where proteins absorb UV light the strongest (Harm, 1980).

Federal guidance provides direction for the validation and dose monitoring of UV systems while regulations define the UV dose requirements for pathogens. The Ultraviolet Disinfection Guidance Manual (USEPA, 2006a) was written to provide guidance to state and federal regulatory agencies and public water systems on the design, operation, maintenance, and validation of UV disinfection systems. The UVDGM provides guidance on reactor validation, dose monitoring and reporting and supplements the UV disinfection requirements listed in the Long Term 2 Enhanced Surface Water Treatment Rule (USEPA, 2006b), which regulates required UV dose. The LT2 also requires that UV reactors use dose monitoring that has been proven through validation testing.

UV reactors in the United States are validated using biodosimetry in which the log inactivation of an organism is measured through a reactor and the corresponding applied average UV dose is back-calculated through a dose-response curve. For validation, test microorganisms or surrogates are typically used; ideal surrogates would match the pathogen in terms of dose

response and action spectrum. Dose response is a measurement of pathogen inactivation as a function of UV dose. The action spectrum of a microorganism is a measure of its spectral sensitivity or its UV inactivation as a function of wavelength for a given UV dose (USEPA, 2003). The dose responses and action of microorganisms and viruses vary across the UV spectrum; differences in these parameters between the pathogens of concern and the test microorganisms lead to errors in validation. For instance, below 240 nm, MS2 has a greater relative spectral sensitivity than *Cryptosporidium* (Linden et al., 2001; Mamane-Gravetz et al., 2005). Therefore, for MP UV lamp systems that don't absorb light below 240 nm, validation testing using MS2 over-predicts the UV dose delivered to *Cryptosporidium*, raising a potential public health concern. The UVDGM requires validation factors be applied to account for validation uncertainty. Differences between the organisms' dose responses at 254 nm are accounted for with a RED (reduction equivalent dose) bias. Differences in the spectral sensitivity or action spectra of the organisms are accounted for with an action spectra correction factor (ASCF).

Validating MP UV reactors requires calculating ASCFs, which requires accurately knowing the action spectra. However, existing action spectra data for waterborne pathogens and UV bioassay test organisms typically do not extend below 220 nm and often not below 240 nm. Nevertheless, the wavelengths below 240 nm are considered responsible for the enhanced efficacy of MP UV over LP UV for disinfecting certain pathogens (Malley et al., 2004; Linden et al., 2007; Eischeid et al., 2009; Beck et al., 2014).

Additionally, many of the existing published action spectra were measured using bandpass optical filters, which can introduce an error that impacts the interpretation of the data. Bandpass filters restrict the UV light from a MP lamp to a given range of wavelengths; however,

the bandpass filters have a bandwidth on the order of 10 nm at half of the maximum peak transmittance and a bandpass of 20 nm at 10 percent of the peak. This breadth essentially allows polychromatic light from the MP source through the filter and decreases the precise delivery of specific wavelengths during action spectra measurements. Use of bandpass filters can cause errors during the action spectra measurement because the effective wavelength of the bandpass filtered light differs from the nominal wavelength of the bandpass filter. Statistically significant error has been shown when the UV dose response of microbes was measured using monochromatic 254 nm light from a LP lamp compared with 254 nm bandpass filtered light from a MP lamp. The doses required for 3-log inactivation of T7 and Q Beta coliphage were 20-34% less when irradiated with the bandpass-filtered MP UV lamp than with the LP UV lamp emitting at the same wavelength (Wright et al., 2007). Mamane-Gravetz et al. (2005) also noted differences (approximately 9-15%) between the inactivation coefficients for MS2 coliphage and *B. subtilis* spores irradiated with a LP UV lamp compared to irradiation from a xenon lamp monochromator centered at 254 nm with a FWHM of 10 nm.

To address these errors, this research measured the action spectra of *Cryptosporidium parvum* and adenovirus 2, as well as MS2, T1UV, Q Beta, T7, and T7m coliphage from 210 nm to 290 nm using a tunable laser that produced precise monochromatic light (bandwidth << 1 nm). To add to the body of knowledge, the action spectrum of *Bacillus pumilus* spores was also determined; however, a MP UV source with bandpass filters was used due to resource limitations. This work was required for calculating accurate action spectra correction factors for MP UV system validation, for matching appropriate test microorganisms to pathogens, and for defining what wavelengths are important for UV dose monitoring.

Action spectra can be used to calculate germicidal UV dose when irradiating with polychromatic UV sources. The suggested practice for calculating UV dose involves weighting the average irradiance of the water sample by a generic DNA absorption spectrum (from *E. coli*), normalized to 254 nm to determine the average germicidal irradiance. Past research has suggested that weighting the MP UV dose calculation by action spectra is more appropriate than the standard practice of weighting by DNA absorption (Malley et al., 2004; Mamane-Gravetz et al., 2005; Hijnen and Medema, 2010; Beck et al., 2014). With a correct MP UV dose calculation, the dose response of the organism to MP UV light would match its response to LP UV light as is the case with *E. coli* and *Mycobacterium terrae* (Bohrerova and Linden, 2006; Guo et al., 2009). In addition to development of the action spectra for numerous microorganisms, in this work the action spectra for MS2 coliphage and adenovirus were used to weight the average irradiance in an MP UV dose calculation and the results were compared to the LP UV dose response.

2.1.1 Pathogens Tested

Cryptosporidium parvum is a protozoan parasite that infects the cell lining of the digestive tract, causing the diarrheal disease, cryptosporidiosis. The pathogen's resistant oocysts, 4 mm to 6 mm in size, can infect humans through multiple transmission pathways and have been associated with numerous waterborne disease outbreaks (Fayer et al., 2000), including one that affected the lives of 400,000 people in Milwaukee in 1993 (Mackenzie et al., 1994). *Cryptosporidium* is important to the water treatment industry due to its resistance to chemical disinfection with chlorine.

Adenovirus is an enteric virus associated with respiratory and gastrointestinal illness in humans, most virulently affecting immunocompromised individuals. It has been associated with

waterborne disease outbreaks (Kukkula, et al., 1997) and has been detected in treated drinking water (Lee and Kim, 2002). As a known public health risk subject to future regulations, it is one of few microbial contaminants listed on the US Environmental Protection Agency's Contaminant Candidate List (CCL 3).

2.1.2 Surrogates Tested

MS2 phage, or male specific 2, is a single-stranded RNA virus that infects the F pilus of male-specific strains of *E. coli*. Frequently used for reactor validation in North America, MS2 is similar in size, shape, and genome length to enteroviruses including poliovirus, echovirus, and coksackievirus, but it is more UV-resistant than these viruses (Hijnen et al., 2006; Park et al., 2011). MS2 has been used as a reactor validation surrogate for *Cryptosporidium* and adenovirus although it has a different dose response and action spectrum than these pathogens.

T1UV coliphage, an organism with a genome similar to coliphage T1, was isolated from swine manure by GAP Environmental Services (London, Ontario Canada). T1UV is a double-stranded DNA virus with a non-contractile tail (Stefan et al., 2007). T1UV has similar sensitivity as *Cryptosporidium* and *Giardia* to low-pressure mercury vapor lamps (253.7 nm) and is often used as a surrogate microorganism for reactor validation.

Q Beta coliphage is a single-stranded RNA virus similar to MS2 that infects *E. coli* through the F pilus of male-specific strains. Q beta has been used for UV reactor validation (USEPA, 2006a) though not frequently. Q Beta is more sensitive to 254 nm UV light than MS2.

T7 coliphage is a double-stranded DNA virus that infects *E. coli.* Like T1UV, T7 coliphage exhibits inactivation kinetics similar to *Cryptosporidium* and *Giardia* and is often used for

reactor validation. **T7m coliphage,** a strain of T7 with a sequence similar to T3 (Lin et al., 2012), is not currently used for validation, but was used in the past.

Bacillus pumilus is a non-pathogenic spore-forming bacterium, highly resistant to monochromatic UV light. Given its UV resistance, *B. pumilus*, in its spore form, is being considered as a surrogate microorganism for adenovirus (Rochelle et al., 2010). The UV dose-response of spores varies by strain and cultivation method.

2.2. MATERIALS AND METHODS

2.2.1 UV Irradiations

UV irradiations were conducted using one of three UV sources: a tunable laser, a LP UV lamp, or an MP UV lamp. *Cryptosporidium*, the five coliphage, and adenovirus 2 were irradiated with a NT242 series Ekspla tunable laser from the National Institute of Standards and Technology (NIST), as described previously. The Ekspla incorporates a pulsed (1 kHz) Nd:YAG pump laser and an optical parametric oscillator (OPO), which provide the capability to tune the laser output between 210 nm and 2600 nm. The 2.5 mm diameter laser beam first passed through a computer-controlled shutter, before being reflected off two dielectric mirrors, which filtered out visible light. A NIST compact array spectrometer (Instrument Systems CAS 140 CT) was used to verify that no visible light reached the samples. The beam traversed next through a beam splitter and an etched, fused silica diffuser (RPC Photonics, Rochester, NY), specifically engineered to modify the laser beam from a collimated oval shape to a uniform diverging beam (10° half-angle) for irradiating the water samples.

For this work, exposures were conducted at 210 nm, 220 nm, 230 nm, 240 nm, 253.7 nm, 260 nm, 270 nm, 280 nm, and 290 nm. The full width at half maximum (FWHM) bandwidth of

the laser radiation was calculated at 0.04 nm at 300 nm emission and 0.07 nm at 210 nm. When measured with a Maya 2000 Pro spectrometer (Ocean Optics, Dunedin, FL), the FWHM varied between 1.1 nm at 210 nm and 1.7 nm at 300 nm; the wider FWHM is caused by the bandwidth of the Maya 2000 Pro. A figure of the NIST tunable laser emission at each wavelength is shown in Figure 2.1. A more detailed description of the tunable laser is included in Appendix B.

For comparison, samples were also exposed to UV light from a LP mercury vapor lamp (Atlantic Ultraviolet G12T6L, Hauppauge, NY), emitting at 253.7 nm, with a full width at half maximum (FWHM) of 2 nm. For *Cryptosporidium*, UV light from the tunable laser was attenuated using a neutral density filter to increase the exposure times to at least 30 s to improve the accuracy of the measured UV dose.

UV irradiations of *B. pumilus* spores were conducted using the LP lamp noted above and with a 1-kW Rayox medium-pressure mercury vapor lamp (Calgon Carbon, Pittsburgh, PA) with bandpass filters (Andover Corporation, Salem, NH), which had a FWHM of 10-12 nm. The emission spectra, shown in Figure 2.1, were measured with an Ocean Optics Maya 2000 Pro spectrometer (Dunedin, FL). The weighted average wavelengths used for irradiation of *B. pumilus* spores were 220, 230, 244, 258, 264, 270, 281, and 292 nm. For each polychromatic irradiation, UV dose was calculated by summing the average UV irradiance over the wavelength range, accounting for absorbance and sample depth, following the Beer-Lambert Law as described previously (Bolton and Linden, 2003; Linden and Darby, 1997). Although the action spectra for *B. pumilus* spores would not be as precise as if it were determined with the NIST tunable laser, the authors chose to include this spectrum with the others because a *B. pumilus* action spectrum has not previously been published in the peer-reviewed literature.

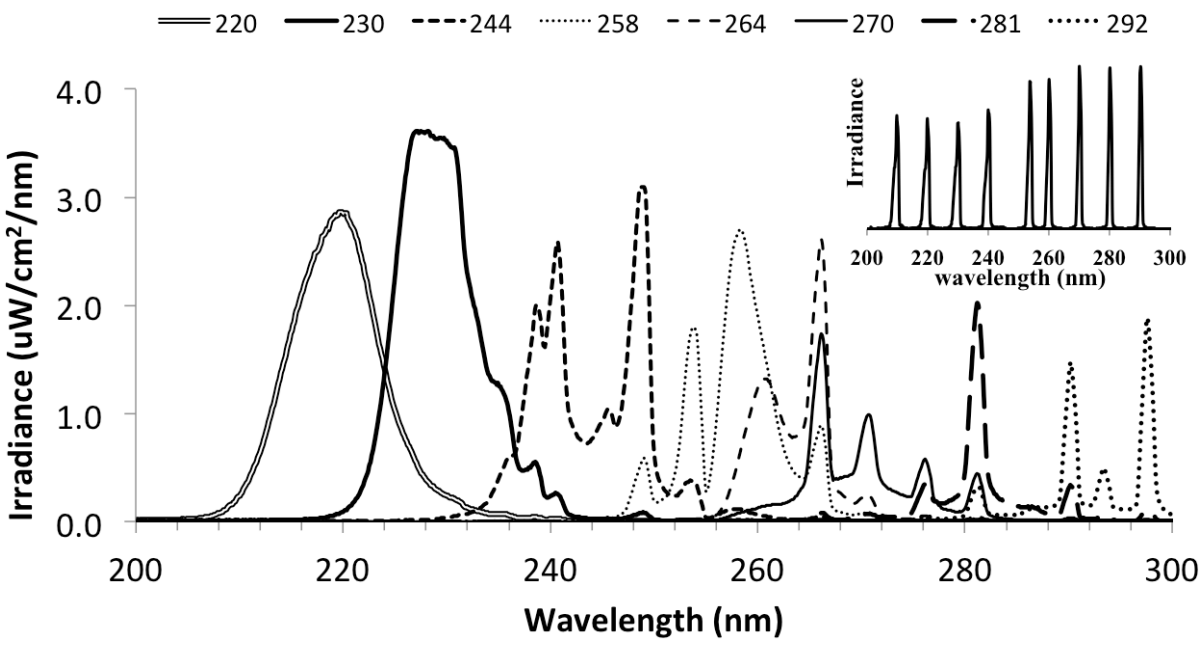

Figure 2.1. Emission spectra of the MP UV lamp through bandpass filters, used for *Bacillus pumilus* irradiations. Insert: for comparison the NIST tunable laser emission at each wavelength is shown.

For all test microorganisms, four collimated beam exposures were conducted at each wavelength to generate a dose response curve up to at least 3-log inactivation of each microorganism. Microbial suspensions of 5 mL in a continuously stirred dish (0.6 cm sample depth) were irradiated by one of the three lamp sources. UV irradiance from the NIST laser was measured by a photodiode detector (IRD SXUV 100, Opto Diode Corporation, Thousand Oaks, CA) comprised of 10 mm x 10 mm windowless silicon and an 8 mm diameter electroformed precision aperture (SK# 030483-1073, Buckbee Mears, Cortland, NY) supplied and calibrated by NIST. At each wavelength, the irradiance uniformity (i.e. Petri factor) of the laser was measured at the water surface plane using a radiometer (model 1400A) and detector (SED 240) and W-diffusor (International Light Technologies, Peabody, MA) with a 1 mm aperture in front of the detector. All petri factors were within the range of 0.94 to 1.05. UV irradiance from the LP UV and MP UV lamp sources were measured at the water surface using the same calibrated

radiometer (model 1400A), detector (SED 240) and W-diffuser. For LP UV exposures, irradiance readings were confirmed using a second radiometer/detector (Gigahertz/Optik X9-11, Newburyport, MA). UV dose was calculated based on average irradiance multiplied by the exposure time where the irradiance accounted for surface reflection, sample depth, UV absorbance, and uniformity across the surface as described previously (Bolton and Linden, 2003). UV doses ranged from 0.5 mJ/cm^2 to 160 mJ/cm^2, depending on the pathogen and the wavelength tested. Immediately after exposure and prior to starting the assays, the irradiated samples were refrigerated at 4°C in the dark.

2.2.2 Stock Preparation and Enumeration

Cryptosporidium parvum

Cryptosporidium parvum oocysts (Iowa isolate) were purchased from Waterborne, Inc. (New Orleans, LA). These had been produced by experimentally infected mice. Feces were collected and purified using sucrose and Percoll density gradient centrifugation. Oocysts were < 1 month old post shedding and had ≥ 5 % infectivity rate for inactivation trials at time of testing.

Cryptosporidium concentrations were assayed using HCT-8 (human ileocaecal adenocarcinoma) cells (American Type Culture Collection, ATCC # CCL-244). The HCT-8 cell stock solutions were prepared by placing the cells in a volume of maintenance media (RPMI), supplemented with antibiotics, an antifungal agent and fetal bovine serum. The flask was incubated at 35 $^{\circ}$C +/- 1.0 for 2-5 days under 5 % CO_2 . When the cells formed a confluent monolayer, they were removed from culture flask by trypsinization, concentrated by slow speed centrifugation at 400 g for 2 min, and re-suspended in maintenance media. A small portion of the re-suspended cells was placed in a sterile flask containing fresh media for continued growth. The

Cryptosporidium infectivity assay was conducted by placing 10^5 HCT-8 cells in each chamber of a well slide containing 8 chambers and incubating at 35 °C +/- 1.0 °C and 5 % CO_2 for 2 to 3 days. When the monolayers in the well chambers were 80 % to 90 % confluent, they were ready to support *C. parvum* infections. HCT-8 cells were discarded after 24 passages.

C. parvum infectivity was measured within 24 hours of UV exposure using a protocol described previously (Johnson et al., 2010). Briefly, oocysts were concentrated using immunomagnetic separation (IMS) as described in US EPA Method 1623 (McCuin and Clancy, 2003) within 2 hours of exposure. Each sample was transferred to an individual Leighton tube containing 1 mL each of SL-A and SL-B buffers. Centrifuge tubes were rinsed with approximately 1 mL to 2 mL of phosphate buffered saline (PBS) to remove residuals and the rinse was transferred to its respective Leighton tube. One hundred microliters each of *Cryptosporidium* IMS beads were added to each tube and were incubated for 1 h at room temperature under constant rotation. Each Leighton tube was then placed in a magnetic particle concentrator (MPC-1) and gently rocked for 2 min, through a 90° angle. The supernatant in each tube was aspirated. The tube was removed from the MPC-1 and the bead-oocyst complex was gently re-suspended in 1 mL PBS. The tube was replaced in the MPC-1 and the bead isolation procedure was repeated and the supernatant discarded. The beads in each tube were re-suspended in 100 µL Hank's Balanced Salts Solution (HBSS) and refrigerated overnight at 4°C.

The following morning, samples and controls (method blanks, heat-inactivated oocysts and unexposed oocysts) were incubated at 35 °C for one hour in acidified HBSS containing a concentration of 1 % trypsin to stimulate excystation of the oocysts. Sample aliquots were rinsed to remove the acidified HBSS and known concentrations of *C. parvum* oocysts were applied to confluent monolayers of HCT-8 cells and then incubated for 68 to 72 hours under 5 % CO_2.

After incubation, inoculated monolayers were washed with phosphate buffered saline and stained with fluorescein isothiocyanate (FITC) conjugated polyclonal antibodies. Detection and enumeration of the intracellular reproductive stages of *C. parvum* oocysts were performed using epifluorescence and differential interference contrast (DIC) microscopy.

Quality assurance/quality control samples were analyzed with each analytical batch. Method blanks, positive controls, a negative control consisting of heat-inactivated oocysts, and inoculation process controls were analyzed. Initial concentrations of oocysts used in each experiment were determined by hemocytometer counts. Initial oocyst infection rates were used to calculate the number of oocysts needed for each exposure to accurately measure the $\log_{10}$ inactivation.

Bacteriophage

Stock solutions of coliphage were prepared by inoculating the propagation media listed in Table 2.1 with the log-phase host bacteria and an aliquot of the phage stock also listed.

TABLE 2.1. Coliphage Propagation Host and Media Specifics

Coliphage (Source /ID)	***Host (Source/ID)***	***Propagation Media***	***Total Time to Propagate***
MS2 (ATCC/15597-B1)	*E. coli HS(pFamp)R (ATCC/700891)*	*Tryptic Soy Broth supplemented with Ampicillin/Streptomycin*	*5 hours*
T1UV (Laval University/HER#468)	*E. coli CN13 (ATCC/700609)*	*Modified TYGB*	*21-27 hours*
Qβ (ATCC/23631-B1)	*E. coli (ATCC/23631)*	*Tryptone Yeast Glucose Broth (TYGB)*	*5 hours*
T7m (ATCC/11303-B38)	*E. coli B (ATCC/11303)*	*Nutrient Broth supplemented with 0.5 % Sodium Chloride*	*7 hours*
T7 (ATCC/BAA-1025-B2)	*E. coli CN13 (ATCC/700609*	*Tryptic Soy Broth*	*24 hours*

The broth was incubated at 35 $^{\circ}$C $\pm$ 0.5 $^{\circ}$C with constant shaking for the time specified in Table 1. Bacterial debris was removed by centrifugation at 5000 g for 30 min. The clarified supernatant containing the phage was decanted to sterile containers and stored at 4 $^{\circ}$C. For some

exposures (i.e., MS2, T1UV, and T7), coliphage stocks were received from other laboratories involved in UV reactor validations.

Phage concentrations were determined using the double agar layer method as described previously (Fallon et al., 2007). Briefly, log phase host bacteria were added to "soft agar" with an aliquot of the sample containing an estimated 20 – 200 plaque forming units (pfu). The inoculated soft agar was poured over an agar plate and allowed to harden. Agar plates were incubated inverted for 16 to 24 hours at 35°C ± 0.5 °C and then examined for plaque formation. Viral plaques were counted to determine the original concentration of coliphage in the original broth culture and the concentrations after exposure to UV light. Each sample was analyzed at multiple dilutions with three replicates plated at each dilution. Controls were analyzed each day samples were analyzed. Negative controls were analyzed at the beginning of each analytical batch and periodically during the plating procedure to ensure the sterility of plating area. A negative control was also analyzed at the end of the plating. A positive control sample was plated each day to ensure the assay was working correctly.

Adenovirus

Virus and cell lines used for inactivation studies were obtained from American Type Culture Collection (ATCC). A549 human lung carcinoma cells (ATCC #CCL-185) were cultured in DMEM high glucose media with 1X penicillin streptomycin (100X solution (Gibco Invitrogen)) and 10% fetal bovine serum and incubated at 37 °C in 5% CO_2 and 95% humidity. Confluent flasks of A549 cells were infected with adenovirus type 2 (ATCC #VR-846), incubated, and checked daily for cytopathic effects (CPE). When the monolayer of A549 cells was 90% destroyed, flasks were freeze-thawed three times and the adenovirus was purified from the flask by centrifugation and polyethylene glycol precipitation, and tittered.

For UV-irradiated samples containing adenovirus, a Most Probable Number (MPN) assay was performed (USEPA, 1996; Cromeans et al., 2008). After exposures, all samples were frozen at -80 °C until cell monolayers were ready for infection. Briefly, 24-well plates were seeded with A549 cells (5 x10^5 cells/1 mL), DMEM supplemented with antibiotics, antimitotic and 10% fetal bovine serum (FBS). The plates were incubated for 1 d to 2 d at 37 °C ± 1 °C and 5% CO_2. Once the monolayers were 90% to 100% confluent, adenovirus samples were removed from the freezer, thawed, and serially diluted. Four sequential dilutions were analyzed, 10 wells per dilution, so that the most dilute applied to the monolayers resulted in no CPE. In each 24-well plate, the first well was a negative control. The media was aseptically removed from the well. A fixed volume (100 µL) of each sample dilution was applied to the monolayer and incubated at 37 °C ± 1 °C for 1 h to 2 h to enhance virus absorption. After the required incubation, 900 µL of DMEM supplemented with antibiotics, antimitotic and 2% fetal bovine serum (FBS) was added to each well. All plates were incubated at 37 °C ± 1 °C and 5% CO2 for 14 d. The media was changed on wells showing no CPE after 5 d to 7 d incubation. An MPN result was determined using a spreadsheet based on the calculation methods given in Standard Methods (APHA, 2005).

Bacillus pumilus

The ASFUVRC strain of *B. pumilus* was isolated from native aerobic spore forming (ASF) bacteria after exposure to high doses of LP UV light. Spore preparation was conducted as described previously (Rochelle et al., 2010). Briefly, spores were cultured for 6 days by incubating at 37 °C in a modified sporulation medium supplemented with 0.1 mM $MnSO_4$. Spores were harvested by centrifuging at 4000 g at 4 °C for 15 min. The resulting cell pellets were washed three times by resuspending in sterile phosphate buffered water (PBW) and centrifuging at 4000 g at 4 °C for 15 min. The final cell pellet was resuspended in 10 mL of

PBW, pasteurized at 80 °C for 20 min to kill vegetative cells, and then stored at 4 °C prior to UV exposure.

B. pumilus spore assays were conducted as described previously (Rochelle et al., 2010). The stock suspension was serially diluted and then aliquots were filtered using 0.45 µm pore-sized mixed cellulose esters membranes. Membranes were applied to plates of tryptic soy agar (TSA) and incubated inverted for 22 to 26 hours at 35 °C. Colonies were enumerated to determine the initial spore concentrations. For exposed samples, sample volumes or dilutions containing and estimated 20 to 60 colony forming units (cfu) per membrane were analyzed to determine $\log_{10}$ inactivation. Each volume analyzed was plated in triplicate.

Quality control samples were analyzed with each batch of samples and include a negative control of the rinse water, a negative control of vegetative bacteria, *E. coli* stock (ATCC #25922) after pasteurization, and a positive control of a known concentration of *B. pumilus*.

2.2.3 Statistical Analysis

Sutherland (2002) and Coohill (1991) describe an action spectrum as constants that map the UV dose response of an organism at different monochromatic wavelengths to its UV dose-response at a reference wavelength, such as 253.7 nm. To determine the constant at a given wavelength, the UV dose-response at 253.7 nm was modeled empirically using a quadratic function:

$$\log I = A \times D + B \times D^2$$

The quadratic function was used for *Cryptosporidium parvum, B. pumilus*, and the coliphage because it accounted for the statistically significant curvature ($p < 0.10$) observed with a majority of the UV dose-response curves measured in this work. The constants were then determined as the values that mapped the UV dose response at each wavelength tested onto the UV dose

response at 253.7 nm, minimizing the sum of the squares of the differences between the measured log inactivation and that predicted using the quadratic function for a given UV dose. The mapping approach was used for determining action spectra because it incorporates all of the dose-response data as opposed to one value at a fixed log inactivation. See Appendix B for a visual illustration of the mapping approach.

With *Bacillus pumilus*, the UV dose response data obtained using the MP UV lamp with bandpass filters was mapped to the UV dose-response data from a LP UV lamp emitting at 253.7 nm. With *Cryptosporidium parvum* and the coliphage, the UV dose response data obtained from the tunable laser emitting at various wavelengths described above was mapped to the UV dose response data obtained using the tunable laser emitting at 253.7 nm.

For adenovirus, the relationship between the log concentration of virus and UV dose was linear, showing no statistically-significant curvature. The kinetic constant for the relationship between log (N) and UV dose was obtained from regression analysis. The log reduction of adenovirus was calculated as:

$$\text{Log reduction} = \log(N_0) - \log(N) \quad ,$$

where $\log(N_0)$ was the log concentration of the unexposed sample obtained from the regression analysis (i.e. the intercept), and log (N) is the measured log concentration. Inactivation rate constants were taken relative to its value at 253.7 nm to illustrate the spectral sensitivity of adenovirus to UV light emission from a LP UV lamp.

The full action spectra were then generated by fitting the averaged values at the wavelength intervals tested with a cubic spline. When applicable the 95% confidence intervals were determined by multiplying the t-statistic (1.96) by the standard deviation and dividing by the square root of the number of samples.

2.2.4 Dose Calculations

The dose response of MS2 and adenovirus to MP UV light was determined given two different MP UV dose calculations. The doses were calculated as described in Linden and Darby (1997) with the spectral weighting being the standard measure of germicidal effectiveness (USEPA, 2006a), the DNA absorption curve, in one calculation and the action spectrum from this study in the other. For MS2, the two MP UV dose response curves were compared with the dose response of MS2 to LP UV light using a dummy variable analysis. For adenovirus, the two MP UV dose response linear regressions were compared to its LP UV dose response using Analysis of Covariance (ANCOVA).

2.3. RESULTS AND DISCUSSION

2.3.1 Cryptosporidium

Results from the three collimated beam trials with *Cryptosporidium parvum* are shown in Figure 2.2. At the tunable laser emission of 253.7 nm, 2-log inactivation was attained at an average UV dose of 1.9 mJ/cm^2. This is consistent with the literature in which 1.7-log inactivation was reported at a LP UV dose of 2 mJ/cm^2 (Shin et al., 2001). The required dose for 2-log inactivation of *Cryptosporidium*, stipulated in the Federal Register is a conservative 5.8 mJ/cm^2 (USEPA 2006b). *Cryptosporidium* dose response exhibited a slight shoulder at each wavelength tested.

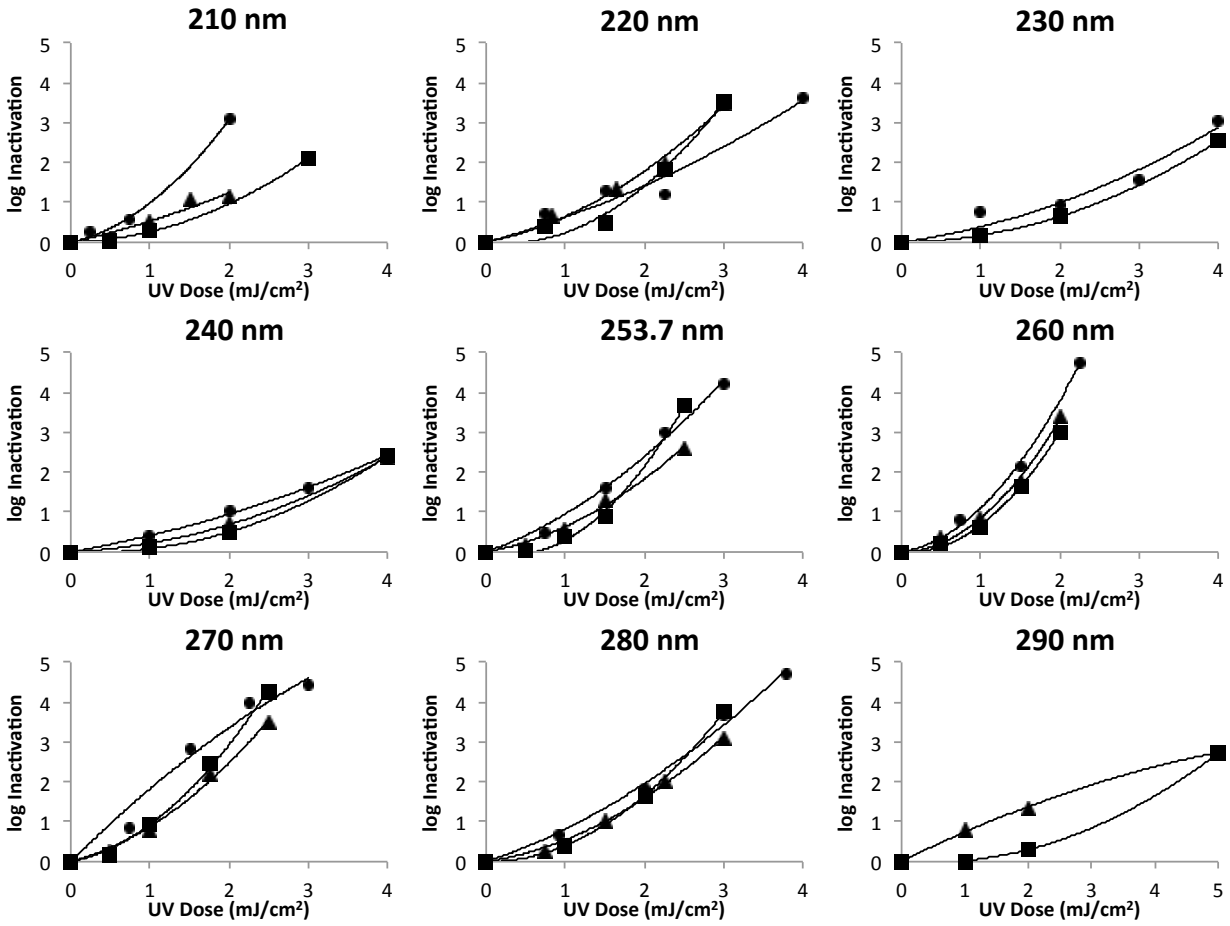

Figure 2.2. Dose response of *Cryptosporidium* to wavelength-specific UV light from the tunable laser. Symbols represent data from three independent trials: R1 (●), R2 (▲), and R3 (■). Average standard deviation between triplicate platings = 8.3 oocysts.

The dose response data was used to determine the spectral sensitivity or action spectrum of *Cryptosporidium parvum* relative to its response at 253.7 nm (Figure 2.3, Appendix B). This spectrum was compared to an action spectrum developed previously from a medium-pressure UV mercury vapor lamp and bandpass filters providing half-peak bandwidths of 9 nm to 11 nm (Linden et al., 2001). Above 240 nm, the two spectra were comparable. Below 240 nm, the spectrum developed in this study displayed a greater relative sensitivity of *Cryptosporidium parvum* to the lower UV wavelengths. This difference could be due to differences between the narrow-band light emitted from the monochromatic tunable laser used in this study and the broader output from the medium-pressure UV lamp with bandpass filters used previously. It

could also be due to differences in the *C. parvum* assays. Nevertheless, unlike for some of the phage presented below, the lower wavelengths from polychromatic lamps do not provide increased inactivation of *C. parvum* relative to inactivation from LP UV light, which is consistent with the previous study (Linden et al., 2001).

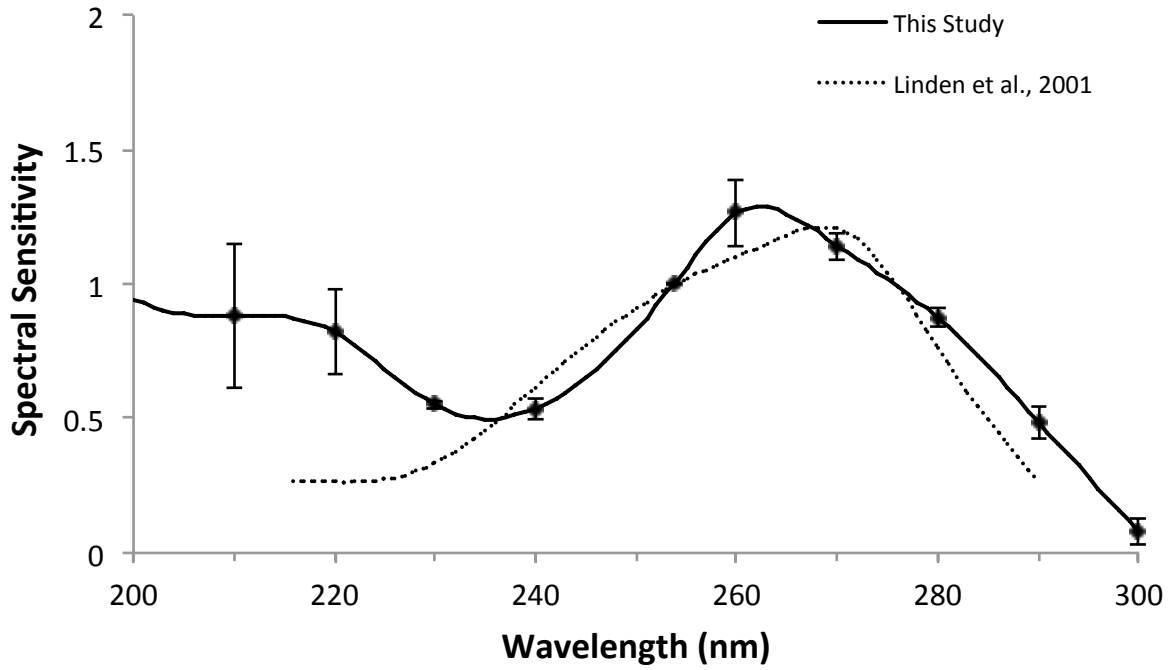

Figure 2.3. Relative spectral sensitivity of *Cryptosporidium parvum* to UV light compared to a previous research study (Linden, Shin et al. 2001). Error bars represent 1 standard deviation from the mean sensitivity value. n = 3 for all wavelengths except 230 nm and 290 nm, where n = 2.

2.3.2 Coliphage

Results from the four collimated beam trials with MS2 Coliphage are shown in Figure 2.4. At the tunable laser emission of 253.7 nm, 2-log inactivation was attained at a UV dose between 29.4 mJ/cm^2 and 41.8 mJ/cm^2. This is consistent with the literature in which 2-log inactivation was reported at LP UV doses of 32.8 mJ/cm^2 and 35.1 mJ/cm^2 (Meng and Gerba, 1996; Park et al., 2011). Four of the six trials lay outside the National Water Research Institute (NWRI) bounds of 34 mJ/cm^2 to 54.5 mJ/cm^2 because the bounds assume a linear dose response

where, in fact, the dose-response have curvature. The bounds were also developed using dose response data where the UV dose calculations did not account for divergence, reflection, or the non-uniformity of the light source across the Petri dish.

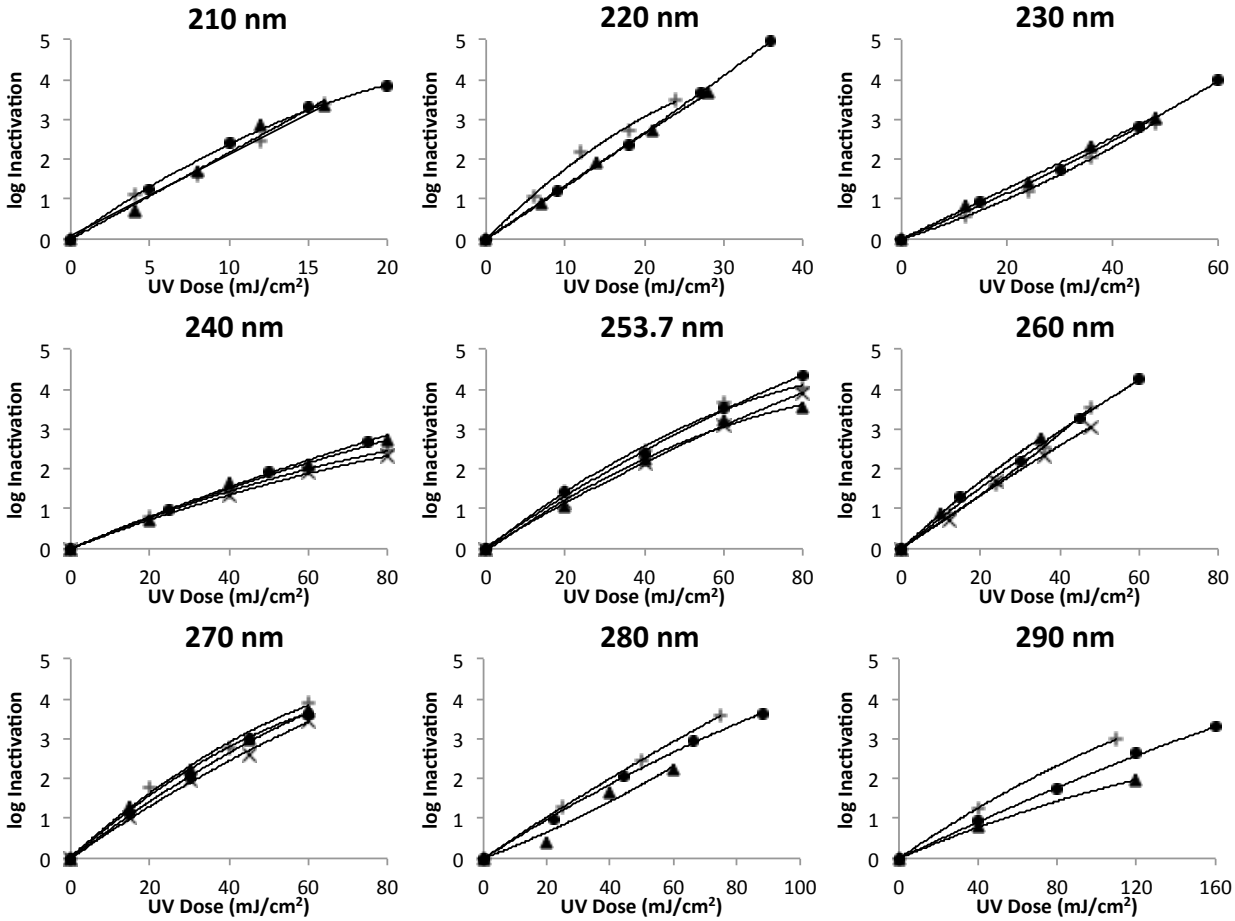

Figure 2.4. Dose response of MS2 Coliphage to wavelength-specific UV light from the tunable laser. Note different x-axis values. Symbols represent data from four separate trials: R1 (●) and R2 (▲) from one laboratory and R3 (+) and R4 (×) from two additional laboratories. Average standard deviation between replicate platings = 6.3 pfu/mL.

The dose response data was used to determine the spectral sensitivity or action spectrum of MS2 Coliphage (Appendix B), which is shown in Figure 2.5, compared with two action spectra from the literature. The MS2 Coliphage action spectrum was first determined in 1965 using a large diffraction grating monochromator, which dispersed monochromatic UV light approximately 1.2 nm in bandwidth (Rauth, 1965). In 2005, the action spectrum was measured with a monochromator with a maximum bandwidth of 10 nm (Mamane-Gravetz, et al., 2005).

The MS2 action spectrum from the present study agrees with the other two, with a relative maximum near 260 nm and an increased sensitivity below 240 nm.

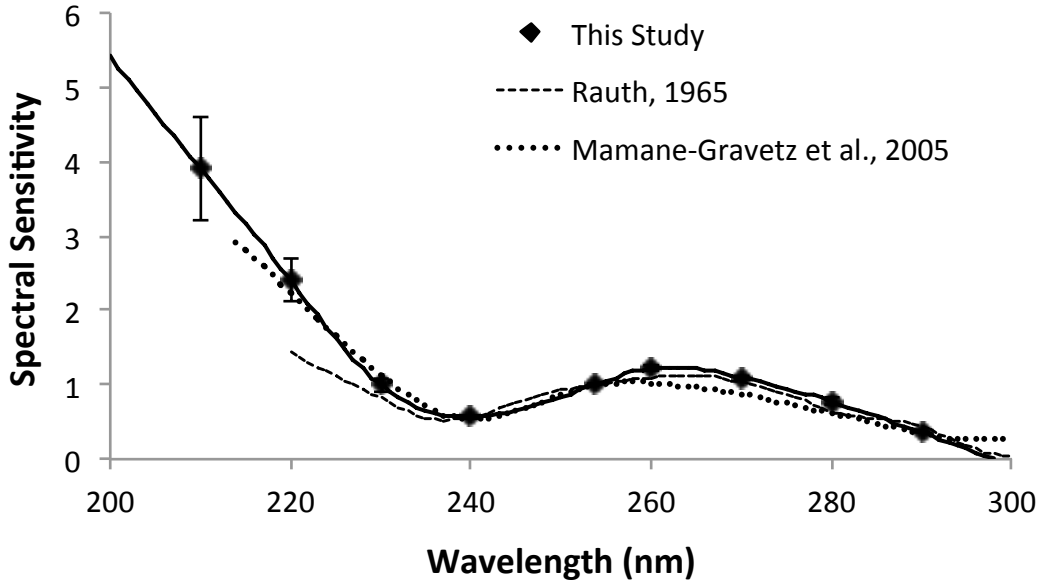

Figure 2.5. Relative spectral sensitivity of MS2 Coliphage to UV light as compared with previous studies (Rauth 1965), (Mamane-Gravetz, Linden et al. 2005). Error bars represent 1 standard deviation from the mean sensitivity value. n = 4 for 240 nm, 253.7 nm, 260 nm, and 270 nm and n = 3 for all other wavelengths tested.

Results from the collimated beam trials with T1UV, Q Beta, T7m, and T7 Coliphage are available in Appendix C. Table 2.2 contains the required UV doses for 1- to 4-log inactivation of each microorganism using the tunable laser emission of 253.7 nm. Also included are results for 2-log inactivation of each microorganism from exposure to low-pressure mercury vapor lamps, from this study and others, for comparison.

Table 2.2 – UV dose response results for coliphage irradiated with the tunable laser at 253.7 nm and LPUV as compared with previous studies.

Coliphage		*Tunable laser at 253.7 nm mJ/cm² (± 95 % CI)*					*LPUV mJ/cm² (± 95 % CI)*		
		n	***1-log***	***2-log***	***3-log***	***4-log***	***n***	***2-log this study***	***2-log past studies***
MS2	*ssRNA*	*6*	*16.0 (± 2.0)*	*33.6 (± 3.8)*	*53.4 (± 5.4)*	*77.6 (± 6.4)*	*4*	*32.8 (± 2.9)*	*32.8[a] 35.1[b]*
T1UV	*dsDNA*	*4*	*4.3 (± 0.4)*	*8.5 (± 0.9)*	*12.8 (± 1.3)*	*17.0 (± 1.8)*	*2*	*8.3 (± 0.1)*	*9.1[c]*
Q Beta	*ssRNA*	*1*	*10.8*	*22.0*	*33.8*	*46.2*	*1*	*19.8*	*23.9[c]*
T7	*dsDNA*	*1*	*1.6*	*3.6*	*6.6*	*--*	*1*	*3.8*	*--*
T7m	*dsDNA*	*2*	*1.7 (± 0.2)*	*3.8 (± 0.4)*	*6.3 (± 0.5)*	*10.6 (± 0.2)*	*2*	*3.4 (± 0.6)*	*--*

[a](Meng and Gerba, 1996); [b](Park et al., 2011); [c](Stefan et al., 2007)

The action spectra for T1UV, Q Beta, T7m and T7 Coliphage are given in Appendix C and shown in Figure 2.6 as compared with the MS2 Coliphage and *C. parvum* action spectra.

The **T1UV Coliphage** action spectrum agreed well with that developed previously using a medium-pressure mercury arc-lamp and bandpass filters (Stefan et al., 2007) at wavelengths above 240 nm, but differed below 240 nm. In both current and past studies, T1UV exhibited a relative peak sensitivity at 265 nm. Because T1UV Coliphage has similar inactivation kinetics at 253.7 nm as the UV dose-requirements for *Cryptosporidium parvum* and *Giardia lamblia*, specified by the LT2ESWTR, it is used as a surrogate organism for those pathogens for UV reactor validation. However, differences in the action spectra of T1UV and *C. parvum* at wavelengths below 240 nm and above 253.7 nm may require application of an action spectra correction factor.

The action spectrum for **Q Beta Coliphage** also agreed well with the spectrum developed previously using an MP UV lamp and bandpass filters (Stefan, 2007). In both studies, Q Beta Coliphage exhibited a peak relative sensitivity between 260 and 265 nm. Note that the action spectrum of Q Beta was very similar to that of MS2.

The action spectrum for **T7 Coliphage** matches that developed previously at 260 nm, where both exhibited a sensitivity of 1.3 (relative to 253.7 nm). However, the spectrum in the literature, obtained with a xenon lamp and a monochromator with 4 nm dispersion, decreased above 260 nm, whereas the T7 Coliphage action spectrum developed in this study increases to a relative peak at 270 nm (Ronto, 1992). **T7m Coliphage** was slightly less sensitive than T7 with a relative peak of 1.1 at 260 nm and a decreasing sensitivity at higher wavelengths.

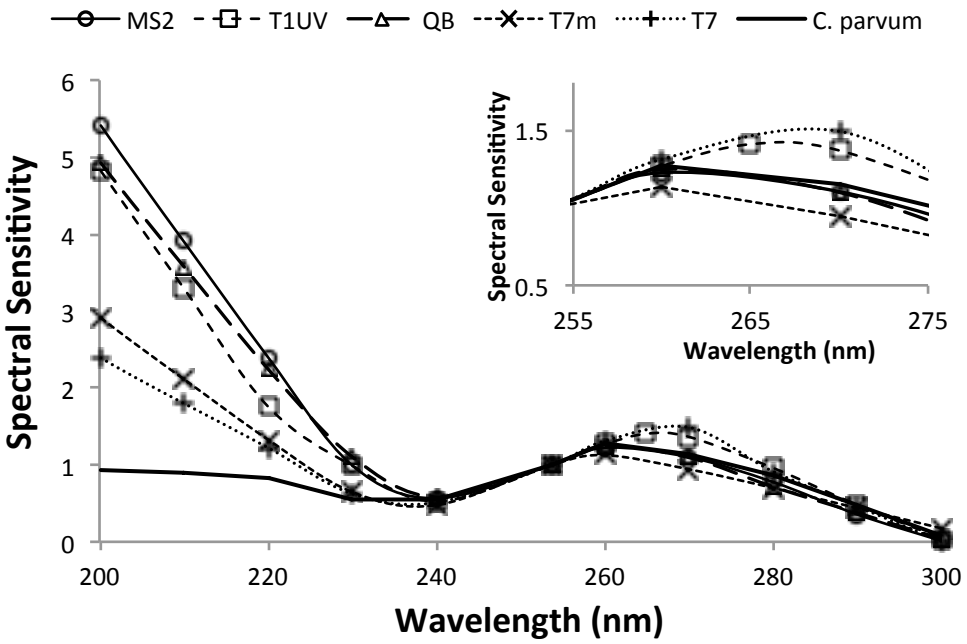

Figure 2.6. Relative spectral sensitivity of MS2, T1UV, Q Beta, T7m, and T7 Coliphage and C. parvum to UV light from the tunable laser. Note data points at 200 and 300 nm are extrapolated.

It was presumed that variations in the peaks of the coliphage action spectra were related, in part, to varying compositions of nucleotide base pairs; however this does not appear to be the case. Adenine has a peak UV absorption near 260 nm. Uracil and thymine peak near 259 nm and 266 nm respectively. Cytosine has a relative peak near 268 nm; and guanine has two peaks: one near 246 nm and one near 277 nm (Jagger, 1967). Given the right shifting of the relative peaks of UV absorbance of T7 and T1UV, it was assumed that they had a higher guanine-cytosine (GC)

content than the other phage. However, of the phage tested, MS2 had the highest GC content (52.1%), followed by T7m (49.9%), Q Beta (48.5%), and T7 (48.4%); the T1UV genome has not yet been sequenced.

The genome's stranded state could have an effect on the sensitivity of phage to UV light and the shape of the action spectra. In the work of Rauth (1965), single-stranded nucleic acid was more sensitive to UV light at 253.7 nm than double-stranded. In this work, that was not the case. MS2 and Q Beta Coliphage, both single-stranded RNA viruses, were more resistant to UV at 253.7 nm than T1UV, T7 or T7m. In Rauth's work, the single-stranded DNA and RNA viruses were more sensitive to the low wavelength light than double-stranded, possibly due to viral protein sensitizing the single-stranded nucleic acid. With the exception of T1UV (dsDNA), this work followed the same trend; MS2 and Q Beta were more sensitive at the lower wavelengths relative to their sensitivity at 253.7 nm, whereas T7m and T7 (both dsDNA phage) were less so. Protein-associated DNA has been shown to be more susceptible to UV-induced photoproducts than isolated DNA (Hegedus et al., 2003). Presumably, this would also be the case with protein-associated RNA.

Proteins also facilitate attachment to and infection of host cells. Amino acids, which compose proteins, absorb strongest below 220 nm (Saidel et al., 1952) and below 230 nm, the UV absorption of total proteins typically exceeds that of total DNA (Jagger, 1967). UV damage to phage proteins could affect attachment to the host cells and contribute to the loss of infectivity observed at those lower wavelengths.

2.3.3 Adenovirus

Dose response results for collimated beam tests with adenovirus 2 are shown in Figure 2.7. From the figure, it's evident that adenovirus 2 was significantly more sensitive at the lower

wavelengths of 210 - 230 nm and least sensitive at 290 nm. Results for the remaining wavelengths were very similar.

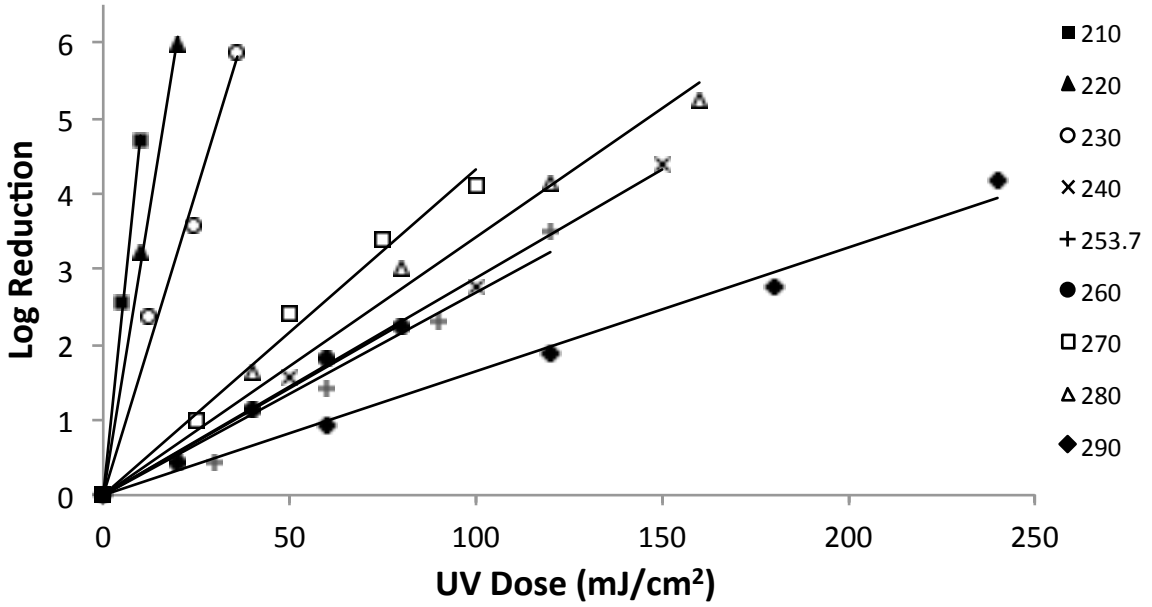

Figure 2.7 Dose response of adenovirus 2 to UV irradiation from a NIST tunable laser.

Adenovirus 2 exhibited a linear dose response. Inactivation rate coefficients at each wavelength were taken relative to the inactivation rate at 253.7 to determine its spectral sensitivity. The resulting spectrum is shown in Figure 2.8 with two different scales to give more definition at the higher wavelengths. The spectrum shown is a linear fit between the points. A cubic spline fit and 5th order polynomial fit both showed a possibly false minimum between 240 and 254 nm, with a spectral sensitivity as low as 0.5 relative to 254 nm. Otherwise, dose response data of adenovirus 2 demonstrated one peak at an apparent maximum of 270 nm and a valley at an apparent minimum between 240 and 260 nm. The spectrum agrees relatively well with a spectrum in the literature (Linden, 2007), which was obtained using a medium-pressure mercury vapor lamp and bandpass filters with a full width at half maximum (FWHM) of 10-12nm.

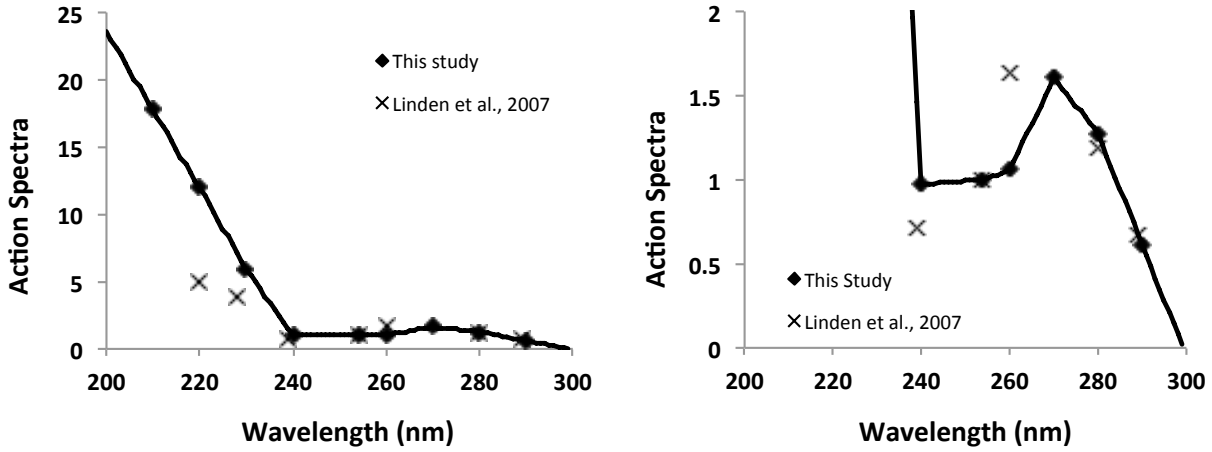

Figure 2.8 Adenovirus 2 action spectrum measured by NIST laser compared with the published data (Linden, 2007).

2.3.4 Bacillus pumilus

Results from the four collimated beam trials with *Bacillus pumilus* spores are given in Appendix C. When irradiated with LP UV light, 2-log inactivation resulted from a UV dose of 174.7 mJ/cm^2. This is a higher dose than that reported for 2-log LP UV inactivation of the same strain of *B. pumilus* spores (102 mJ/cm^2), cultivated under the same conditions (0.1 mmole/L $MnSO_4$) for a shorter incubation time (5 days versus 6 days). A longer incubation time would result in increased accumulation of manganese, which is required for efficient sporulation and would increase the UV resistance.

The action spectrum for *Bacillus pumilus* spore ASFUVRC (Figure 6, Table S1) was consistent with that developed previously (Rochelle et al., 2010) for spores cultivated with a slightly different method (1 mmole/L $MnSO_4$ for 5 days). Although the UV resistance between the studies varied, as described above, the spectra were very similar. *B. pumilus* spores exhibited a relative peak in the 260 to 265 nm range. At 220 nm, the spores were 8 to 9 times more sensitive than at 253.7 nm. The increased effectiveness of this low wavelength light is presumed to be due to damage to the small acid-soluble proteins (SASP). SASPs bind to the spore DNA and mitigate DNA damage by forming thymidyl-thymidine spore photoproducts upon UV

irradiation as opposed to thymine dimers (Setlow, 2006). These spore photoproducts can be repaired by the spore photoproduct (SP) lyase enzyme (Setlow, 2001). The 253.7 nm light wouldn't damage this SP repair mechanism; however, the lower UV wavelengths, near 220 nm, would damage the DNA binding proteins as well as the SP lyase enzyme that would otherwise repair the damage.

From 220 to 290 nm, the *Bacillus pumilus* spore action spectrum is very similar to the action spectrum for adenovirus 2 (Figure 2.9), which also was developed for this study and published previously (Beck et al., 2014). This similarity between *B. pumilus* spore and adenovirus 2 is consistent with other research (Rochelle et al., 2010). However, the relative spectral sensitivity of *B. pumilus* spore may decrease sharply below 220 nm given the absorbance of the spore homogenate (Rochelle et al., 2010). The adenovirus 2 action spectrum does not decrease sharply below 220 nm (Beck et al., 2014); adenovirus 2 is more sensitive than *B. pumilus* spore between 200 and 220 nm.

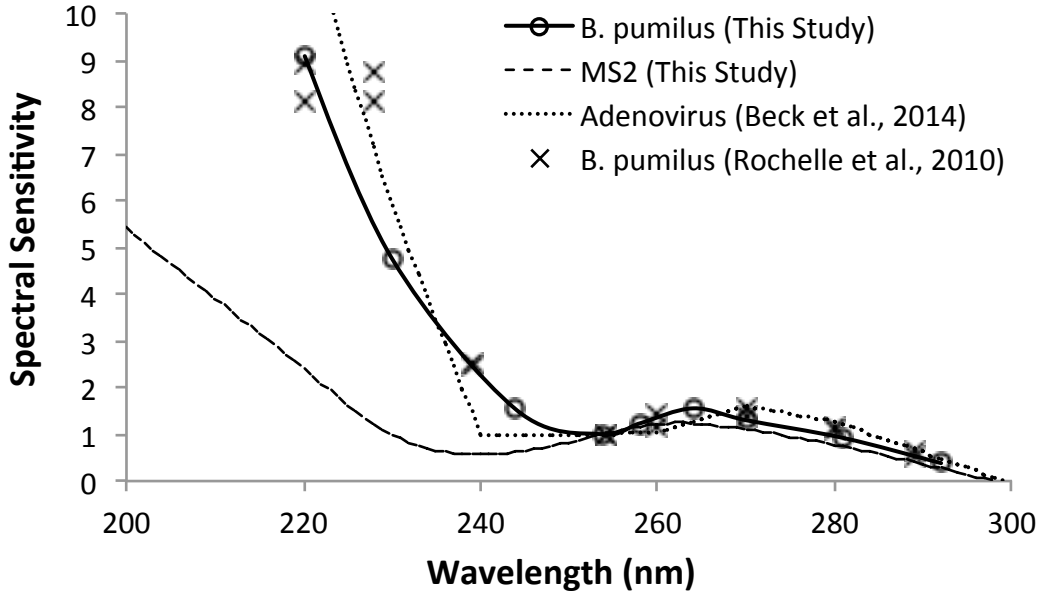

Figure 2.9. Relative spectral sensitivity of *Bacillus pumilus* to MP UV light with bandpass filters as compared with a *B. pumilus* spectrum from the literature (Rochelle et al., 2010) and the MS2 and adenovirus 2 (Beck et al. 2014) spectral sensitivity to UV light from the tunable laser.

2.3.5 Dose Calculations

Figure 2.10 shows a comparison of the dose response of MS2 to LP UV and MP UV light with the MP UV dose calculated two different ways. When the MP UV emission spectrum was weighted by the DNA absorption, the dose response of MS2 was significantly different than its response to LP UV light. Weighting the MP UV dose calculation by the action spectrum measured in this paper also yielded a statistically different response compared to the MS2 dose response to LP UV light. However, when the MP UV dose was weighted by the action spectrum measured in this paper, the dose response of MS2 was closer to its response to LP UV light, as illustrated in Figure 2.10. Differences in the two dose responses could be due to experimental variability. Nevertheless, this theoretical comparison shows that there is better agreement when weighting with action spectrum than with a DNA absorption curve. It also suggests that the low wavelengths, which are less prominent in a DNA weighted UV dose, play a role in MS2 coliphage inactivation.

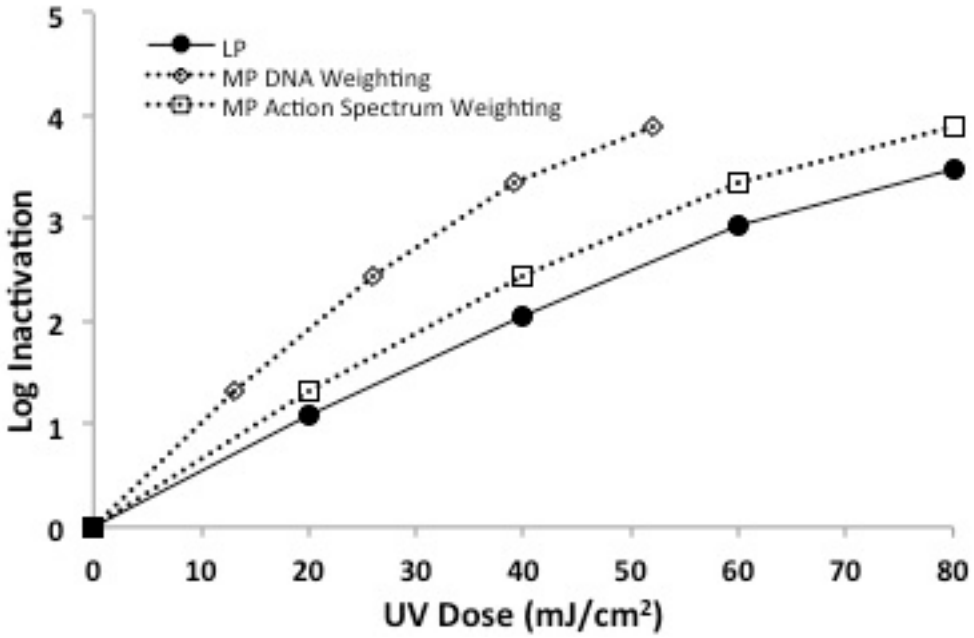

Figure 2.10 Dose response of MS2 coliphage to LP UV light and MP UV light with the MP UV dose determined by weighting the lamp emission with the DNA absorption or the MS2 action spectrum.

The action spectrum of adenovirus 2 was used to calculate UV dose delivered by a collimated beam apparatus equipped with a medium pressure lamp. Figure 2.11 shows the dose response of adenovirus 2 to LP UV and MP UV light. When the MP UV dose was calculated by weighting the MP UV emission spectrum by adenoviral DNA absorption, the LP UV and MP UV results differed considerably (ANCOVA $p = 1.5x10^{-4}$) and MP UV was significantly more effective than LP UV. However, when the MP UV dose was determined by weighting the MP UV emission by the adenovirus action spectrum, the dose response of adenovirus to MP UV light was similar to its response to LP UV light (ANCOVA $p = 0.592$). This theoretical comparison confirms that the adenovirus action spectrum, which was developed relative to 254 nm, is accurate. It also highlights the importance of the low wavelengths for adenovirus disinfection, which are not accounted for as strongly in dosimetry using DNA absorption weighting.

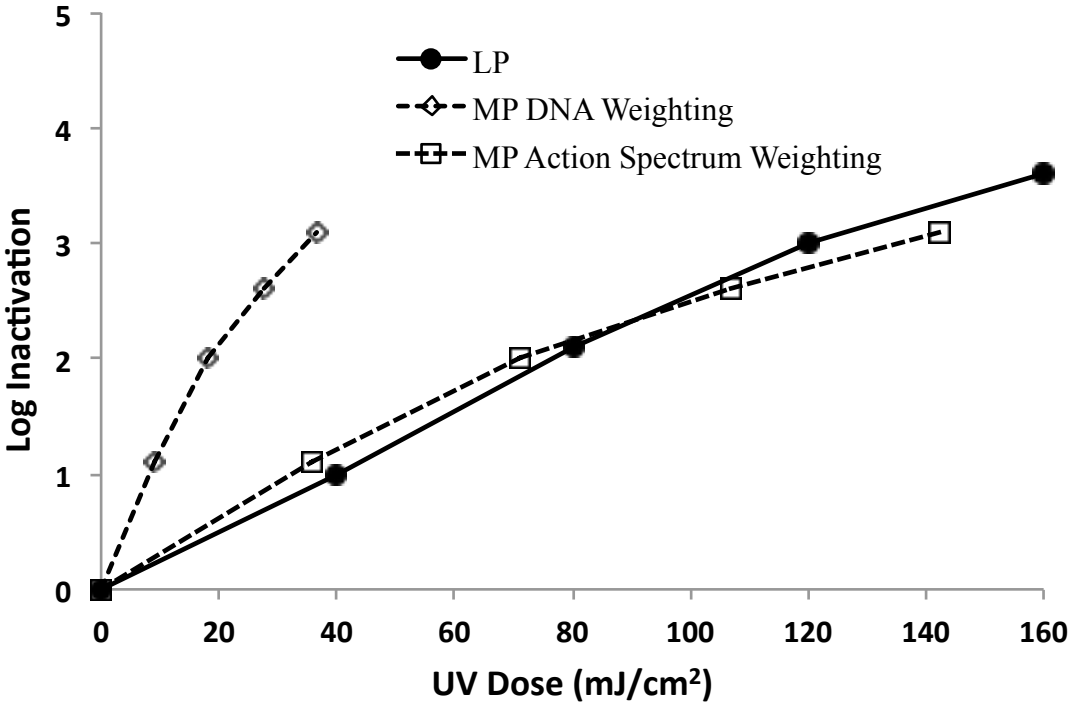

Figure 2.11 Dose response of adenovirus 2 to LP UV light and MP UV light with the MP UV dose determined by weighting the lamp emission with DNA absorption or the adenovirus action spectrum as measured by cell culture infectivity.

2.4. CONCLUSIONS

This research defined the UV action spectra of the pathogens *Cryptosporidium parvum* and adenovirus 2, and surrogates MS2, T1UV, Q Beta, T7, and T7m Coliphage, as well as *Bacillus pumilus*. These action spectra are essential for properly calculating action spectra correction factors for polychromatic UV systems such as during validation of MP UV systems and targeting UV sensors toward the most relevant wavelengths for dose monitoring.

Knowledge of action spectra for a suite of surrogates is important for matching appropriate challenge microorganisms to pathogens, and for improving UV dose monitoring. These action spectra can also serve as a guide for development of effective wavelength-targeted UV disinfection technologies such as excimer lamps, lasers and UV light emitting diodes (LEDs).

CHAPTER 3

COMPARISON OF LOSS OF INFECTIVITY AND RNA DAMAGE IN MS2 COLIPHAGE ACROSS GERMICIDAL UV WAVELENGTHS

This chapter discusses the wavelength-specific effects of UV light on the MS2 Coliphage genome for comparison with the previously published reduction in viral infectivity.

The work described in this chapter is being submitted for publication. (Beck, S.E., Rodriguez, R.A., Hawkins, M., Linden, K.G., Hargy, T.M., Larason, T.L. 2015. Comparison of Loss of Infectivity and RNA Damage in MS2 Coliphage Across Germicidal UV Wavelengths).

3.1 INTRODUCTION

Ultraviolet (UV) light is a common method of disinfection in the water treatment industry. UV light induces damage to the genomes of bacteria, protozoa, and viruses, breaking bonds and forming photodimeric lesions in the nucleic acids, DNA and RNA (Adams et al., 1986). These lesions prevent transcription and replication and ultimately lead to inactivation of the microorganism or virus (Wellinger and Thoma, 1996; Smith et al., 1998). Direct UV damage to nucleic acids occurs at the wavelengths absorbed by DNA and RNA, in the germicidal UV region between 200 and 300 nm (Besaratinia et al., 2011; Rosenstein, 1987). In this wavelength range, however, UV light also damages other cellular and viral components, causing, for example, photochemical reactions in proteins and enzymes (Jagger, 1967; Harm, 1980). For this reason, UV sources that emit polychromatic light, across the germicidal UV spectrum, are considered more effective at inactivating certain pathogens than sources that emit monochromatic light at 253.7 nm (Hijnen et al., 2006; Eischeid and Linden, 2011; Beck et al., 2014; Linden, K.G. et al., 2007). As polychromatic sources become more common, more research is being undertaken to understand the mechanisms of inactivation occurring in pathogens exposed to polychromatic UV light.

Male specific (MS2) coliphage is a single-stranded, RNA virus. It infects strains of *E. coli* that produce the F+ pili, which serves as the viral receptor. The virion consists of a short single-stranded RNA genome (3569 base pairs (bp)), surrounded by an icosahedral protein capsid, 27 nm in diameter (Valegard, K et al., 1997). MS2 is commonly used in the water treatment industry as a surrogate for enteroviruses because of its similar size, shape, and genome composition (Hijnen, 2006 et al.; Park et al., 2011). It serves as a biodosimeter for UV disinfection studies (Chen et al., 2009) and for UV reactor validation in North America (Park et

al., 2011; Mackey et al., 2002). For reactor validation, MS2 is also used as a surrogate for *Cryptosporidium* and adenovirus, despite the differences in UV sensitivity and spectral sensitivity between these microorganisms. Recent interest has grown about microbial and viral sensitivity to UV light below 240 nm. Light from some newer medium-pressure mercury vapor lamps is richer in wavelengths below 240 nm. Type 219 quartz sleeves, for example, which were commonly used in practice and are standard in European applications of MP UV, absorb most of the low wavelength light. Recently, however, vendors have been replacing the Type 219 sleeves with Type 214 sleeves, which transmit 51% of the light at 200 nm, or with synthetic quartz sleeves, which transmit 89% of the 200 nm light (Wright et al., 2009).

Using lamp systems with Type 214 and synthetic quartz sleeves with MS2 as a validation test organism for pathogens such as *Cryptosporidium,* can over-predict the UV dose delivered, raising a potential public health concern (Wright et al., 2009). Additionally, in adenovirus, it was shown that UV light below 240 nm induces damage to a viral component other than nucleic acid, contributing significantly to its loss of infectivity (Beck et al., 2014). Knowledge about inactivation at the lower UV wavelengths prompted the desire to understand more about the inactivation mechanisms involved at these wavelengths. It was particularly important to test MS2, given its importance to the water treatment industry and its use as a surrogate for both *Cryptosporidium* and adenovirus.

Many studies have compared the spectral sensitivity or action spectrum of an organism or virus to the absorbance of its DNA (Chen et al., 2009; Lakretz et al., 2010; Maezawa, 1984; Mamane-Gravetz et al., 2005; Stefan et al., 2007). Fewer studies have measured the damage that occurs within the DNA or RNA as a result of that absorbance of UV irradiation (Besaratinia et al., 2011; Beck et al., 2014). This research analyzes the wavelength-specific effects of UV light

on the bacteriophage MS2 by analyzing damage to its viral RNA. RNA differs from DNA in composition primarily with the presence of uracil nucleotides instead of thymine. UV irradiation forms several RNA photoproducts, primarily from adjacent pyrimidine nucleotides, such as uracil dimers (Miller and Plagemann, 1974; Smith, 1963), as well as RNA-protein crosslinks (Wurtmann and Wolin, 2009). These lesions, which inhibit RNA synthesis primarily through the formation of 6-4 photoproducts (Petit-Frere et al., 1996), also block the reverse transcriptase enzyme (Smith et al., 1998) from transcribing strands of complementary DNA, making the reverse transcription-qPCR assay suitable for detecting damage to the viral RNA. Past research used reverse transcription-quantitative PCR to confirm that, after exposure to UV light at 253.7 nm, the loss of viral infectivity of MS2 was due to genomic (Simonet and Gantzer, 2006). This research examined the role of other wavelengths emitted by polychromatic UV systems to determine whether that finding extended across the other wavelengths in the germicidal UV range.

3.2 MATERIALS AND METHODS

3.2.1 UV Irradiations

UV irradiations of MS2 coliphage suspended in phosphate buffered saline (PBS) were conducted using a NT242 series Ekspla tunable laser provided by the National Institute of Standards and Technology (NIST, Gaithersburg, MD). As described previously (Beck et al., 2014), the tunable laser provided precise UV irradiations (bandwidth < 0.1 nm) at wavelengths between 210 and 290 nm at approximate 10 nm intervals. At each wavelength, four collimated beam exposures were conducted to generate a dose response curve demonstrating up to 3-log inactivation of MS2 coliphage. Irradiance was measured at the water surface by a photodiode

detector (IRD SXUV 100, Opto Diode Corporation, Thousand Oaks, CA) and precision aperture (SK#030483-1073, Buckbee Mears, Cortland, NY), both supplied by NIST.

Average UV doses were determined as described in Bolton and Linden (2003), adjusting for reflection off the water surface, UV absorption (measured by a Spectronic Genesys 10uv™ spectrophotometer, Thermo Electron Scientific Instruments Corp, Madison, WI), depth of the water sample, and the non-uniform distribution of light across the sample surface. Quiescently stirred samples of 5 mL (0.6 cm depth) were irradiated in 3.5 cm diameter petri dishes. Laser irradiance varied with each wavelength examined between 11.4 μW/cm^2 and 221 μW/cm^2 and UV doses ranged from 4 mJ/cm^2 to 160 mJ/cm^2, depending on wavelength tested. Beam divergence was assumed to be negligible from the laser diffuser, but measured and accounted for in the mercury lamp irradiations described below.

Immediately after exposure, the irradiated samples were assayed for phage infectivity and the remainders were stored at -80 ºC. An aliquot of each sample from the -80 ºC freezer was shipped to University of Colorado Boulder for molecular analysis.

3.2.2 Reverse Transcription and Quantitative Polymerase Chain Reaction (RT-qPCR)

The two-step Reverse Transcription Quantitative Polymerase Chain Reaction (RT-qPCR) method detects UV damage in large fragments of the MS2 genome. It was adapted from Simonet and Gantzer (2006), using the primer set for Real-Time PCR described previously (Ogorzaly and Gantzer, 2003) (Table 3.1).

The viral RNA was extracted using a QIAmp Viral RNA kit (Qiagen, Valencia, CA) according to the manufacturer's instructions. The reverse transcription step consisted of 2 μL of reverse primer, 25 mM, for each 10 μL sample of extracted RNA. The sample was heated at 70°C for 5 min to anneal the primers and then rapidly chilled on ice for 1 min. The analysis was

conducted with two separate reverse primers to analyze the MS2 dose response resulting in two different lengths of cDNA produced. Reverse primer #3424 and #2440 given in Table 3.1 were used to analyze fragments of 2169 and 1185 base pairs, respectively.

The samples described above were combined with a reverse transcription mix containing 1 μL of Improm II reverse transcription enzyme (200 units/μL, Promega, Madison, WI), 5 μL of its 5X reaction buffer, 3 μL of 25 mM $MgCl_2$ (Promega), 1 μL of dNTP nucleotide mix (10 mM, Fermentas, Thermo Fischer Scientific, Waltham, MA), 0.5 μL of ribonuclease inhibitor (RNasin, 20–40u/µl, Promega), and nuclease free water for a total volume of 25 μL per sample. The mixture was heated to 42°C for 60 min for complementary cDNA transcription followed by chilling on ice.

Quantitative Polymerase Chain Reaction (qPCR) was used to quantify the RT products. A 2 μL volume of the cDNA was combined with a reaction mix containing 12.5 μL of QuantiTect Probe PCR Master Mix (Qiagen), 0.5 μL of 7.5 mM forward and reverse primer, 0.5 μL of 7.5 mM probe, and nuclease-free water for a total reaction volume of 25 μL. The primers and probes, synthesized by Integrated DNA Technologies (Coralville, IA), are given in Table 3.1. The qPCR assays were performed in duplicate using a MJ MiniOpticon™ Real-Time PCR machine (Bio-Rad, Hercules, CA). In the thermocycle program, the samples were heated to 94°C for 10 min before repeating 50x a cycle of 10 s at 94°C to denature the DNA strands, followed by 1 min at 60°C to anneal the primer and probe and synthesize new DNA. The fluorescence signal was read at the end of each cycle.

Table 3.1. Primers and probe used for reverse transcription and quantitative PCR.

Purpose	Sequence	Genome Region	Amplicon Size (bp)*	Reference
Reverse Transcription				
Reverse Primer 3424	TCT TTC GAG CAC ACC CAC C	3405-3424	2,169	a
Reverse Primer 2440	TCT ATA CCA ACG GAT TTG AGC C	2418-2440	1,185	This paper
quantitative PCR				
Forward Primer	TCG ATG GTC CAT ACC TTA GAT GC	1255-1277		b
Reverse Primer	ACC CCG TTA GCG AAG TTG CT	1404-1423		b
Probe	5'6-FAM/TC TCG TCG ACA ATG GC/ 3' BHQ-2	1362-1375		b

* Size of the RNA analyzed using this reverse primer for reverse transcription and in reference to the site used for the real-time PCR assay.

a. Ogorzaly and Gantzer, 2003

b. Simonet and Gantzer, 2006

3.2.3 UV Absorption of RNA

Viral RNA from the MS2 coliphage stock (10^8 pfu/mL) was extracted as described above. The UV absorption was determined from 220 nm to 300 nm using a UV spectrophotometer (Nano Drop 1000, Thermo Fischer Scientific, Wilmington, DE) to compare with the spectral sensitivity of RNA measured with RT-qPCR. The ratio of UV absorption at 260 nm and 280 nm was 2.55, confirming the purity of the RNA.

3.2.4 Statistical Analysis

For the RT-qPCR analyses, serial, 10-fold dilution curves were developed to correlate the PCR cross threshold value (Ct) with MS2 concentration and measure changes in the log concentration of gene copies for each fragment. The following linear equation was used for calculating $\log_{10}$ copies when performing RT-qPCR with the 1185-base pair amplicon from the MS2 stock.

$$\log_{10} \text{copies} = -(0.3244 \times Ct) + 6.9639. \qquad r^2 = 0.996 \qquad [1]$$

For the 2169-base pair fragment, the following stock dilution curve was used:

$\log_{10}$ copies = -(0.3145 x Ct) + 12.958 $\quad r^2 = 0.981$ [2]

The results, which reflected log reduction for each amplicon, must be adjusted to apply to the whole genome. Pecson et al. (2011) discusses methods for relating genome damage, measured by qPCR, to loss of MS2 infectivity following exposure to UV light. They introduced a theoretical framework to adjust the results using the ratio of genome size to amplicon size. However, different regions of the MS2 genome have different susceptibilities to UV damage (Pecson et al., 2011); therefore, the results were adjusted using another method proposed in the same publication: by calibrating the qPCR results to empirical infectivity measurements at 253.7 nm (Pecson et al., 2011).

A calibration factor, c, was calculated as the ratio of the lesion rate in each amplicon relative to the lesion rate in the whole genome, as described previously and given in equation 3.

$$\boldsymbol{c} = \frac{\ln\left(\boldsymbol{Proportion}(\boldsymbol{undamaged\ genome})\right)}{\ln\left(\boldsymbol{Proportion}(\boldsymbol{undamaged\ amplicon})\right)} \quad [3]$$

The factor, c, was determined by dividing the ln of damage to the viral genome, estimated for a given dose using the linear regression from plaque assay infectivity results, by the ln of damage to the genome from RT-qPCR. Ratios from each point of the dose response curve at 253.7 nm were averaged to determine the calibration factor for data collected with that amplicon. The calibration factors determined with the data at 253.7 nm were used for extrapolating RT-qPCR data from each fragment to the whole genome at all other wavelengths tested. The 253.7 nm results were used as the point of comparison because action spectra were taken relative to 253.7 nm.

This analysis assumes single-hit inactivation, in other words, that a single lesion leads to the inactivation of the virus and prevents PCR amplification, an assumption that has been used previously for MS2 (Simonet and Gantzer, 2006; Pecson 2011).

The RT-qPCR results displayed first order kinetics and no statistically significant curvature. RNA damage was compared to the loss of infectivity results reported previously (Beck et al., 2015), using analysis of covariance (ANCOVA).

The kinetic constant for the relationship between log (N) and UV dose was obtained from regression analysis. The log reduction of MS2 was calculated as

$$\text{Log reduction} = \log(N_0) - \log(N) \quad [4]$$

where log (N_0) was the log concentration of the unexposed sample obtained from the regression analysis and log (N) is the measured log concentration.

To illustrate the action spectra or spectral sensitivity of the MS2 RNA to UV light, the UV dose response results at each wavelength tested were mapped to the UV dose response at the reference wavelength of 253.7 nm to obtain a scalar reference value (Sutherland, 2002). For mapping, the dose response data obtained using RT-qPCR with both fragment sizes was fit using a second order polynomial equation; mapping constants were defined using:

$$\log I_\lambda = A \times (\alpha_\lambda \times D_\lambda) + B \times (\alpha_\lambda \times D_\lambda)^2 \quad [5]$$

where logIλ is the predicted log inactivation, Dλ is the UV dose, λ is the wavelength associated with logIλ and Dλ, αλ is the action spectrum constant at wavelength λ, and A and B are constants defining the UV dose-response at 253.7 nm. The values of the action spectra constants were identified as the constants that maximized the R-squared value of the relation between measured logI λ and Dλ. The full action spectra were then generated by fitting the averaged values at the wavelength intervals tested with a cubic spline.

3.3 RESULTS AND DISCUSSION

The qPCR results were adjusted to reflect UV damage to the entire genome using Eq. 3, as described above. The calibration factor, c, was 2.47 for the 1185 base pair amplicon and 0.98 for the 2169 base pair amplicon.

Inactivation of MS2 using the NIST laser at 253.7 nm is presented in Figure 3.1. The inactivation rate was 0.050 ($p = 3.6 \times 10^{-7}$) when measured using plaque assay infectivity. The RT-qPCR data points at 253.7 nm calibrated to this infectivity data, yielded inactivation rates of 0.046 ($p = 6.2 \times 10^{-4}$) for data collected with the 1185 bp amplicon and 0.058 ($p = 1.7 \times 10^{-3}$) for data from the 2169 bp amplicon.

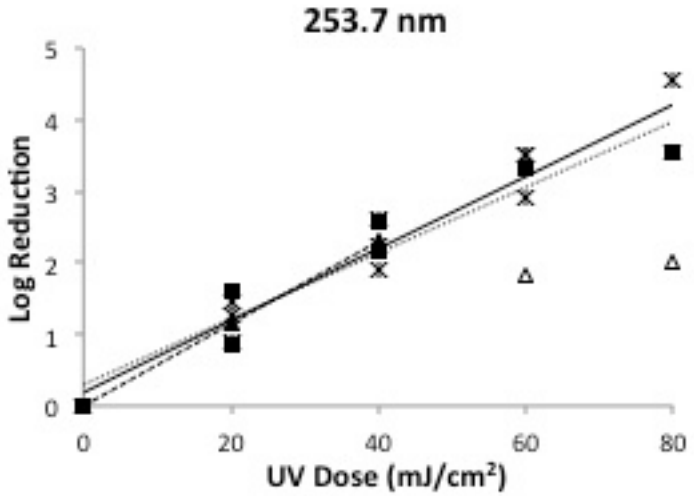

Figure 3.1. Dose response of MS2 coliphage exposed to UV light from a tunable laser at 253.7 nm as measured by RT-qPCR using two fragment lengths, 1185 base pairs (squares) and 2169 base pairs (triangles), after calibration with plaque assay infectivity (asterisks) (Beck et al., 2015, Chapter2). Open symbols were not used in data analysis.

MS2 coliphage consists of a protein capsid surrounding a single-stranded RNA core. Since the coliphage is composed of two primary components: RNA and proteins, loss of infectivity at a given wavelength must be due to damage to the RNA, damage to the viral proteins, or both. Inactivation of MS2 and its RNA by the NIST laser at 210 nm, 220 nm, 230 nm, 240 nm, 260 nm, 270 nm, 280 nm, and 290 nm as a function of UV dose is given in Figure

3.2. The results shown represent damage to the full genome, determined with RT-qPCR from the two different amplicons as compared with the dose response of the viral infectivity, published previously (Beck et al., 2015). The results indicate that across the germicidal UV spectrum, from 210 nm to 290 nm, the rate of damage to the MS2 genome observed closely mirrored the loss of viral infectivity.

Dose response results of damage to the MS2 viral genome measured using RT-qPCR with the 1185 base pair amplicon best correlated to the dose response of viral infectivity; these results are presented in Table 3.2. According to the ANCOVA analysis, the susceptibility of the MS2 genome to UV light was statistically similar to the susceptibility of the virus to UV light emitted at 210 nm, 220 nm, 253.7 nm, 260 nm, 270 nm, 280 nm, and 290 nm. At 230 nm and 240 nm, dose response results representing RNA damage and viral infectivity were found with ANCOVA to be statistically different, in part because both data sets had small analytical errors at those wavelengths. However, 95% confidence intervals created for both data sets overlapped at all wavelengths tested. The statistical similarity between loss of viral infectivity and genome damage at both the low UV wavelengths (< 240 nm) and the higher UV wavelengths (> 240 nm) suggests that genome damage is the primary mechanism responsible in UV inactivation for MS2 across the germicidal UV spectrum.

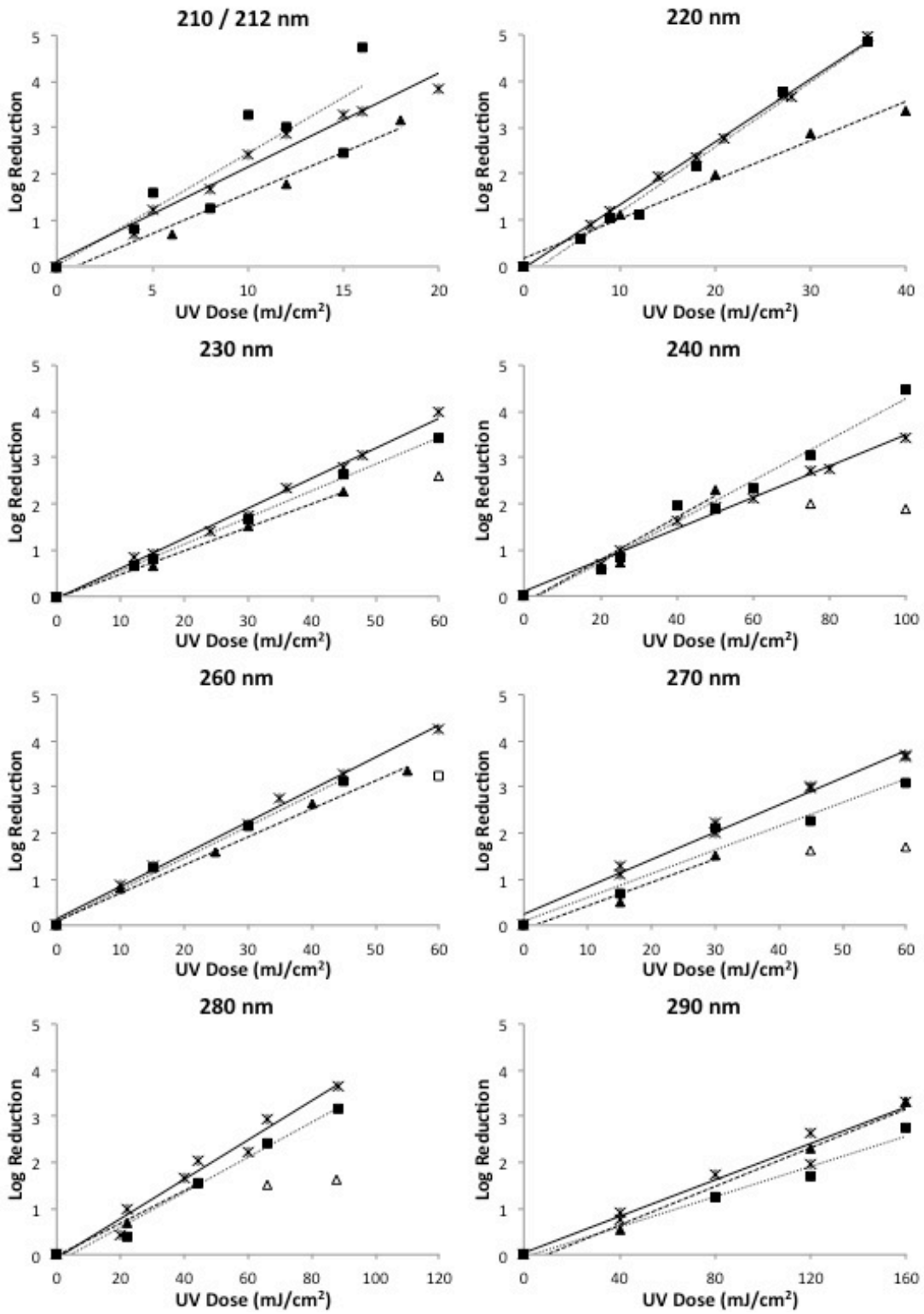

Figure 3.2. Dose response of MS2 coliphage to monochromatic UV light from a tunable laser as measured by RT-qPCR using two fragment lengths, 1185 base pairs (squares) and 2169 base pairs (triangles), for comparison with plaque assay infectivity (asterisks) (Beck et al., 2015). Open symbols were not used in data analysis. Note different x-axes values.

Table 3.2: Wavelength-Specific Inactivation Rate Constants (in cm^2/mJ), Comparing Genome Damage (1185 bp amplicon) to Loss of Viral Infectivity for MS2 Coliphage.

Wavelength (nm)	RNA Damage 1185 bp fragment k (±95% CI; p-value)	Infectivity[a] k (±95% CI; p-value)	ANCOVA[b] p-value
210	0.243 (0.1257; 3.2×10^{-3})	0.203 (0.0297; 8.3×10^{-7})	0.421
220	0.141 (0.0180; 5.7×10^{-6})	0.136 (0.0055; 1.1×10^{-10})	0.502
230	0.058 (0.0022; 2.0×10^{-7})	0.065 (0.0044; 4.2×10^{-9})	0.009
240	0.044 (0.0063; 2.5×10^{-6})	0.034 (0.0028; 1.4×10^{-8})	0.002
253.7	0.046 (0.0155; 6.2×10^{-4})	0.050 (0.0095; 3.6×10^{-7})	0.557
260	0.069 (0.0149; 2.6×10^{-3})	0.070 (0.0059; 7.0×10^{-7})	0.739
270	0.051 (0.0216; 4.8×10^{-3})	0.059 (0.0065; 1.2×10^{-7})	0.233
280	0.038 (0.0088; 8.5×10^{-4})	0.043 (0.0075; 8.7×10^{-6})	0.300
290	0.016 (0.0071; 9.9×10^{-3})	0.020 (0.0043; 7.6×10^{-5})	0.214

a. Beck et al., 2015
b. ANCOVA, statistical significance was defined as $p < 0.05$.

Table 3.3 compares the dose response data for damage to the MS2 genome measured with the longer, 2169 base pair, amplicon, with the infectivity results. The results correlated well with infectivity; however, the longer amplicon was unable to detect damage at high UV doses. PCR is limited because the amplicons are susceptible to saturation from multiple photon hits. One lesion prevents the DNA polymerase from carrying through a reaction to transcribe a strand of complementary DNA. PCR only detects the reduction in amplifiable genome fragments; therefore, multiple damage sites are measured as a single point of damage, the log reduction will not increase, and tailing occurs. In some cases, the assay detection limit for RT-qPCR with the 2169 amplicon was 1.5-log reduction. In those cases, the UV dose response curve plateaued.

Those points, which are represented with open symbols in Figure 3.2, were omitted from the regression analysis; only the linear points were included in calculating the inactivation rate. Through ANCOVA, it was shown that the susceptibility of the MS2 genome to UV light was not statistically different to the susceptibility of the MS2 virus at 210 nm, 253.7 nm, 270 nm, 280 nm, and 290 nm. At 220 nm, 230 nm, 240 nm, and 260 nm, 95% confidence intervals from both datasets overlapped.

Table 3.3: Wavelength-Specific Inactivation Rate Constants (in cm^2/mJ), Comparing Genome Damage (2169 bp amplicon) to Loss of Viral Infectivity for MS2 Coliphage.

Wavelength (nm)	RNA Damage 2169 fragment k (±95% CI; p-value)	Infectivity[a] k (±95% CI; p-value)	ANCOVA[b] p-value
210	0.176 (0.0780; 0.0104)	0.203 (0.0297; 8.3×10^{-7})	0.232
220	0.085 (0.0203; 9.3×10^{-4})	0.136 (0.0055; 1.1×10^{-10})	4.0×10^{-6}
230	0.051 (0.0064; 8.7×10^{-4})	0.065 (0.0044; 4.2×10^{-9})	1.7×10^{-4}
240	0.046 (0.1278; 0.136)	0.034 (0.0028; 1.4×10^{-8})	0.035
253.7	0.058 (0.0020; 1.7×10^{-3})	0.050 (0.0095; 3.6×10^{-7})	0.515
260	0.061 (0.0079; 1.5×10^{-4})	0.070 (0.0059; 7.0×10^{-7})	0.028
270	0.051 (0.1243; 0.122)	0.059 (0.0065; 1.2×10^{-7})	0.349
280	0.035 (0.0233; 0.033)	0.043 (0.0075; 8.7×10^{-6})	0.353
290	0.021 (0.0052; 1.0×10^{-3})	0.020 (0.0043; 7.6×10^{-5})	0.624

a. Beck et al., 2015
b. ANCOVA, statistical significance was defined as $p < 0.05$.

More important than a comparison of the dose response at each wavelength is a comparison of the spectral sensitivity of MS2 and its genome. The spectral sensitivity or action spectrum of MS2 and the viral genome relative to their sensitivity at 253.7 nm are given in Figure 3.3. The MS2 action spectrum from plaque assay infectivity (Beck et al., 2015) exhibited

a relative peak at 260 nm, decreased with UV wavelength down to 240 nm and then increased below 240 nm. This same trend was observed for the spectral sensitivity of the MS2 genome. When measured with the shorter, 1185 bp amplicon, and the longer, 2169 bp amplicon, the MS2 genome sensitivity also exhibited a relative peak near 260 nm, decreased to 240 nm, and then increased below 240 nm.

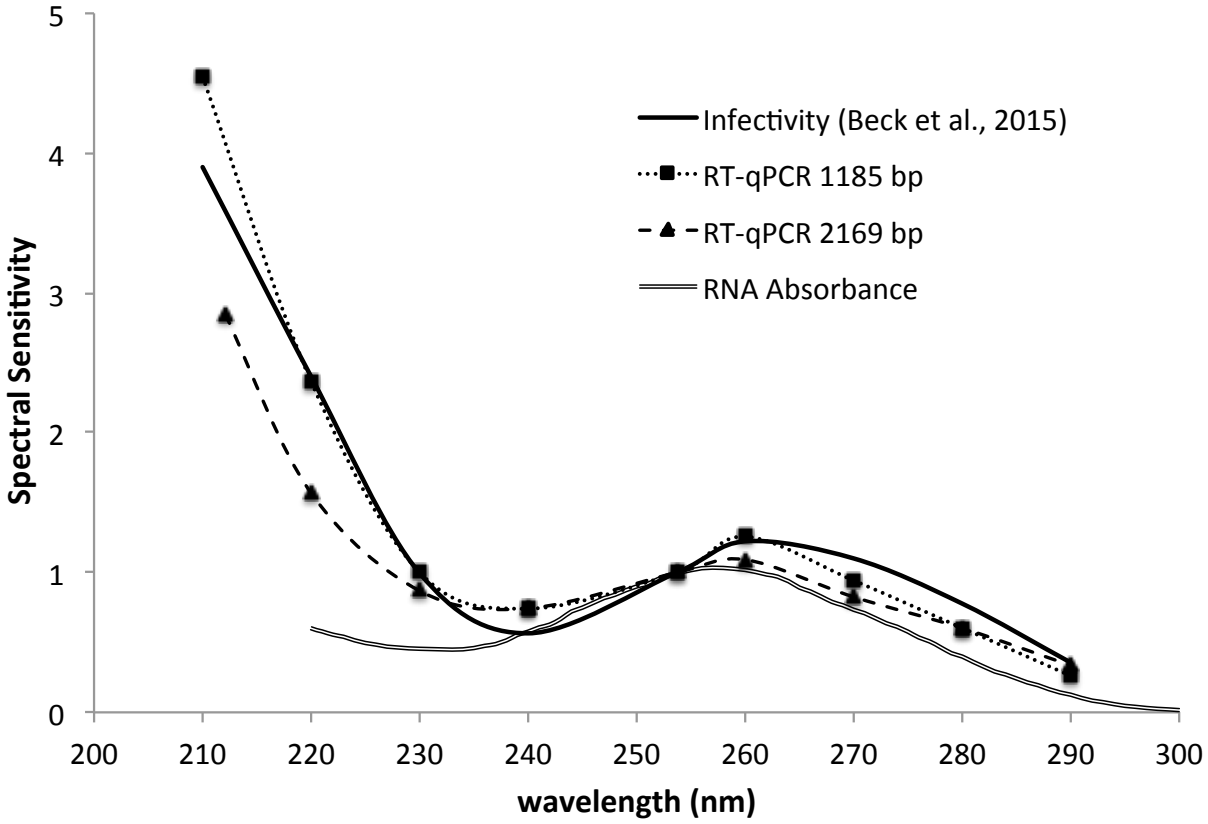

Figure 3.3. Action spectrum of MS2 Coliphage (Beck et al., 2015, Chapter 2) and its nucleic acid (RNA damage) between 210 nm and 290 nm as compared to the UV absorption of MS2 RNA measured.

Whereas the spectral sensitivity of adenovirus diverged from the sensitivity of its genome at wavelengths below 240 nm (Beck et al., 2014), the MS2 action spectrum did not. For MS2 coliphage, damage to the nucleic acid is therefore considered the primary cause for loss of infectivity across the germicidal UV spectrum. Although UV light causes photoproducts or structural modifications in capsid proteins (Miller and Plagemann, 1974) and genome-mediated

protein damage has been demonstrated in MS2 (Wigginton et al., 2012), that damage does not appear to contribute significantly to a loss of infectivity of MS2. MS2 infects by attaching its maturation protein to the viral receptor on the F pilus of *E. coli*. The maturation protein exists as a single copy, relative to the 180 copies of coat protein (Valegard et al., 1997). Adenovirus, in contrast, has a more complicated protein structure. It consists of 13 structural proteins, which play an integral role in the infection process (Seth, 1999), initially via the fiber proteins, which protrude from 12 vertices and are responsible for contact with the host cell receptor (Russell, 2009).

It is interesting to note, however, that the spectral sensitivity of RNA damage diverges from the RNA absorbance at wavelengths below 240 nm. One explanation is that proteins absorbing at those wavelengths could be transferring the UV energy to the RNA. A study on protein association of DNA showed that protein-associated DNA is more susceptible to UV damage than isolated DNA (Hegedus et al., 2003). UV-induced RNA-protein crosslinking has been described in the scientific literature (Wurtnmann and Wolin, 2009). For MS2 coliphage, the most abundant protein, the coat protein, binds a stem-loop structure in the viral RNA (Valegard, 1997; Peabody, 1993) and the maturation protein is bound to the RNA at two sites, at the 5' end and at the 3' end (Shiba and Suzuki, 1981). At these sites, UV energy could induce a covalent crosslink between the protein and the RNA or the proteins could transfer the UV energy directly to the RNA, forming a RNA photoproduct. Wigginton et al. (2012) showed that the presence of viral RNA contributed to site-specific protein damage following UV radiation at 253.7 nm, suggesting an energy transfer from RNA to viral proteins. At wavelengths below 240 nm, perhaps the energy transfer would occur in the opposite direction; energy absorbed by proteins could be generating site-specific RNA damage, resulting in a loss of viral infectivity. Regardless

of the pathways involved, this research shows that inactivation of the RNA bacteriophage MS2 is dominated by damage to the nucleic acids throughout the germicidal wavelength range.

CHAPTER 4

WAVELENGTH DEPENDENT UV INACTIVATION AND DNA DAMAGE OF ADENOVIRUS AS MEASURED BY CELL CULTURE INFECTIVITY AND LONG RANGE QUANTITATIVE PCR

This chapter discusses the wavelength-specific effects of UV light on adenovirus type 2 by analyzing in parallel the reduction in viral infectivity and damage to the viral genome. The research goal was to understand why polychromatic UV light is more effective at inactivating this resistant pathogen than monochromatic UV light sources emitting at 254 nm. The research showed that below 240 nm, reduction of viral infectivity was significantly greater than the reduction of DNA amplification, suggesting that UV damage to a viral component other than DNA contributed to the loss of infectivity at those wavelengths.

The work described in this chapter has been published. (Beck, S.E., Rodriguez, R.A., Linden, K.G., Hargy, T.M., Larason, T.L., Wright, H.B. 2014. Wavelength-Dependent UV Inactivation of Adenovirus as Measured by Cell Culture Infectivity and Quantitative PCR. *Environ. Sci. Technol*. 48 (1), 591-8).

4.1 INTRODUCTION

Adenovirus is an enteric virus associated with respiratory and gastrointestinal illness in humans, most virulently affecting immunocompromised individuals. It has been associated with waterborne disease outbreaks (Kukkula et al., 1997) and has been detected in treated drinking water (Lee and Kim, 2002). As a known public health risk subject to future regulations, it is one of few microbial contaminants listed on the US Environmental Protection Agency's Contaminant Candidate List (CCL 3). Relative to other pathogens, adenovirus demonstrates strong resistance to UV light. When disinfecting with monochromatic, low-pressure (LP) ultraviolet (UV) light at 253.7 nm, 4-log inactivation requires a dose between 120 mJ/cm^2 to 170 mJ/cm^2, four times greater than that required for inactivating other enteric viruses, including echovirus, coxsackievirus, and poliovirus (Gerba et al., 2002; Linden et al., 2009; Shin et al., 2005; Thompson, et al., 2003). Given this resistance, adenovirus governs the US Environmental Protection Agency regulations for virus inactivation. The Long-Term 2 Enhanced Surface Water Treatment Rule (LT2), which requires 4-log inactivation of viruses, stipulates a minimum UV dose of 186 mJ/cm^2, based on statistical analysis of empirical results of adenovirus inactivation by LP UV light (USEPA, 2003; USEPA, 2006a; Yates et al., 2006). For groundwater treatment, the US EPA Groundwater Rule declared that UV is not a sufficient standalone treatment for viruses unless adequate inactivation is demonstrated through a field-scale challenge test (USEPA, 2006b).

Although adenovirus has demonstrated a resistance to LP UV light, polychromatic UV light from medium-pressure (MP) mercury vapor lamps is two to four times more effective (Linden et al., 2009; Linden et al., 2007). A MP UV dose of 40 mJ/cm^2 to 80 mJ/cm^2 is necessary for 4-log inactivation, where germicidal dose is calculated using the UV absorbance of

DNA (Linden and Darby, 1997). The high resistance of adenovirus to LP UV could be the result of nucleic acid damage being repaired during infectivity assays. When adenovirus was assayed using a cell line with limited DNA repair capability (XP17BE) the doses for 4-log inactivation using LP and MP UV lamps were as low as 57 mJ/cm^2 and 42 mJ/cm^2, respectively (Guo et al., 2010). Although more effective than LP UV light, the mechanisms behind the enhanced efficacy of MP UV light have not been well characterized. UV light is generally subdivided into UVC (100 nm to 280 nm), UVB (280 nm to 315 nm) and UVA (315 nm to 400 nm). The region between 200 nm and 300 nm is directly absorbed by DNA and therefore considered the germicidal UV region. Kuluncsics et al. found that UVC is 10^5 times more effective than UVA at inducing cyclobutane pyrimidine dimers (CPDs), the dominant form of UV-induced DNA damage (1999). Besaratinia et al. determined that the formation of CPDs and other photodimeric lesions is dependent upon wavelength (2011). In both previous studies, the DNA was isolated prior to exposure to UV light, limiting the potential insights into interactions between DNA and proteins that could occur in vivo with a water treatment application.

Measuring nucleic acid damage gives insight into the mechanisms involved in UV inactivation. DNA damaged by UV light inhibits Taq DNA polymerase progression through the template DNA strand (Van Houten et al., 2000). The longer the DNA strand, the higher the possibility of the polymerase to encounter damage. Therefore, Polymerase Chain Reaction (PCR) assays with the ability to amplify long fragments of DNA allow for greater sensitivity by enabling the detection of biologically relevant DNA damage (Cheng et al., 1995; Ayala-Torres et al., 2000). When assaying equal amounts of DNA using PCR, a reduction in amplification corresponds to DNA damage; the method is therefore a useful tool for quantifying damage to the viral genome (Eischeid et al., 2009). A long-range quantitative PCR method was adapted for

adenovirus and proposed as an alternative to cell culture for detecting adenovirus inactivation by UV light.20 When direct DNA damage is measured, LP and MP UV light are equally effective at damaging the adenovirus genome despite their difference in efficacy at inactivating the virus as determined by cell culture assays (Eischeid et al., 2009).

The goal of this study was to provide more insight into the fundamental mechanisms of adenovirus inactivation from polychromatic germicidal UV light by determining the impact of specific UV wavelengths in inactivating adenovirus, particularly at lower wavelengths (< 240 nm). In this study, a tunable laser from the National Institute of Standards and Technology was used to isolate monochromatic wavelengths from 210 nm to 290 nm. At each wavelength, the viral infectivity and genome damage were analyzed to determine the spectral sensitivity of adenovirus and its genome and enhance our understanding of the link between UV-induced nucleic acid damage and loss of infectivity.

To our knowledge, this is the first study analyzing the spectral sensitivity of DNA across the deep UVC spectrum, applying novel and precise irradiation techniques via a tunable laser for wavelength-specific UV inactivation in combination with analysis of spectral sensitivity of adenovirus on the molecular level. Understanding the wavelength-specific effects of UV light on nucleic acids can help us understand the effect of low-wavelength (< 240 nm) UV light, which could have a significant impact on MP UV system validation and potentially encourage the use of MP UV systems for virus inactivation in groundwater. The research can also assist with the design of novel, tailored-wavelength UV disinfection technologies, combining, for example, light emitting diodes (LEDs) with specific output spectra.

4.2 MATERIALS AND METHODS

4.2.1 UV Irradiations

UV irradiations of adenovirus suspended in phosphate buffered saline (PBS) were conducted using a NT242 series Ekspla tunable laser provided by the National Institute of Standards and Technology (NIST, Gaithersburg, MD), described in Chapter 2. At wavelengths between 210 and 290 nm in 10 nm intervals, four collimated beam exposures were conducted to generate a dose response curve up to 3-log inactivation. Irradiance was measured at the water surface by a photodiode detector (IRD SXUV 100, Opto Diode Corporation, Thousand Oaks, CA) and precision aperture (SK#030483-1073, Buckbee Mears, Cortland, NY), both supplied by NIST. Average UV doses were determined as described in Bolton and Linden (2003), adjusting for reflection off the water surface, UV absorption (measured by a Spectronic Genesys 10uv™ spectrophotometer, Thermo Electron Scientific Instruments Corp, Madison, WI), depth of the water sample, as well as the non-uniform distribution of light across the sample surface. Beam divergence was assumed to be negligible from the laser diffuser, but measured and accounted for in the mercury lamp irradiations. Quiescently stirred samples of 5 mL (0.6 cm depth) were irradiated in 3.5 cm diameter petri dishes. UV doses ranged from 8 mJ/cm^2 to 160 mJ/cm^2, depending on the wavelength. Laser irradiance varied across wavelengths between 10 μW/cm^2 and 300 μW/cm^2. For DNA-based analysis, two independent experiments were conducted to collect a replicate set of samples at each wavelength. Immediately after exposure and prior to the plaque assay, the irradiated samples were stored at -80 ^{o}C. An aliquot of each sample from the -80 ^{o}C freezer was also shipped to University of Colorado Boulder for molecular DNA-based analysis.

Collimated beam exposures were also conducted to compare the adenovirus dose response to LP UV light. UV doses with the low-pressure mercury vapor lamp (G12T6L, Atlantic Ultraviolet, Hauppauge, NY) were determined as described above, following the Bolton and Linden (2003) protocol.

4.2.2 Cell and Virus Propagation and Enumeration

Adenovirus 2 (ATCC #VR-846) was propagated in A549 human lung carcinoma cells (ATCC #CCL-185). For UV-irradiated samples containing adenovirus, a Most Probable Number (MPN) assay was performed (USEPA, 1996, Cromeans et al., 2008). An MPN result was determined using a spreadsheet based on the calculation methods given in Standard Methods (APHA, 2005). Detailed information regarding cell and virus propagation and virus enumeration can be found in Chapter 2.

4.2.3 Long Range and Quantitative Polymerase Chain Reaction Assay (LR-qPCR)

A two-step Long Range Quantitative Polymerase Chain Reaction (LR-qPCR) procedure was used to detect UV damage to the viral genome (Rodriguez et al., 2013; Bounty et al., 2012). In the first step, Long Range PCR was performed to amplify intact DNA fragments 1.1 kilobase pairs (kbp) long. In the second step, qPCR was used to quantify the products of the LR PCR. Viral DNA was extracted using a DNeasy Blood and Tissue Kit (Qiagen, Valencia, CA) according to manufacturer's instructions. The LR-PCR procedure was modified to use the hot-start, DNA polymerase enzyme (GoTaq, Promega, Madison, WI) to simplify the PCR assay. The master mix for the LR-PCR consisted of 2 units of GoTaq polymerase, 1X of GoTaq buffer (5 µL of 5X buffer solution), 1µL of 7.5 µM forward and reverse primer, 5 µL of extracted DNA, and water for a total volume of 25µL. The primers used are presented in Table S1. The temperature cycles for the LR-PCR were an initial denaturation step of 1.5 minutes at 95 °C,

followed by 10 cycles of 15 seconds at 94 °C and 10 minutes at 65 °C, with a final extension step of 10 minutes at 72 °C. Purification of the product from the LR-PCR and quantification using real-time, quantitative (q) PCR were performed as described previously (Rodriguez et al., 2013). The LR-qPCR process was calibrated with serial dilutions of adenovirus 2 stock of a known viral concentration. Primer and probe nucleic acid sequence information are given in Table 4.1

Table 4.1. Primers and probe used for long range and quantitative PCR

Purpose	Sequence	Genome Region	Fragment Size (bp)
Long Range PCR			
Adapter	CAC GGA GAG ATG GCT ATG CG	None	
Forward Primer	CAC GGA GAG ATG GCT ATG CGC GGC GGT ATC CTG CCC CTC C	Adapter + 17,822-18,996	1,174
Reverse Primer	CGT AGG TGC CAC CGT GGG GTT TT AAA C	18,969-18,996	
qPCR			
Forward Primer	CAC GGA GAG ATG GCT ATG CG	Adapter	177
Reverse Primer	CAA GCG AGC GTG AGA CTC C	17,961-17,979	
Probe	FAM/TTG CAT CCG TGG CCT TGC AGG CGC A/BHQ	17,884-17,908	

4.2.4 UV Absorption of DNA

Viral DNA from the adenovirus 2 stock (10^8 pfu/mL) was extracted as described above. The UV absorption was determined from 200 nm to 300 nm using a UV spectrophotometer (Nano Drop 1000, Thermo Fischer Scientific, Wilmington, DE) to compare with the spectral sensitivity of DNA measured with LR-qPCR. The ratio of UV absorption at 260 nm and 280 nm was 1.83, confirming the purity of the DNA.

4.2.5 Statistical Analysis

For the LR-qPCR analysis, a serial, 10-fold dilution curve was developed to correlate the PCR cross threshold value (Ct) with adenovirus concentration and measure changes in the log concentration of gene copies. The viral stock concentration in genome copies was determined using a calibrated real-time PCR for the adenovirus hexon gene described previously (Jothikumar et al., 2005). The calibration of the Hexon gene real-time PCR was performed as described previously (Rodriguez et al., 2013). The following linear equation was used for calculating $\log_{10}$ copies when using the LR-qPCR from adenovirus stock.

$$\log_{10}\text{copies} = -(0.3059 \times Ct) + 14.684. \qquad r^2 = 0.962 \qquad [1]$$

Analysis of the relation between $\log_{10}$ copies and UV dose showed a linear response with no statistically-significant curvature. Dummy variable regression analysis (Draper et al., 1998) showed that repeated UV dose-response curves at a given wavelength had the same slope ($p < 0.05$) but different intercepts. The kinetic constants for the relation between $\log_{10}$ copies and UV dose reported here, as well as their 95% confidence intervals, were obtained from the dummy variable regression analysis.

The log reduction of amplifiable DNA was calculated as:

$$\text{Log reduction} = \log_{10}\text{copies}\,(D_0) - \log_{10}\text{copies}\,(D)\ , \qquad [2]$$

where $\log_{10}$ copies (D_0) is the PCR response of the unexposed sample predicted by the dummy variable regression analysis (i.e. the intercept) and $\log_{10}$ copies (D) is the PCR response obtained with a given UV dose, D.

The relationship between the log concentration of adenovirus and UV dose was also linear, showing no statistically-significant curvature. The kinetic constant for the relationship

between log (N) and UV dose was obtained from regression analysis. The log reduction of adenovirus was calculated as:

$$\text{Log reduction} = \log(N_0) - \log(N) \quad , \qquad [3]$$

where log (N_0) was the log concentration of the unexposed sample obtained from the regression analysis (i.e. the intercept), and log (N) is the measured log concentration.

Analysis of covariance (ANCOVA) was used to compare the linear regression for DNA damage with the linear regression for infectivity to determine if they were statistically similar ($p > 0.05$). Inactivation rate constants for infectivity and DNA damage were taken relative to their values at 253.7 nm to illustrate the action spectrum or spectral sensitivity of adenovirus and its DNA to UV light emission from a LP UV lamp. ANCOVA was also used to compare the LP UV and MP UV dose response given different MP UV fluence calculations.

4.3 RESULTS AND DISCUSSION

Inactivation of adenovirus 2 using LP UV light and the NIST laser at 253.7 nm are presented in Figure 4.1. For LP UV, the inactivation rate (k, cm^2/mJ) was 0.023 ($p = 4.4 \times 10^{-4}$) for cell culture infectivity and 0.022 ($p = 3.3 \times 10^{-9}$) for the 1.1 kbp fragments analyzed with the LR-qPCR assay. For the NIST laser at 253.7 nm, the inactivation rates were 0.030 ($p = 1.3 \times 10^{-3}$) for cell culture infectivity and 0.025 ($p = 1.9 \times 10^{-13}$) with LR-qPCR. Using ANCOVA, the adenovirus 2 dose response measured by DNA damage was not significantly different ($\alpha = 0.05$) from the dose response measured by cell culture infectivity ($p = 0.63$ for LP UV, $p = 0.64$ for NIST laser at 253.7 nm) for both light sources. Additionally, the dose response of adenovirus 2 to LP UV irradiation was not considered statistically different from its response to the NIST laser at 253.7 nm when measured by both infectivity ($p = 0.052$) and LR-qPCR ($p = 0.18$) as

determined by ANCOVA. This work verified the equivalency of UV exposure between both UV emission systems.

Four-log inactivation of adenovirus 2 was observed using a LP UV lamp at a UV dose of 174 mJ/cm^2. This is comparable to previous studies, which noted 4-log inactivation at doses between 120 mJ/cm^2 and 168 mJ/cm^2. [3-6] Two-log reduction in DNA amplification of adenovirus 2 was observed using a LP UV dose of 68 mJ/cm^2 when analyzing a fragment size of 1.1 kbp. This differed from two previous studies, which showed 2-log reduction of DNA amplification after approximately 50 mJ/cm^2.[19,20] The difference in dose response could be attributed to inherent variability in adenovirus dose response as reported in the literature, yet could also be due to variations in the methods, such as using different DNA polymerases from different vendors. Previous work on adenovirus DNA damage was performed using rTth polymerase from Applied Biosystems. This present work used GoTaq polymerase and respective buffer from Promega. However, the results in this study demonstrated that the simplified PCR assay, using the hot-start polymerase, could achieve a linear relationship of up to 3-log reduction of PCR signal due to UV damage (Figure 4.1). In addition, the LR-qPCR assay demonstrated good agreement between the reduction in DNA and the reduction in viral infectivity for exposure at 253.7 nm from either source (Figure 4.1).

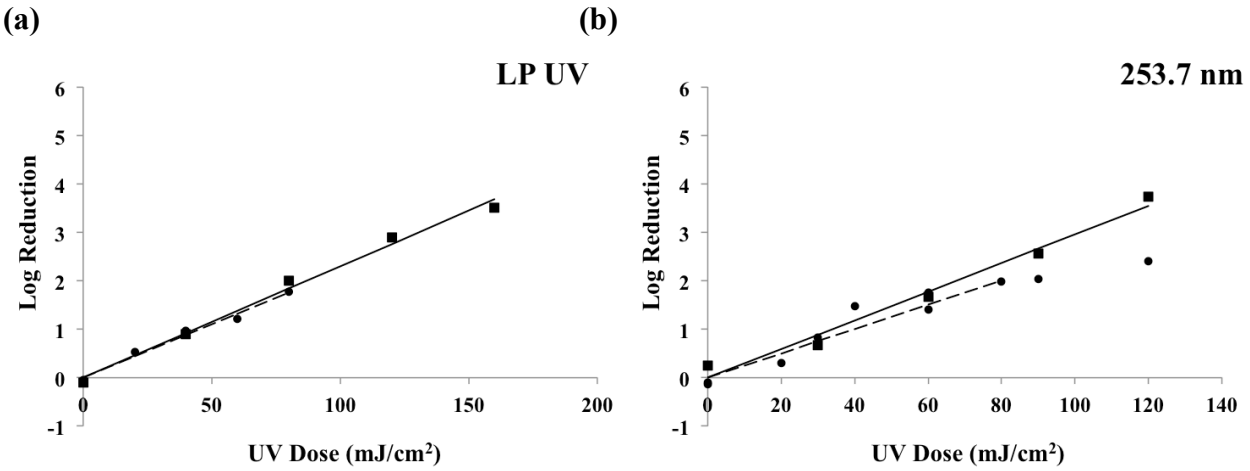

Figure 4.1. Dose response of adenovirus 2 for irradiation with low-pressure UV light (a) and the NIST laser at 253.7 nm (b) as measured by cell culture infectivity (■) and DNA amplification (●).

Adenovirus is a non-enveloped, icosahedral particle consisting of a protein capsid surrounding a DNA-protein core. Since the viral particle is composed of two primary components: DNA and proteins, loss of infectivity at a given wavelength is assumed to be due to damage to DNA, damage to viral proteins, or both. Inactivation of adenovirus 2 by the NIST laser at 210 nm, 220 nm, 230 nm, 240 nm, 260 nm, 270 nm, 280 nm, and 290 nm is shown in Figure 4.2 as a function of UV dose. It is important to highlight that the fragments used in the Long Range PCR for these experiments were 1.1 kbp in length. Therefore, the results should be considered as damage observed in a 1.1 kbp fragment of the adenovirus genome. This sensitivity level allows the levels in reduction in PCR signal to be similar to the levels in reduction in viral infectivity when adenovirus is irradiated with LP UV light, which is the point of comparison. The results indicate that at 240 nm and below, the loss of viral infectivity was significantly greater than the observed damage to the viral genome; therefore, damage to the nucleic acids was not the only cause for the loss of adenoviral infectivity at those wavelengths. At 260 nm, the opposite was true. At 270 nm, 280 nm, and 290 nm, as with 253.7 nm, the sensitivity of the genome and the virus were statistically similar.

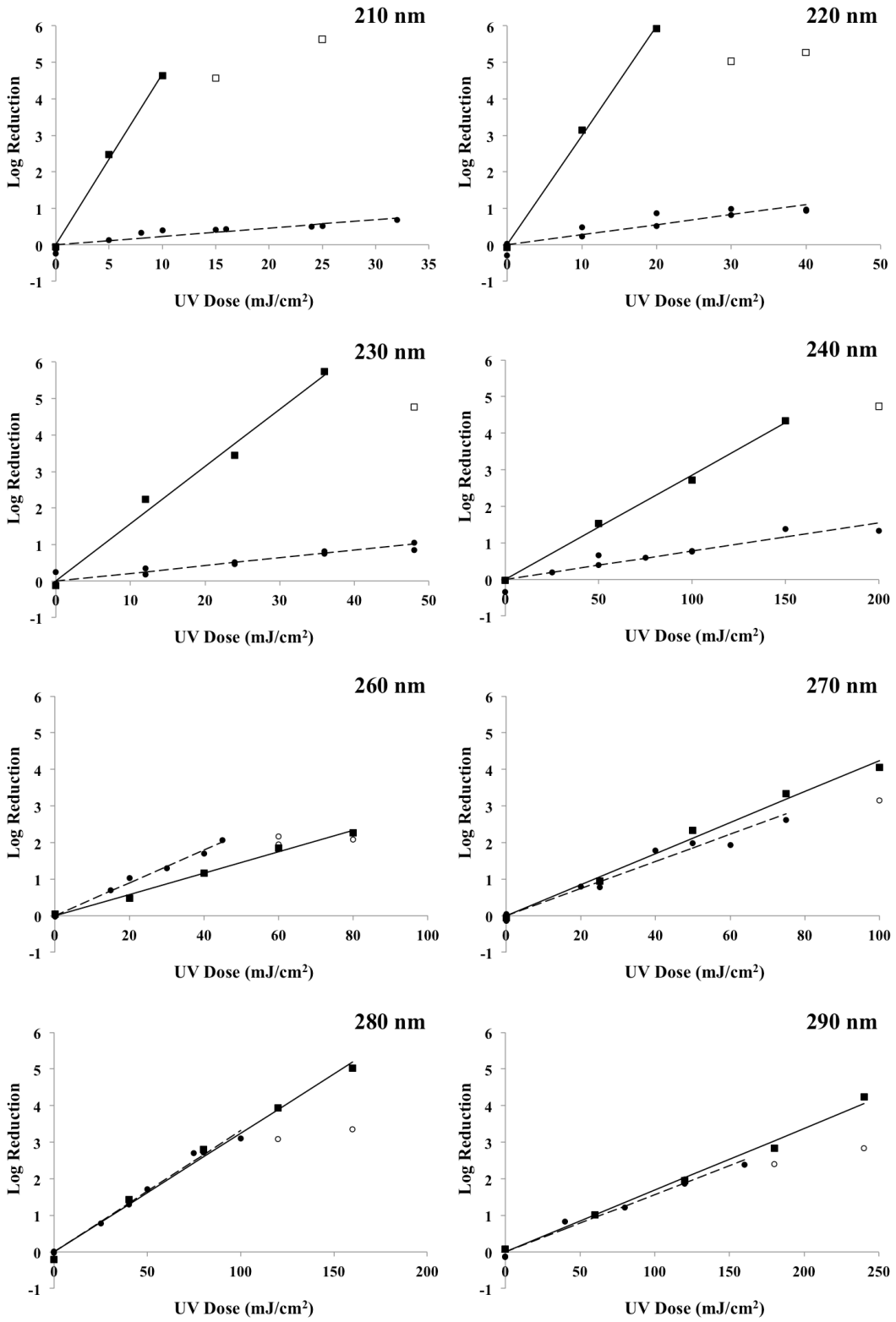

Figure 4.2. Dose response of adenovirus 2 to monochromatic UV light from the NIST laser at various wavelengths as measured by infectivity (■) and DNA amplification (•). Note different x and y axes labels. Open symbols represent data points not included in statistical analysis due to indications of tailing (genome damage) or from reaching the detection limit (cell culture assay).

Linear inactivation rate constants (cm^2/mJ) for each wavelength are given (Table 4.2) as determined through infectivity and DNA damage. For the calculations of the inactivation rate constants, some points were not used as indicated in Figure 4.2. In the case of the infectivity assay, the assay detection limit was reached after obtaining a 5-log reduction; therefore, these points were not used for the calculation of rate. In the case of genome damage determined by LR-qPCR, it was observed previously that tailing occurs after obtaining 2.5- to 3-log reduction in amplifiable genome fragments (Rodriguez et al., 2013). This tailing occurs when the genome fragment is saturated with damage and exposed to multiple hits. Multiple damage sites in the same fragment are measured as one point of damage because the PCR can only detect the reduction in amplifiable genome fragments regardless of the number of damage sites per genome. As a result, the log reduction cannot increase and tailing occurs. Therefore, these points were not used for the calculation of rate.

Analysis of covariance (ANCOVA) at each wavelength confirmed a statistical difference ($p < 0.05$) between DNA damage and infectivity at 210 nm, 220 nm, 230 nm, 240 nm, and 260 nm. At 240 nm and below, loss of viral infectivity was significantly greater than the loss of DNA amplification. This implies that damage to a viral component other than the viral genome contributed to loss of infectivity at those wavelengths. The significantly higher loss of infectivity at these low wavelengths is likely due to damage to the viral proteins, which play an integral role in the infection process by initiating adenoviral infection in a suitable host cell, lysing endosomes, and facilitating the release of DNA in the host cell nucleus (Seth, 1999). At 240 nm and below, the UV absorption of proteins is higher, primarily because of the absorption of peptide bonds, which are prevalent in protein structures as the link between amino acids (Jagger, 1967; Harm, 1980).

Table 4.2. Wavelength-specific inactivation rate constants (in cm^2/mJ) for adenovirus 2. For ANCOVA, significance was defined as $p < 0.05$.

Wavelength (nm)	Cell Culture Infectivity k (±95%CI; p-value)	DNA Damage k (±95%CI; p-value)	ANCOVA p-value
210	0.469 (0.2740; 2.9E-02)	0.023 (0.0108; 1.3E-04)	2.6E-09
220	0.299 (0.1594; 2.7E-02)	0.028 (0.0110; 8.1E-06)	1.3E-08
230	0.157 (0.0577; 7.2E-03)	0.021 (0.0054; 2.0E-08)	7.2E-09
240	0.029 (0.0048; 1.5E-03)	0.008 (0.0016; 6.7E-10)	2.9E-06
253.7	0.030 (0.0080; 1.3E-03)	0.025 (0.0034; 1.9E-13)	0.64
260	0.029 (0.0045; 2.6E-04)	0.045 (0.0037; 1.1E-12)	1.4E-04
270	0.042 (0.0081; 4.7E-04)	0.036 (0.0043; 8.7E-15)	0.12
280	0.032 (0.0052; 2.8E-04)	0.033 (0.0020; 7.0E-06)	0.68
290	0.017 (0.0029; 3.5E-04)	0.016 (0.0019; 4.6E-10)	0.43
LP UV	0.023 (0.0043; 4.4E-04)	0.022 (0.0022; 3.3E-09)	0.63

At 260 nm, loss of DNA amplification was statistically greater than the loss of viral infectivity. This relatively greater DNA damage could be the result of damaged DNA being repaired during the infectivity assay. Although this phenomenon was not demonstrated directly in this study, the possible role of viral DNA repair has been demonstrated using cell lines with limited repair capability (Guo, 2010). Repair of photodimeric lesions likely occurred across the germicidal UV spectrum. However, it was not specifically measured in this study in part because the LR-qPCR assay used to measure DNA damage before repair was calibrated to cell culture infectivity, which can be influenced by host cell repair mechanisms. At 254 nm, 270 nm, 280 nm, and 290 nm, differences between loss of viral infectivity and DNA damage were not

statistically different, indicating that at those wavelengths loss of viral infectivity is linked primarily to genomic damage. At 280 nm, the UV absorption of proteins has a relative peak due to the absorption of tryptophan and tyrosine amino acids; however, their absorption at 280 nm is an order of magnitude lower than DNA absorption (Harm, 1980). These results are consistent with the high UV absorption of DNA relative to proteins at those wavelengths.

Figure 4.3 shows the spectral sensitivity (action spectra) of adenovirus 2 inactivation and its genome damage, obtained by taking the inactivation rate constants relative to their values at 253.7 nm. The figure highlights the significant difference between the rate constants of inactivation and genome damage at wavelengths below 240 nm as well as their relative similarities at wavelengths above 240 nm. At 210 nm, the loss of viral infectivity was almost 16 times greater than at 254 nm; at 220 nm, it was over 10 times greater. Above 240 nm, the action spectrum of inactivation peaked at 270 nm and was relatively flat from 240 to 260 nm. The action spectrum of inactivation follows the same trend as reported in the literature (Figure 4.3a), which showed five to six times greater inactivation at 222 nm and four to six times greater inactivation at 228 nm (Linden et al., 2007). In contrast to this study, the reported action spectrum (Linden et al., 2007) above 240 nm peaked at 260 nm. Differences in spectral sensitivity could be attributed to inherent variability in adenovirus dose-response in cell culture as evidenced by the literature; however, they could also be attributed to the UV light sources used. The previous study used MP UV light with bandpass filters, which provided half-peak bandwidths of approximately 10 nm wide compared to less than 1 nm wide for this study.

Figure 4.3b compares the action spectra of UV inactivation and genome damage to the UV absorption of adenoviral DNA measured in this study. The action spectrum of genome damage and the UV absorption both peaked at 260 nm. This observation is expected because UV

energy must be absorbed to cause damage to the genome. At 260 nm, the genome was 1.8 times as sensitive to damage as at 253.7 nm. Above 260 nm, the DNA damage sensitivity decreased with increasing wavelength, which is consistent with a past study of cyclobutane dimer formation at wavelengths between 261 nm and 305 nm (Besaratinia et al., 2011). The adenoviral genome was least sensitive to damage at 240 nm, near the relative minimum of DNA absorption at 230 nm. The viral genome exhibited a higher sensitivity to damage at 220 nm than at 210 nm, which was unexpected. The UV absorption of the intact virus peaks between 210 nm and 220 nm (Guo et al., 2010). It is possible that proteins absorbing at those wavelengths could transfer the UV energy to the DNA. Protein-associated DNA is more susceptible to UV-induced photoproducts than isolated DNA (Hegedus et al., 2003.

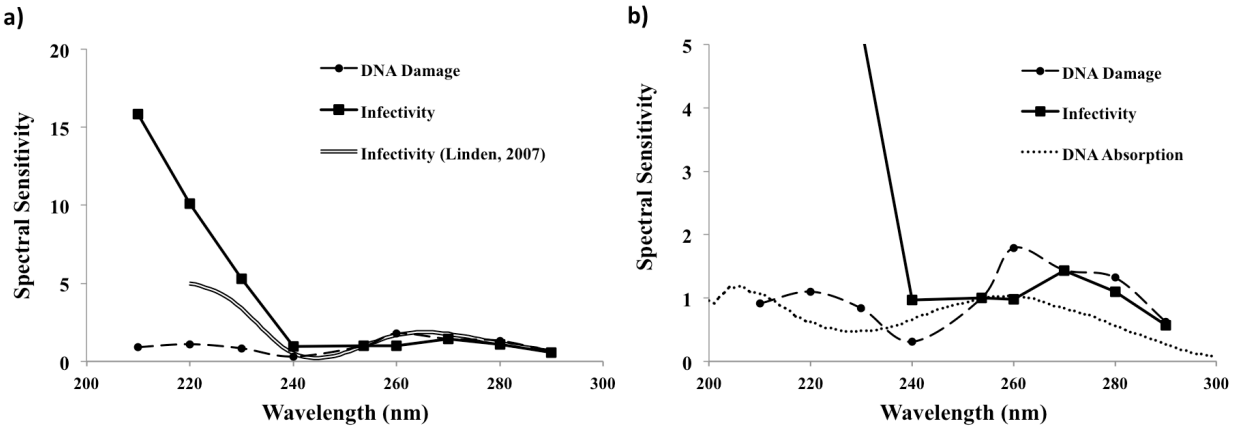

Figure 4.3. Spectral sensitivity of adenovirus 2 and its nucleic acid (DNA damage) between 210 nm and 290 nm as compared to (a) the action spectrum in the literature (Linden et al., 2007) and (b) the UV absorption of adenoviral DNA measured. Note different y-axes values.

The observation that the action spectrum of adenovirus 2 inactivation was relatively flat from 240 to 260 nm but peaked at 270 nm is unusual. Action spectra of other viruses such as rotavirus (dsRNA), MS2 coliphage (ssRNA), T7 coliphage (dsDNA), T1UV Coliphage (dsDNA), and Q beta Coliphage (ssRNA) all show a local minimum at 240 nm and local maximum between 259-265 nm (Mamane-Gravetz et al., 2005; USEPA, 1996; Rauth, 1965;

Stefan et al., 2007; Ronto et al., 1992). Other organisms such as *E. coli*, *S. typhimurium*, *P. aeruginosa*, *B. subtilis* also have relative peak sensitivities in the 260 nm to 265 nm region (Gates, 1930; Chen et al., 2009; Lakretz and Ron, 2010). The nucleotide base pairs of adenine, thymine, cytosine, and uracil have relative peak absorption values between 260 nm to 265 nm with guanine peaking closer to 245 nm and 275 nm (Davidson, 1976). Few action spectra are available for dsDNA viruses. Herpes simplex virus exhibited relative peak sensitivities at 270 nm and 280 nm (Detsch, 1980); however, herpes simplex has an envelope, which could impact its UV sensitivity. T7 and T1UV, both dsDNA coliphage, showed a peak sensitivity between 260 and 265 nm (Ronto et al., 1992). However, T7 and T1UV do not infect human cells and their bacterial assays are performed in the dark; dark repair of DNA does not usually occur when the host is growing at log phase.

The lack of increased sensitivity of adenovirus near 260 nm could be an artifact of experimental variability or an indication of DNA damage repair by the host cells used in the infectivity assay. However, statistical analysis demonstrated that adenovirus dose response to 260 nm was statistically different than at 270 nm, but not different than the dose response at 240 or 254 nm; this suggests that the spectral sensitivity is not an artifact of experimental variability. As a double stranded (ds) DNA virus, adenovirus is susceptible to host cell DNA repair, which could affect its infectivity-based spectral sensitivity. At 260 nm, the virus is most sensitive to DNA damage and DNA damage is the dominant mechanism for loss of infectivity; therefore, DNA repair could restore its viral infectivity and affect its infectivity action spectrum. The impact of potential repair of DNA damage in the estimation of UV inactivation of dsDNA viruses during infectivity assays has been investigated with cells deficient in DNA repair mechanisms, demonstrating a significant reduction in dose required compared to repair proficient

cells (Go et al., 2010). In addition, the adenovirus genome has been demonstrated to sustain damage from LP lamps (254 nm) that did not translate to reduction in viral infectivity (Rodriguez et al., 2013), suggesting the potential role of DNA repair mechanisms in the resistance of adenovirus to UV disinfection. The type of DNA damage and potential repair obtained at different wavelengths is not well understood and merits further research.

This research provides fundamental insight into the action of ultraviolet light on adenoviruses and the molecular level viral responses to UV irradiation. The data clearly indicate that nucleic acid damage is not the only mechanism responsible for virus inactivation from polychromatic UV lamps, including MP UV lamps, which are commonly used in the water and wastewater treatment industries. It has significant broader impacts with the potential to improve current UV disinfection and system validation, by demonstrating the importance of low wavelengths in inactivating adenoviruses, which drive the UV disinfection requirements. It also has the potential to improve the design of UV technologies by making the case for tailored wavelength units, which could combine a wavelength in the germicidal range, such as 254 nm or 260 nm, with a wavelength in the protein absorbance region, such as 220 nm or 230 nm, to optimize pathogen inactivation and minimize energy costs. Future research would complement this study by evaluating the spectral sensitivity of adenoviral proteins, specifically the fiber proteins and DNA binding proteins.

CHAPTER 5

WAVELENGTH DEPENDENT DAMAGE TO ADENOVIRAL PROTEINS ACROSS THE GERMICIDAL UV SPECTRUM

Understanding why polychromatic UV light is more effective at inactivating adenovirus 2 than monochromatic UV light emitting at 254 nm required studying wavelength-specific damage to both viral components: DNA and proteins. Chapter showed that UV damage to DNA was not the sole contributor to the loss of adenovirus infectivity. This chapter takes that one step further by showing damage to adenoviral proteins across the germicidal UV spectrum. SDS-PAGE (sodium dodecyl sulfate polyacrylamide gel electrophoresis) was used to demonstrate protein damage at various wavelengths between 200 and 300 nm. Adenoviral protein damage was significantly greater at wavelengths below 240 nm than at 254 nm or above.

The work described in this chapter will contribute to a publication on this topic.

5.1 INTRODUCTION

Adenovirus is a common cause of respiratory illnesses, including bronchitis and pneumonia, as well as gastrointestinal infections. Immunocompromised individuals, infants, and children are the most at risk of adenovirus infection; however, it has historically caused acute respiratory illness in military recruits as well (Russell, 2006). As a waterborne pathogen, adenovirus has been found in both contaminated and treated drinking water (Kukkula et al, 1997; Lee and Kim, 2002) and raw and treated wastewaters (Crabtree et al., 1997). It is of significant interest in the water treatment industry, particularly with regard to ultraviolet (UV) disinfection, because of its resistance to UV irradiation relative to other pathogens. When disinfecting with traditional low-pressure (LP) UV irradiation, emitting at 254 nm, 4-log inactivation of adenovirus type 2 occurs a UV dose of approximately four times greater than those required for inactivating other enteric viruses, including echovirus, coxsackievirus, and poliovirus (Gerba, Gramos, & Nwachuku, 2002; Linden et al., 2009; Shin, Linden, & Sobsey, 2005; Thompson et al., 2003). This increased resistance drives regulations set by the US Environmental Protection Agency (USEPA) for virus inactivation by UV irradiation. To demonstrate 4-log inactivation of all viruses, the Surface Water Treatment Rule requires a UV dose of 186 mJ/cm^2, based on empirical results of adenovirus inactivation (USEPA, 2003; USEPA, 2006a). For groundwater disinfection, UV is not considered sufficient standalone treatment for viruses unless demonstrated through a field-scale challenge test (USEPA, 2006b).

Despite its demonstrated resistance to monochromatic irradiation emitted from low-pressure UV lamps, adenovirus has shown an increased sensitivity to polychromatic UV irradiation from medium-pressure (MP) mercury vapor lamps. MP UV lamps were two to four times more effective than LP UV lamps (Linden et al., 2009; Shin et al., 2009; Linden et al.,

2007, Guo et al., 2010; Rodriguez et al., 2013), inactivating adenovirus by 4-log at doses of 40-80 mJ/cm^2. Although research comparing monochromatic and polychromatic inactivation of viruses is limited, polychromatic irradiation has been shown to be twice as effective as monochromatic irradiation at inactivating rotavirus, calicivirus, and MS2 bacteriophage (Malley, 2004).

This enhanced viral inactivation from polychromatic lamps is attributed, in part, to the method for calculating dose for MP UV lamps (Malley, 2004; Hijnen, 2010). Current practice is to determine the polychromatic UV dose by weighting the average irradiance in the water sample germicidally, based on the absorbance of DNA as detailed in Linden and Darby (1997). When direct DNA damage was measured with a PCR assay, however, monochromatic and polychromatic light from LP and MP UV sources were equally effective at damaging DNA, inducing the same amount of DNA lesions per kilobase (Eischeid et al., 2009). The enhanced susceptibility of adenovirus 2 to polychromatic UV irradiation is due to UV damage of viral components other than nucleic acid, particularly below 240 nm (Beck et al., 2014). Polychromatic UV irradiation emitted by MP UV lamps is more effective than monochromatic UV irradiation at damaging viral proteins, impacting the ability of the viruses to infect (Eischeid and Linden, 2011).

Adenovirus has a relatively complicated viral protein structure, consisting of 13 structural proteins, which play an integral role in the infection process. The proteins were historically assigned roman numerals in decreasing molecular weight order, corresponding to their migration order through an SDS-PAGE (sodium dodecyl sulfate polyacrylamide gel electrophoresis) gel (Maisel et al., 1968). Fiber proteins (polypeptide IV) protruding from 12 vertices, initiate contact with the host cell receptor, primarily the coxsackie-adenovirus receptor (CAR) on human lung

cells (Russell, 2009). The penton base of the fiber protein (polypeptide III) is responsible for the virion entry into the host cell; it binds to integrin coreceptors on the cell surface, which stimulates endocytosis and results in internalization of the virus (Wickham et al., 1993; Salone et al., 2003). The hexon protein (polypeptide II), which has the highest molecular weight of the adenoviral proteins, is characterized for its remarkable stability due to a highly folded design; it maintains the structural stability of the virus during infection (Russell, 2009, San Martin, 2012). The release of polypeptides VI and VIII, which bridge the DNA core to the viral capsid, enables the entry of the viral DNA, core proteins V, and the terminal protein into the host cell's nucleus (Seth, 1999; Russell, 2009). UV-induced damage to these viral proteins impacts multiple stages of the viral infection, preventing the virion from attaching and entering the host cell, utilizing its machinery, and ultimately releasing its DNA into the host cell nucleus to begin replication.

A previous study used SDS-PAGE to show enhanced protein damage from MP UV irradiation over LP UV (Eischeid and Linden, 2011). Another study showed that DNA damage was not the sole mechanism responsible for loss of viral infectivity at wavelengths below 240 nm (Beck et al., 2014). This present study expands on the previous works, demonstrating the protein damage (primarily from wavelengths below 240 nm) that contributes to increased virus inactivation by polychromatic UV sources. The study used a deuterium lamp with bandpass filters, a LP UV lamp, and UVC LEDs to irradiate adenovirus 2 across the germicidal UV spectrum between 200 nm and 300 nm. SDS-PAGE separated the proteins by molecular weight; the hexon, penton, minor capsid, fiber, and core protein bands were analyzed for UV-induced damage.

5.2. MATERIALS AND METHODS

5.2.1 Adenovirus Propagation and Enumeration

Adenovirus stocks were provided from the US Environmental Protection Agency in Cincinnati, OH. Human adenovirus 2 was obtained from the American Type Tissue Collection (ATCC VR-846, Manassas, VA) and propagated in A549 human lung carcinoma cells (ATCC CCL-185). Briefly, A549 cells were planted in 175 cm^2 vented tissue culture flasks (Greiner, Monroe, NC) in Dulbecco's Minimum Essential Medium (DMEM) (Thermo Fisher Scientific Inc., Waltham, MA) supplemented with 10% fetal calf serum (Thermo Fisher Scientific Inc.), and maintained in 5% (vol/vol) CO_2. The cells were infected with stock adenovirus 2, and the cells were incubated for up to two weeks or until cytopathogenic effects (CPE) were observed. Cells underwent three freeze-thaw cycles and a portion of the cell lysate was passaged onto fresh A549 cells for further propagation. Cell lysates from all passages were combined to obtain maximal viral stock. Lysates were centrifuged at 2500 × g for 30 minutes to remove cell debris. The supernatant containing virus was then centrifuged at 10,000 × g for 10 minutes to remove any remaining small cellular debris. In order to remove any potential viral clumps, remove any remnant of growth media, and further purify the viral stock, the virus supernatant was further concentrated using celite, as described by McMinn et al. (2012). Following celite concentration, viral stocks were further concentrated using 30 kDa MWCO Vivaspin-20 ultrafilters (Sartorius-Stedim, Aubagne, France) as described previously (Cashdollar et al., 2013). Viral stocks, estimated at 3.2 x 10^9 pfu/mL, were stored at -80°C until UV exposure experiments.

5.2.2 UV Irradiations

Adenovirus suspensions, diluted 50% by double-processed tissue culture water, were irradiated by a deuterium lamp, UV LEDs, and a low-pressure (LP) mercury vapor lamp. The

200 W deuterium lamp (Hi-Tech Lamps, Inc, Mountain View, CA) spectrum was attenuated with bandpass filters to filter its emissions to roughly 10 nm intervals within the germicidal UVC range. The filtered deuterium lamp spectra (Figure 5.1), measured with a Maya 2000 Pro spectrometer (Ocean Optics, Dunedin, FL) exhibited peak wavelength emissions at 213.4 nm, 220.0 nm, 226.3 nm, 239.8 nm, and 267.6 nm with full width at half maximum (FWHM) bandwidths measuring between 9.6 and 12.4 nm. The spectra from the turnkey UV-C LED unit (Dot Metrics Technologies, Charlotte, NC), measured with the Maya 2000 Pro, peaked at 259.6 nm and 276.6 nm with FWHM bandwidths at 12.6 nm and 9.8 nm respectively (Figure 5.1). The deuterium lamp and UV LED sources were set up in a bench-scale collimated beam apparatus as described in Bolton and Linden (2003). For reference, adenovirus 2 suspensions were also irradiated by a custom-made LP UV system built with four 15 W mercury vapor lamps emitting monochromatic irradiation at 254 nm (Figure 5.1) through a four inch aperture.

The adenovirus 2 exposures were conducted across the germicidal UV spectrum. Specific wavelengths were analyzed in more detail. The 220 nm was of particular interest as a wavelength below 240 nm where protein damage was expected to be greatest due to the high protein absorbance (Jagger, 1967; Harm, 1980, Beck et al., 2014). At 220 nm, the virus was exposed to UV doses of 0. 10. 20, 30, 40, and 50 mJ/cm^2. At the common reference wavelength of 254 nm, the emission of the low-pressure mercury vapor lamp, protein damage was measured at UV doses of 0, 100, 200, 300, 400 mJ/cm^2. Protein damage from both LEDs, emitting at 260 nm and 280 nm, was also measured; 280 nm is of research importance as a relative peak of protein absorbance. The LED exposures were also conducted at 100, 200, 300, and 400 mJ/cm^2.

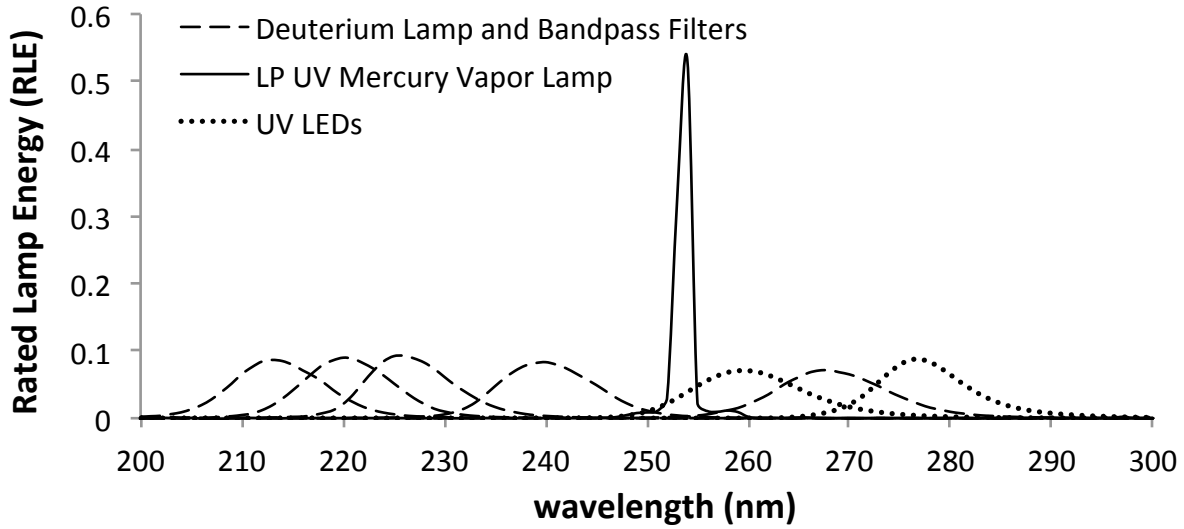

Figure 5.1. Emission spectra from the deuterium lamp with bandpass filters, the LP mercury vapor lamp and the UV LEDs.

Adenovirus suspensions were exposed to the UV sources in continuously stirred, 2 mL volumes (0.2 cm sample depth, 3.5 cm diameter Petri dishes). Irradiance was measured at the water surface with an IL-1700 radiometer, SED 240 detector, and W-diffuser (International Light, Peabody, MA). For exposures involving the deuterium lamp with bandpass filters, irradiance was significantly lower than for the other two sources, ranging from 0.0102 mW/cm^2 to 0.025 mW/cm^2. For the UV LEDs, irradiance ranged between 0.193 to 0.337 mW/cm^2. For the LP UV lamp, irradiance at the water surface was 0.95 mW/cm^2.

Average UV doses for the collimated beam tests were determined as described previously (Bolton and Linden, 2003), adjusting for reflection off the water surface, UV absorption (Cary 100 spectrophotometer, Agilent Technologies, Santa Clara, CA), depth of the water sample, as well as the uniformity of the distribution of light across the surface of the sample. Petri factors ranged from 0.90 to 0.92 for the deuterium lamp with bandpass filters, 0.88 to 0.93 for the UV LEDs, and 1.0 for the LP UV mercury vapor lamp.

Because the deuterium lamp with bandpass filters and the UV LEDs are polychromatic light sources, the UV dose accounted for the relative lamp emission (RLE) of the light source (Figure 5.1) and the sensitivity of the radiometer used to measure irradiance, which was given with the radiometer calibration data (Linden and Darby, 1997; USEPA, 2006). The RLE and radiometer sensitivity were taken relative to the weighted average wavelength of each source (i.e. 214 nm, 220 nm, 227 nm, 240 nm, and 268 nm for the deuterium lamp, and 261 nm and 278 nm for the UV LEDs. Average irradiance was used, rather than germicidal irradiance, for the UV dose calculations.

Irradiations were conducted at room temperature. The deuterium lamp operated on a chiller, which cooled the lamp unit to between 2 ^{o}C and 15 ^{o}C. The LED unit contained a closed-loop thermal management system to regulate internal UV LED temperatures. Sample volumes were measured after irradiation. For the deuterium exposures, from 0% to 10% of the volume, and therefore the sample depth, was lost to evaporation. For the UV LED exposures, from 0% to 20% of the volume was lost. In the case of evaporation, water was added back to each sample. Samples were placed in the -80^{o}C freezer prior to the SDS PAGE assay.

5.2.3 SDS-PAGE Analysis

Adenovirus 2 protein damage was measured by sodium dodecyl sulfate polyacrylamide gel electrophoresis (SDS-PAGE) using a method modified from that described previously (Eischeid and Linden, 2009). Of the 2 mL irradiated samples, 150 μL was used for the analysis. Each volume was spiked with 2 μL of 0.5 mg/mL aprotinin, an internal protein standard (MP Biomedicals, Santa Ana, CA) and pretreated by incubating for 10 minutes at room temperature with 32 μL of 2% sodium deoxycholate (Sigma Aldrich, St Louis, MO). Samples were precipitated with trichloroacetic acid, adding 25% by volume (37.5 μL), and chilled on ice for 30

min. Samples were then centrifuged for 30 min at 4°C (20,000 x g), washed with acetone, and centrifuged again. The precipitated and dried protein pellets were resuspended in Laemmli buffer (Bio-Rad, Berkeley, CA) with 5% beta mercaptoethanol, diluted with SDS running buffer (Tris/glycine/SDS, Bio-Rad, Berkeley, CA). Resuspended proteins were heated to 95 °C, to further denature the proteins, prior to injection into 4 to 20% gradient Tris-HCL precast gels (Bio-Rad). After the gel electrophoresis (150 V, 95 min), gels were fixed in a 7% acetic acid/10% methanol solution for 30 minutes with gentle agitation, stained overnight with SYPRO Ruby protein gel stain (Bio-Rad) according to manufacturer's instructions, and destained with the acetic acid methanol solution. Gels were imaged with a Gel-Doc imager and individual protein bands were identified by molecular weight (van Oostrum, 1985; Rux and Burnett, 1999; Vellinga et al., 2005) with the aid of the broad-range molecular weight protein standard (Bio-Rad). Proteins were quantified from image densitometry using Image-J software, relative to the internal protein standard (aprotinin, 6.6 kDa).

5.2.4 Statistical Analysis

At the time of this writing, the duplicate protein assay was not completed so statistical analysis has not yet been conducted.

5.3 RESULTS AND DISCUSSION

The SDS-PAGE gel in Figure 5.2 shows adenoviral protein damage across the germicidal UV spectrum. Proteins were identified by the molecular weight (kDa) labeled on the left side of the image, which corresponds the protein ladder in lane 1. Lanes 2-8 show adenoviral proteins across the UV spectrum after exposure to the wavelengths given at the top of the image. UV dose, shown at the bottom of the image was 50 mJ/cm^2 at wavelengths of 240 nm and above. Below 240 nm, the UV doses steadily decreased to ensure protein detection by the SDS-PAGE

assay. Adenoviral proteins, labeled on the right hand side, were historically assigned roman numerals corresponding to their migration order through the gel, in decreasing molecular weight order (Maisel et al., 1968). In this present study, the hexon (polypeptide II, 109 kDa), penton base (polypeptide III, 63.3, 67 kDa), minor capsid (IIIa, 63.3 kDa), fiber (IV, 62 kDa) and core (V, 41.6 kDa) proteins were selected for analysis. The bright band labeled as capsid IIIa is believed to be a combination of capsid IIIa as well as part of the penton base (III) given their corresponding 63.3 kDa molecular weights; however, it was analyzed here as capsid IIIa.

The gel clearly shows damage to adenoviral proteins, particularly at the low wavelengths below 240 nm. The spiked protein standard (6.6 kDa) is strong across all lanes in the gel. In the first three lanes, the protein signature of the virus is very weak; individual protein bands are not distinct and are blended throughout each lane. This indicates protein degradation or denaturing, causing a change to the molecular weights, particularly at those low wavelengths (214 nm, 220 nm, 227 nm). The low wavelength lanes also show the strongest protein signal in the well itself, at the top of the gel, indicating that the proteins are folding or changing in a structure that prevents them from migrating through the gel.

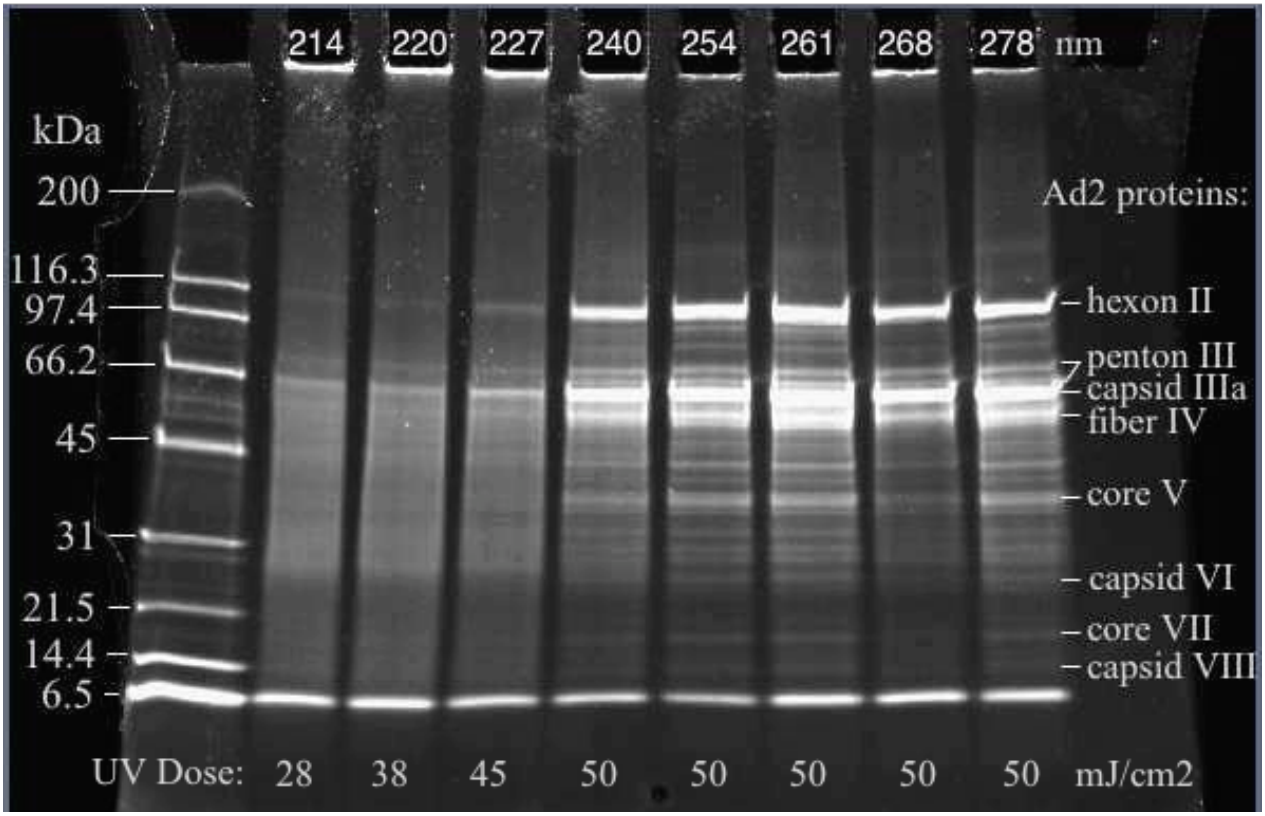

Figure 5.2. Adenovirus protein damage across the germicidal UV spectrum as measured by SDS PAGE. Molecular weight is given on the left-hand side. Adenovirus proteins are identified on the right-hand side. Wavelengths used for irradiation are identified at the top and UV doses given at the bottom.

The Image J analysis of the protein gel in Figure 5.2 yielded the quantitative relative protein damage data shown in Figure 5.3. The relative protein damage followed the same trend of the UV absorption of adenovirus 2 (Figure 5.3 inset), increasing prominently below 240 nm where the UV absorption, measured with the UV spectrophotometer described above, is highest. The protein damage from adenovirus exposure to 38 mJ/cm^2 at 220 nm was 3.6 times greater than the protein damage from exposure to 50 mJ/cm^2 at 254 nm. Protein absorbance is significantly higher at wavelengths below 240 nm, primarily due to the high absorbances of the peptide bond (Jagger, 1967; Harm, 1980). Peptide bonds are prevalent in protein structures as the link between amino acids used to form the protein structure. The increased protein damage at 268 nm seen relative to 254 nm was unexpected. Adenovirus has a relative peak absorbance at

270 nm, but that is insignificant when compared with wavelengths below 240 nm. This warrants further research that was not feasible in this study given the very long exposure times required for the deuterium lamp with bandpass filters emitting at 268 nm.

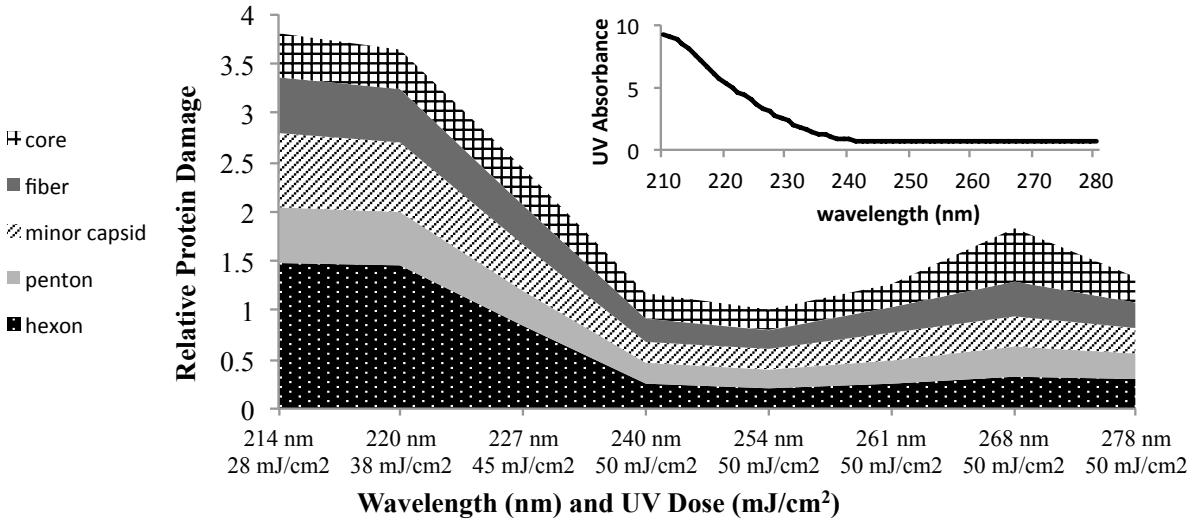

Figure 5.3. Damage to adenovirus 2 proteins across the germicidal UV spectrum relative to their protein damage at 254 nm, shown alongside relative UV absorbance (inset).

The impact of adenoviral protein damage at 220 nm is shown in the gel in Figure 5.4a. The protein signature, while strong in the unexposed (0 mJ/cm^2) sample, is significantly degraded in the exposed samples. Proteins signals are weak, individual bands not distinct, but rather blended together, and a strong protein signal is seen in the injection wells. The data in Figure 5.4b quantifies this damage, revealing that just 10 mJ/cm^2 of 220 nm irradiation decreased the protein quantity by approximately 60% for all five proteins analyzed. Relative protein quantity continued to decrease with increasing UV dose for the hexon, penton, minor capsid, and fiber proteins. For the core protein, however, the damage leveled off. Eischeid (2009) also reported that the core proteins were least susceptible to UV damage, perhaps from being shielded from the UV light (Nermut, 1979).

a)

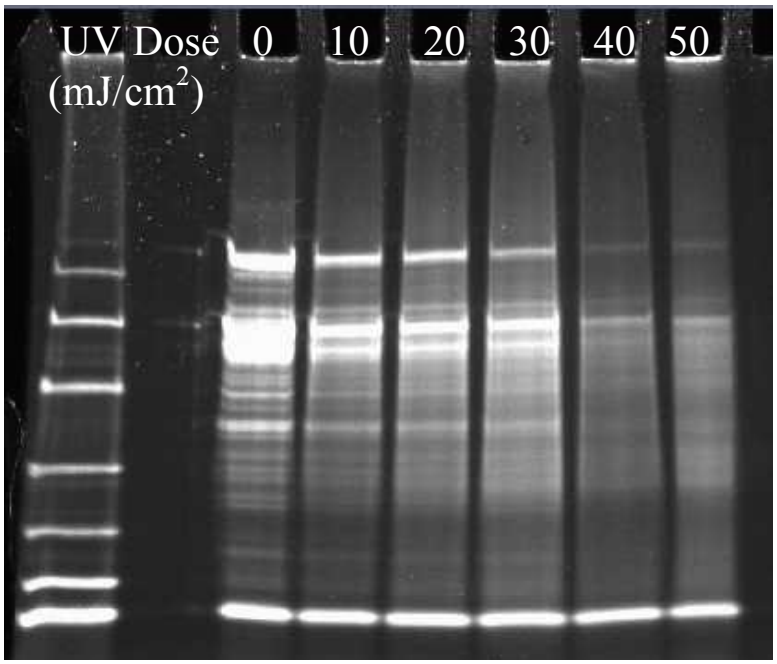

b)

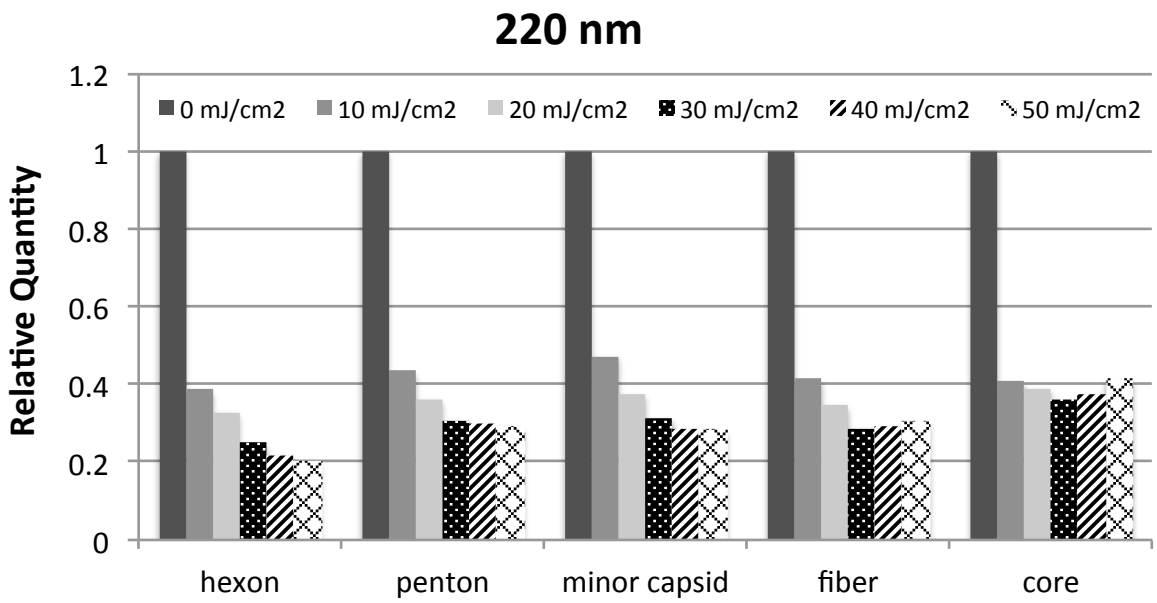

Figure 5.4. Adenoviral protein damage induced from UV light emitting at 220 nm for 10, 20, 30, 40, and 50 mJ/cm^2, shown in the SDS-PAGE gel (a) and from the corresponding quantification (b).

Adenoviral protein damage from 254 nm UV light emitted by the low-pressure mercury vapor lamp is shown in Figure 5.5a. Protein degradation was not visually detected in the gel. Individual bands were still clearly distinct and there was little protein signal in the wells at the top of the gel. The variability in the corresponding bar chart in Figure 5.5b is believed to represent the inherent error in the SDS-PAGE method.

a)

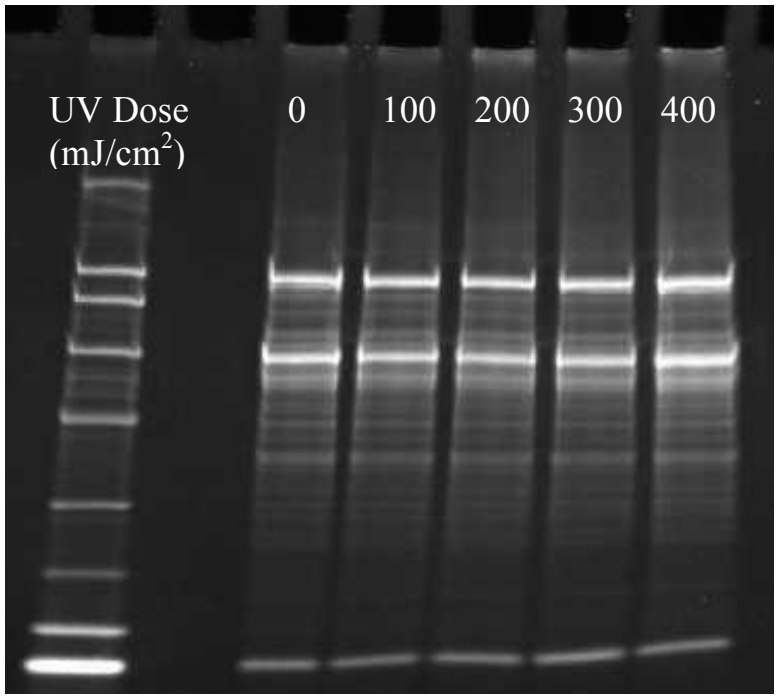

b)

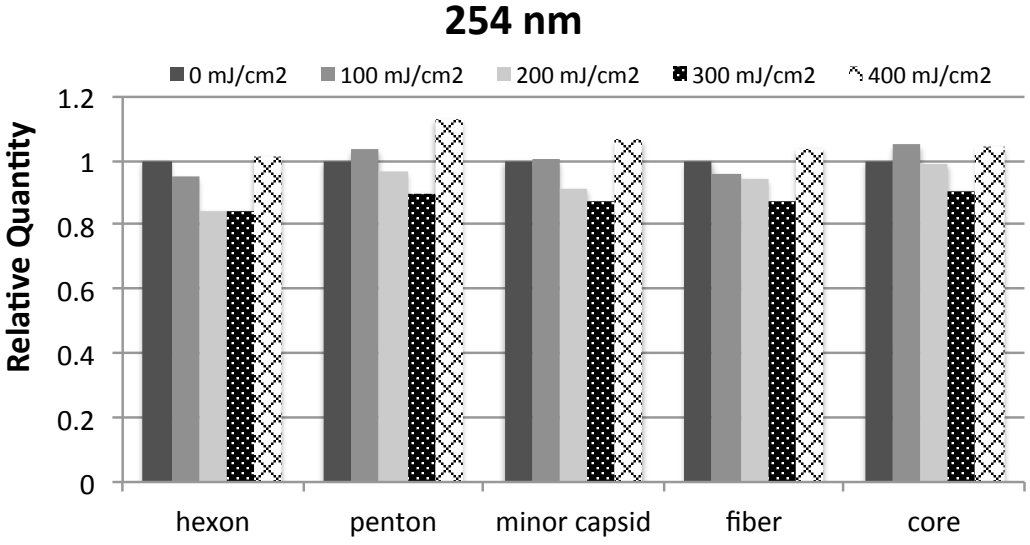

Figure 5.5. Adenoviral protein damage induced from UV light emitting at 254 nm for 100, 200, 300, and 400 mJ/cm^2, shown in the SDS-PAGE gel (a) and from the corresponding quantification (b).

Figure 5.6 shows adenoviral protein damage from 260 nm UV light emitted by the UVC LEDs. Although very slight, UV-induced protein degradation was detected at the high UV doses, unlike at 254 nm. Visually, protein signals were slightly weaker, protein bands were less distinct, and a protein signal was detected in the wells at the top of the gel. The image densitometry quantification showed up to 25% protein reduction at 400 mJ/cm^2 from the average of two gels. Protein degradation of 25% seems high relative to the visual interpretation of the gel. This experiment merits replication. Duplicate results were not ready at the time of publication.

a)

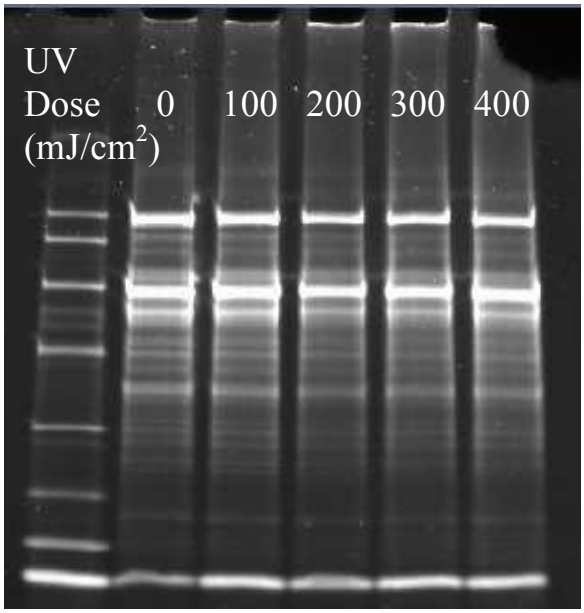

b)

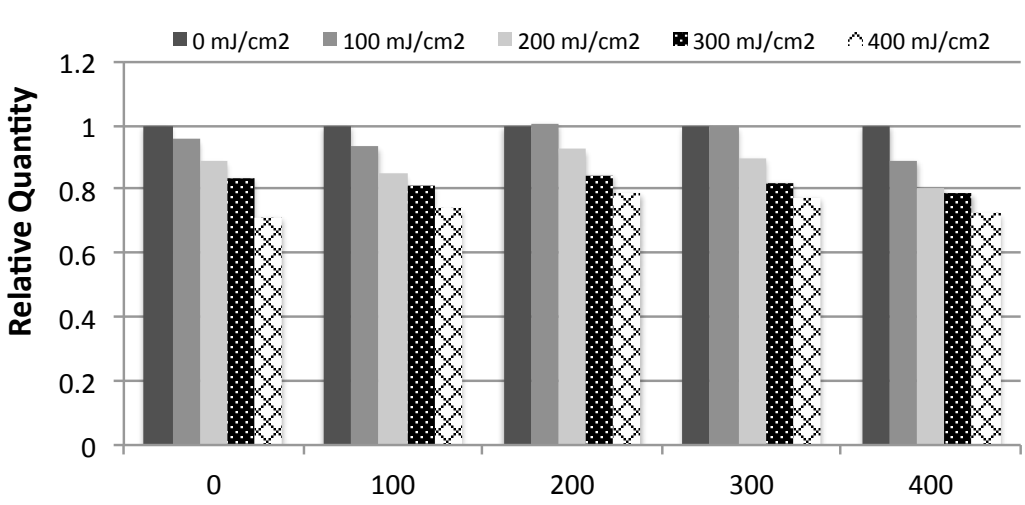

Figure 5.6. Adenoviral protein damage induced from UV light emitting at 260 nm for 100, 200, 300, and 400 mJ/cm^2, shown in a SDS-PAGE gel (a) and from the corresponding quantification (b).

Lastly, the damage to adenoviral proteins from a 280 nm UVC LED is shown in Figure 5.7. Protein degradation from the LEDs at 280 nm was very similar to that detected at 260 nm. The protein damage is characterized visually by slight degradation of the protein bands, blending of different molecular weights, and an increasing protein signal in the SDS-PAGE gel wells. The image densitometry quantification; however, showed no protein degradation. In fact, an increase in relative quantity of proteins was detected at 400 mJ/cm^2, most likely due to a relatively low reference protein signature at that dose. This, again, highlights the inherent error in the SDS-PAGE assay. These results also merit replication; however, duplicate results were not yet available at the time of publication.

The protein damage results at 280 nm were unexpected. In general, proteins have a relative peak UV absorbance near 280 nm due to the absorbance of aromatic amino acids such as tryptophan, tyrosine, and cystine, the Cys-Cys disulphide bond (Pace et al., 1995). In fact, purified proteins are often measured using the UV absorbance of a sample at 280 nm relative to its absorbance at 260 nm to determine their purity or concentration relative to known amounts of protein (Aitken and Learmonth, 2002; Simonian and Smith, 2006). Therefore, more protein degradation was expected in adenovirus 2 at 280 nm. The 280 nm LEDs did not appear to contribute to significantly enhanced protein damage relative to 260 nm. One possible explanation is that at 280 nm, the absorbance of amino acids is an order of magnitude lower than DNA absorbance (Harm, 1980). Also, the relative peak absorbance of adenovirus 2 is closer to 270 nm than 280 nm. The 270 nm UV source, a deuterium lamp with bandpass filters was not used to further analyze protein damage at that wavelength due to the long exposure times required.

a)

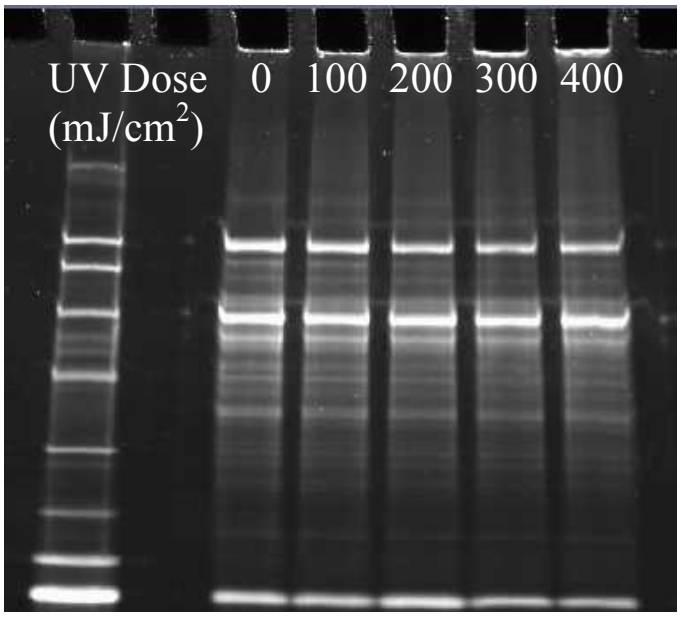

b)

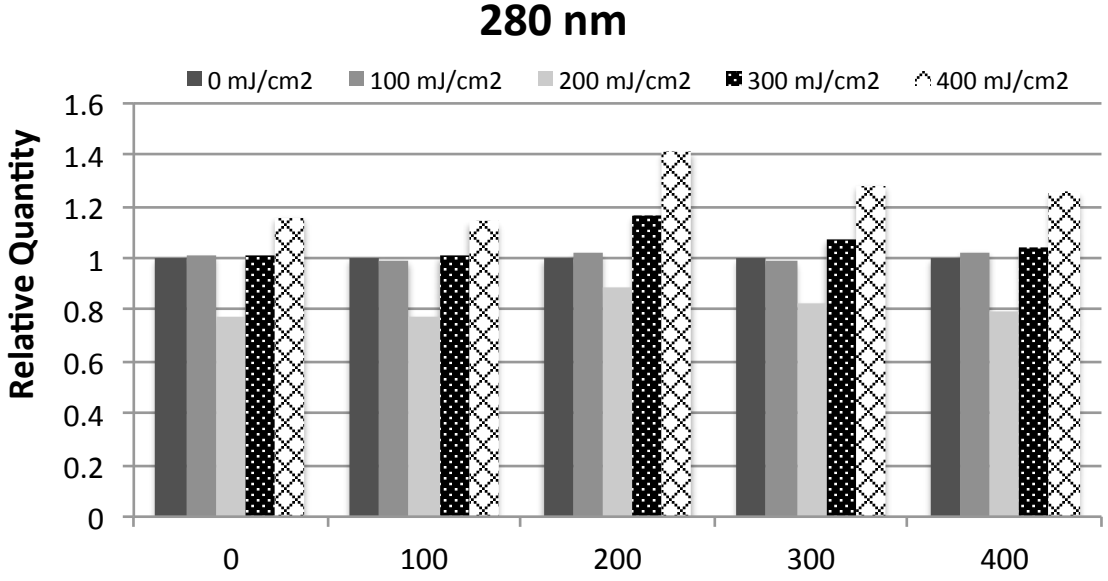

Figure 5.7. Adenoviral protein damage induced from UV light emitting at 280 nm for 100, 200, 300, and 400 mJ/cm^2, shown in a SDS-PAGE gel (a) and from the corresponding quantification (b).

The SDS-PAGE assay has limitations, due to its inherent error, which has not yet been measured in conjunction with these experiments. Nevertheless, the assay was sufficient to show undeniable protein damage to the adenovirus 2 hexon, penton, minor capsid, fiber, and core proteins, primarily at wavelengths below 240 nm. This research supplements previous work (Eischeid, 2011; Beck et al., 2014) to show without a doubt that the low wavelengths below 240 nm are causing the protein damage that is ultimately responsible for the enhanced efficacy of medium-pressure UV light over low-pressure UV light.

CHAPTER 6

OPTIMIZING PATHOGEN INACTIVATION AT LOW ENERGY COST WITH A TAILORED, MULTIPLE-WAVELENGTH UV LED UNIT

The research discussed in Chapters 2 through 4 informed the design of a tailored, multiple-wavelength UVC LED unit for comparison with UV inactivation from other polychromatic UV sources. The chapter evaluated the unit, which combined LEDs emitting at 260 nm and 280 nm for its efficacy at inactivating the common water-borne pathogens, fecal indicators, and surrogates *E. coli*, MS2 Coliphage, adenovirus 2, and *Bacillus pumilus* spores. Inactivation by 260 nm and 280 nm LEDs separately and simultaneously was compared with the efficacy of the medium-pressure (MP) and low- pressure UV lamp.

The UVC LEDs were competitive with mercury vapor lamps for water disinfection; however, at the present time, they require more energy per log reduction of MS2, adenovirus 2, and *B. pumilus* spores. The 280 nm UV LED was more efficient (per log reduction) for inactivating *E. coli*.

The combination of the 260 nm and 280 nm UVC LED wavelengths was also evaluated for potential synergistic effects. For all four microorganisms and viruses tested, no dual-wavelength synergy was detected in bacterial or viral inactivation nor in damage to the DNA or RNA.

The work described in this chapter is being submitted for publication. (Beck, S.E., Ryu, H., Boczek, L., Cashdollar, J.L., Jeanis, K.M., Rosenblum, J.S., Lawal, O.R., Linden, K.G. 2015. Optimizing pathogen inactivation at low energy cost with a tailored, multiple-wavelength UV LED unit.)

6.1 INTRODUCTION

Ultraviolet (UV) light emitting diodes (LEDs) are an emerging technology for water and wastewater disinfection. Deep UV LEDs emitting UVC irradiation have proven effective in inactivating bacterial, viral and protozoan pathogen surrogates (Bowker et al., 2011) and have been demonstrated for point-of-use water disinfection (Chatterley and Linden, 2010). UV LEDs have enormous potential since they are smaller, lighter, and have lower power consumption than traditional mercury vapor lamps used for ultraviolet light disinfection (Vilhunen 2010). Given the small size of the UV LEDs, less than 1 mm^2, multiple diodes can emit from different angles as opposed to traditional collimated beam sources. As a result, they were less affected by the presence of particles than traditional UV sources (Crook et al., 2014). Additionally, UV LEDs are mercury-free and provide the capability to be turned on or off instantaneously.

Considerable research is being employed to evaluate UVC LEDs at various wavelengths for pathogen inactivation. Several studies have evaluated the efficacy of germicidal irradiation from UV LEDs emitting in relatively narrow bandwidths at or near 255 nm, 265 nm, 269 nm, and 275 nm, and 280 nm for inactivating *E. coli* (Oguma et al., 2003; Bowker et al, 2011; Chatterley and Linden, 2010; Vilhunen, 2009). At least two studies evaluated UVC LEDs emitting at or near 250 nm, 270 nm, and 282 for inactivating *Bacillus subtilis* spores (Morris, 2012; Wurtele et al., 2011). Another study evaluated UV LEDs emitting at 255 nm and 275 nm for inactivating coliphage MS2 and T7 (Bowker et al., 2011).

As an emerging technology, LEDs are constantly improving in energy efficiency, lifespan, and affordability, all of which will make them more practical for widespread use (Ibrahim, 2014). A recent (2014) analysis on the economic viability of UV LEDs predicts “water disinfection systems employing UV LEDs should start to appreciably penetrate the residential

and industrial market within the next 5 years" (Ibrahim et al., 2014). With the rapid research and development in UV LED technology, broad potential exists for its use as a sustainable, point-of-use disinfection technology in drinking waters through photovoltaic (PV) powered systems, such as that previously suggested by Lui, G.Y. et al. (2014).

Among the primary advantages of UV LEDs is that given their compact size, LEDs of different outputs can be combined to optimize pathogen inactivation; and, given their low power consumption, this inactivation can potentially occur at a very low energy cost. Some UV LED disinfection studies have evaluated the combination of multiple UV wavelengths on pathogens and non-pathogenic surrogate microorganisms used for research purposes or for validating UV disinfection systems. Chevremont et al. (2012) combined LEDs emitting in the UVA and UVC range to try and achieve both microbial disinfection and chemical degradation for wastewater treatment. Oguma et al. (2013) combined LEDs emitting in the germicidal range, measuring their collective inactivation of *E. coli.*

Tailoring multiple wavelengths is a way to optimize inactivation of target pathogens. Ideally, a tailored UV disinfection system would target bacteria and viruses by combining a wavelength from the dominant germicidal region (250 - 280 nm) with a wavelength from the polypeptide absorbance region below 240 nm (i.e. 230 nm). This type of combination would simulate UV emissions from a medium-pressure mercury lamp, which has been shown to be more effective than low-pressure UV lamps at inactivating certain pathogens (Hijnen et al., 2006; Malley et al., 2004). In particular, the polychromatic emission from MP UV lamps has been shown to be more effective than LP UV lamps against adenovirus due to increased damage to viral proteins (Eischeid and Linden, 2011; Linden, K.G. et al., 2007; Beck et al., 2014). Although, 230 nm LEDs are not at a practical stage of development for this application, 280 nm

LEDs are widely available and 280 nm is the location of a relative peak UV absorbance of proteins (Jagger, 1967).

For this research, the authors utilized a UV disinfection unit that combined UV LEDs emitting at 260 nm, which is the relative peak absorption of DNA and RNA, with UV LEDs emitting at 280 nm, the relative peak absorption of proteins, to target genomic and protein-based regions of bacterial and viral organisms. It was hypothesized that this polychromatic UVC LED system could attain similar levels of bacterial and viral inactivation as the medium-pressure (MP) mercury vapor lamp, but at a much lower energy cost. The efficacy of a germicidal UV system combining 260 nm and 280 nm LEDs was compared with the efficacy of an MP UV system and a low-pressure (LP) UV system, for inactivating *E. coli*, MS2 coliphage, adenovirus 2, and *Bacillus pumilus* spores. *E. coli* was chosen as a common microorganism and fecal indicator, frequently used to evaluate UV LED disinfection systems. Adenovirus 2 was chosen because it is known as the most resistant pathogen to UV irradiation, which drives the UV disinfection requirements for viruses (USEPA, 2006) and also as a virus that has demonstrated enhanced inactivation due to protein damage (Eischeid and Linden, 2011; Beck et al., 2014). MS2 coliphage and *B. pumilus* spores were chosen because of their use in validating polychromatic UV disinfection systems for obtaining adenovirus credit.

Also within this study, inactivation of microorganisms and viruses by 260 nm and 280 nm light emitted separately from the UV LED unit was summed together and compared with inactivation from both wavelengths combined to investigate potential synergistic effects. To provide insight into mechanisms of possible dual-wavelength synergy, the direct genome damage of adenovirus 2 and MS2 coliphage was also quantified.

6.2 MATERIALS AND METHODS

6.2.1 UV Irradiations

Bacterial and viral suspensions were irradiated with a bench-top UVC LED unit supplied by Aquionics (Erlanger, KY). The unit, a prototype of a turnkey UV-C LED CB system from Dot Metrics Technologies (Charlotte, NC) was set up in a collimated beam apparatus similar to that described in Bolton and Linden (2003). Microorganism and virus suspensions were exposed to 260 nm light, 280 nm light, and the combination of 260 nm and 280 nm together (260|280). The LED spectra (Figure 6.1a), measured with a Maya 2000 Pro spectrometer (Ocean Optics, Dunedin, FL) exhibited peak wavelength emissions at 259.6 nm and 276.6 nm, with full width at half maximum (FWHM) bandwidths of 12.6 nm and 9.8 nm respectively. When the 260|280 nm LEDs were illuminated simultaneously (Figure 6.1b), the 260 nm LEDs comprised 47.5% of the total irradiance and the 280 nm LEDs comprised the remaining 52.5%. These emission spectra are compared to that from the medium-pressure mercury vapor lamp used (Rayox, 1kW, Calgon Carbon Corporation, Pittsburgh, PA) as illustrated in Figure 6.1c.

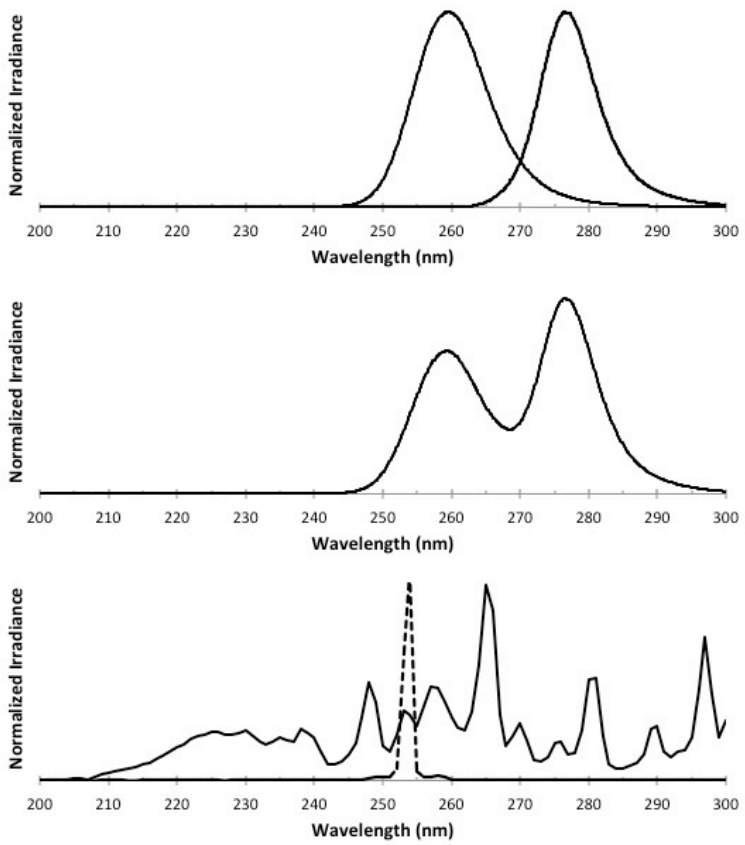

Figure 6.1. Emission spectra from a) the 260 nm and 280 nm LEDs when illuminated separately, b) the unit with 260 nm and 280 nm LEDs illuminated together (260|280) and c) a medium-pressure (solid) and low-pressure (dashed) mercury vapor lamp.

At each wavelength, four collimated beam exposures were conducted in triplicate to generate a dose response curve up to 3-log inactivation for each microorganism. Stirred suspensions of 5 mL (0.6 cm sample depth) were irradiated in 3.5 cm diameter dishes at a distance of 4 cm from the UVC LED source. Irradiance was measured at the water surface with an IL-1700 radiometer, SED 240 detector, and W-diffuser (International Light, Peabody, MA). Incident LED irradiance varied from 0.19 to 0.55 mW/cm^2. For the MP UV work, incident irradiance ranged from 0.35 – 1.17 mW/cm^2. For the LP UV exposures, incident irradiance ranged from 0.3 – 0.75 mW/cm^2.

Average UV doses for the collimated beam tests were determined as described previously (Bolton and Linden, 2003), adjusting for reflection off the water surface, UV absorption (Cary

100 spectrophotometer, Agilent Technologies, Santa Clara, CA), depth of the water sample, as well as the uniformity of the distribution of light across the surface of the sample. Petri factors ranged from 0.9 to 0.95 for the UV LED work and were consistently 1.0 for the MP UV and LP UV exposures.

The UVC LEDs and medium-pressure UV lamp are each polychromatic light sources. As such, the UV dose accounted for the relative lamp emission (RLE) of the light source (as measured by the Maya 2000 Pro spectrometer) and the sensitivity of the radiometer used to measure irradiance (from the radiometer calibration data). For the UV LED exposures, the RLE and radiometer sensitivity were taken relative to the weighted average wavelength of each LED (i.e. 261 nm for the 260 nm LED, 278 nm for the 280 nm LED, and 271 nm for the 260|280 nm LED combination). For the MP UV lamp, the RLE and radiometer sensitivity were taken relative to 254 nm.

For the LED synergy calculations, UV doses for the 260 nm, 280 nm, and 260|280 nm combined irradiation were determined using calculations of average irradiance throughout the water sample. When comparing the LED efficacy to MP UV, the average irradiance was weighted germicidally, based on the absorption of DNA as is standard for polychromatic UV sources (Linden and Darby, 1997; USEPA, 2006).

Irradiations were conducted in triplicate, at room temperature, with the LED unit containing a closed-loop thermal management system to regulate internal UV LED temperatures. Immediately after exposure to the UV LEDs or the MP or LP UV sources, the irradiated samples were refrigerated at 4^{o}C prior to shipping to the Environmental Protection Agency (adenovirus 2 and *B. pumilus* spores), or prior to their analysis at the University of Colorado Boulder on the

same day (*E. coli* and MS2). An aliquot of each *E. coli*, MS2 coliphage, and adenovirus 2 sample was also placed in a -80^{o}C freezer for subsequent DNA or RNA analysis.

6.2.2 Synergy

To test synergy, the dose response results from the 260 nm LEDs were multiplied by 0.475, the percentage that the 260 nm LEDs contributed to the total irradiance by the 260|280 nm LED unit. The dose response results from the 280 nm LEDs were multiplied by 0.525, their percentage of total irradiance from the combined unit. Those results were summed together and compared with the dose response results from the 260|280 nm LEDs combined using a two-tailed independent paired t-test, where significance was defined as less than 0.05.

6.2.3 Energy

The electrical energy per order, E_{EO} is a parameter for characterizing the electrical energy efficiency of disinfection systems. Described previously (Bolton and Stefan, 2002; Sharpless and Linden, 2005), the E_{EO} defines the amount of energy (Ws) required to decrease the concentration of a contaminant or microorganism by one order of magnitude in a known volume of water.

$$E_{EO} = \frac{P}{k_D \times I} \qquad [1]$$

where P is the power in Watts, k_D is the fluence-based inactivation constant (cm^2/mJ) and I is the germicidal irradiance (mW/cm^2), measured at a distance of 4 cm from the light source. The known volume of water was the 5 ml sample used for all of the experiments. Extrapolating the results from this small-scale laboratory experiment for application in a large-scale water treatment facility was beyond the scope of this work. The current, voltage draw, and power of

the LED unit in each configuration as well as the MP UV and LP UV lamps (Table 6.1) were measured at the outlet using a Kill-A-Watt electricity monitor (P3 International, New York, NY).

Table 6.1. Energy draw for the three UV LED configurations, the MP UV lamp, and the LP UV lamp used.

UV Source	Voltage (V)	Current (A)	Power (W)
260 nm LED	119.5	0.33	39.4 W
280 nm LED	119.5	0.26	31.1 W
260|280 nm LED	119.5	0.55	65.7 W
MP UV Lamp	114.0	9.43	1075 W
LP UV Lamp	117.5	1.22	143.4 W

In the case of adenovirus 2 and *Bacillus pumilus*, where the dose response results either followed a linear inactivation that did not originate at the origin or when the data was best fit with a 2nd order polynomial curve, the electrical energy for a specific log reduction, N, of each sample, $E_{EL,N}$, was calculated. The dose required for obtaining that log reduction, D_N, was substituted in Eqn. 1, above, as the inverse of the fluence-based inactivation rate constant:

$$E_{EL,N} = \frac{D_N \times P}{I} \quad [2]$$

It's important to note that the electrical energy per order, E_{EO}, and the electrical energy for a specific log reduction $E_{EL,N}$, for the exposed samples both apply to the current state of the disinfection technologies compared. Energy efficiencies are continuously improving, particularly for the developing UV LED technology. Following trends of visible LEDs, a UV LED with a 2% wall plug efficiency in 2010 is projected to have a 75% wall plug efficiency in 2020 (Ibrahim et al., 2014). Similarly, a UV LED outputting 0.36 mW in 2010 is expected to output 675 mW by 2020 (Ibrahim et al., 2014).

6.2.4 Propagation and Enumeration

Escherichia coli

A frozen stock culture of Escherichia coli K12 (ATCC #29425) was thawed and inoculated into 50 mL of sterile tryptic soy broth (TSB) and placed within a shaking incubator at 37 ^{o}C for 24 hours. One mL of the overnight E coli culture was then passed to a fresh 100 mL of TSB and incubated until log phase, determined by optical density. The cells were then centrifuged at 5,000 rpm for 5 min, with the supernatant being discarded, and the pellet being re-suspended in sterile phosphate buffered saline (PBS), repeated three times. This cell suspension was then diluted with PBS to achieve a working stock solution of approximately 10^6 CFU/mL.

Following *E. coli* irradiations, a sample was removed from the Petri dish and stored at 4 ^{o}C for the infectivity analysis with another sample taken and stored at -20 ^{o}C for DNA analysis. The sample for infectivity analysis was serially diluted in PBS. Within 2 hours of the *E. coli* irradiations, the samples were enumerated using a spread plate technique. Volumes of 100 uL of the diluted sample were spread on tryptic soy agar (TSA) and incubated inverted at 37 ^{o}C for 18 to 24 h. Samples were plated in duplicate and plates yielding 0 to 200 colonies were included in the analysis.

MS2 Coliphage

For MS2 coliphage, tryptic soy broth supplemented with ampicillin/streptomycin was inoculated with log-phase host bacteria, *E. coli* F amp (ATCC/700891), and an aliquot of MS2 Coliphage (ATCC/15597-B1). The broth was incubated with constant shaking for 5 hours at 37 ± 0.5°C. After the bacterial debris was removed by centrifugation, the clarified supernatant was decanted to sterile containers and stored at -20 °C.

The coliphage stock was diluted to a working concentration of 5 x 10^6 pfu/mL. After exposure to UV irradiation, samples were serially diluted and enumerated following EPA double agar layer Method 1601 (USEPA, 2001). Briefly, 100 uL of each dilution were added to a soft agar containing the log-phase host bacteria. The inoculated soft agar was poured over an agar plate and allowed to harden. Plates were inverted and incubated at 37 ± 0.5°C for 16-24 hr. Viral plaques were counted to determine the concentration of coliphage in the stock culture. Each sample was analyzed in duplicate.

Adenovirus

Human Adenovirus 2 was obtained from the American Type Tissue Collection (ATCC VR-846, Manassas, VA) and propagated in A549 human lung carcinoma cells (ATCC CCL-185). Briefly, A549 cells were planted in 175 cm^2 vented tissue culture flasks (Greiner, Monroe, NC) in Dulbecco's Minimum Essential Medium (DMEM) (Thermo Fisher Scientific Inc., Waltham, MA) supplemented with 10% fetal calf serum (Thermo Fisher Scientific Inc.), and maintained in 5% (vol/vol) CO_2. The cells were infected with stock adenovirus 2, and the cells were incubated for up to two weeks or until cytopathogenic effects (CPE) were observed. Cells underwent three freeze-thaw cycles and a portion of the cell lysate was passaged onto fresh A549 cells for further propagation. Cell lysates from all passages were combined to obtain maximal viral stock. Lysates were centrifuged at 2500 × g for 30 minutes to remove cell debris. The supernatant containing virus was then centrifuged at 10,000 × g for 10 minutes to remove any remaining small cellular debris. In order to remove any potential viral clumps, remove any remnant of growth media, and further purify the viral stock, the virus supernatant was further concentrated using celite, as described by McMinn et al. (2012). Following celite concentration,

viral stocks were further concentrated using 30 kDa MWCO Vivaspin-20 ultrafilters (Sartorius-Stedim, Aubagne, France) as described previously (Cashdollar et al., 2013). This resulted in stock titers of 10^{10} MPN/ml for use in the system evaluation. Viral stocks were stored at -80°C until UV exposure experiments.

Adenovirus was enumerated using Integrated Cell Culture Quantitative PCR (ICC-qPCR), modified from Gerrity et al. (2008), which quantifies infectious adenoviruses from viral DNA harvested from a cell culture monolayer. Test cultures for ICC-qPCR were grown in 24-well cell culture trays (Thermo Fisher Scientific Inc.) in the same media as described above. Sample inoculation procedures were followed as described above for the total culturable virus assay (TCVA) with the exception of adding 100 µl of inoculum to each of three wells per dilution. In addition to post-UV exposure samples, five 10-fold serial dilutions from virus stock (i.e., 10^5 to 10 MPN/100 µl) were inoculated to four wells per dilution for generating ICC-qPCR standard curve. The trays were then incubated for 48 hr at 37°C in a 5% CO_2 incubator. After incubation, the cell monolayers were washed five times with 1 mL of PBS to remove extracellular viruses and then harvested by scraping after a freeze-thaw cycle. These wash steps would not remove non-infectious virus attached to cells completely, which could cause false positive signals. To overcome this, four rinse control replicates were processed along with each set of ICC-qPCR standards, and their mean copy numbers were subtracted for respective samples. Viral DNA from cell harvest with infectious viruses was extracted and purified with the DNeasy 96 Blood and Tissue Kit (QIAGEN, Valencia, CA) according to the manufacturer's instructions. DNA extracts were stored at -20°C until the qPCR assay.

The ICC-qPCR standard curve was constructed using five 10-fold serial dilutions from human adenovirus 2 stock as described above. Briefly, based on the quantities resulting from the

ICC-qPCR assay (x) and the original number of infectious adenovirus 2 spiked into each dilution (y), the regression analysis was performed for determining unknown parameter (a) in the standard curve (i.e., y=ax+b). The concentrations of infectious adenovirus 2 in pre-inoculation samples (i.e., the dependent variable, y=the original virus concentration prior to replication) were estimated using the regression equation with ICC-qPCR quantities (i.e., the independent variable, x). The estimated y values were used to calculate log inactivation of human adenovirus 2.

Bacillus pumilus

Bacillus pumilus (ATCC 27142) was obtained from Mesa Laboratories (Omaha, NE). Spores were produced by inoculating vegetative cells of *B. pumilus* into half strength (0.5x) Columbia broth (Remel, Lenexa, KS) supplemented with 1 mM of $MnSO_4$. Cultures were then incubated at 35 °C for five days with shaking at 100 rpm. Spores were purified by gradient separation using 58 % (v/v) RenoCal-76 (Bracco Diagnostics, Princeton, NJ). Spore preparations were stored in 40% (v/v) ethanol at 4 °C until UV experiments were conducted.

Prior to UV exposure, spores were washed with Butterfields buffer (Hardy Diagnostics, Santa Clara, CA) 3 times by centrifugation (5184 x g, 15 min) as outlined in Standard Method 9050.C.1.a (APHA, 2005). Spores were resuspended and diluted with Butterfield's buffer for a final, working concentration of 10^5 CFU/mL. After UV exposure, samples were held at 4 °C and then shipped in a chilled container to the U.S. EPA for analysis.

Spore enumeration followed the membrane filtration method outlined in Standard Method 9218B section 3.C (APHA, 2005). Filters were placed onto nutrient agar (BD, Sparks, MD) supplemented by trypan blue dye and incubated at 35 °C for 18-24 hr.

6.2.5 Synergistic Damage to the Viral DNA and RNA

This study also measured potential synergistic damage to the viral genomes after exposure to UV irradiation from the combined 260|280 nm emissions.

DNA damage of adenovirus was measured as previously described using a long-range quantitative polymerase chain reaction (LR-qPCR) procedure to analyze damage to a 1.1 kilobase pair long fragment (Beck et al., 2014). The LR-qPCR method, which yields the log reduction in amplification of the adenoviral genome, was previously correlated to adenovirus inactivation as measured by cell culture infectivity at 254 nm (Rodriguez et al., 2013).

RNA damage of MS2 coliphage was also measured as described previously using a Reverse Transcription (RT) PCR method (Beck et al, in press). The method, adapted from previous publications (Simonet and Gantzer, 2006; Ogorzaly and Gantzer, 2003) analyzed damage to an 1185 base pair fragment. The results, which reflected log reduction for each amplicon, were adjusted to apply to the whole genome using a calculation originating from Pecson et al. (2011); this was detailed specifically for this procedure in Beck et al. (in press). As described above, potential synergy was measured by comparing the log reduction in amplification after exposure to the 260|280 nm LED unit with the sum of log reduction in amplification from the respective contributions of the 260 nm (47.5%) and 280 nm (52.5%) LEDs. A two-tailed independent paired t-test was used to detect significance (< 0.05).

6.2.6 Statistical Analysis

For *E. coli* and MS2 coliphage, log inactivation was calculated as $\log (N_o/N)$ where N_o is the number of colony forming units, CFU/mL, or plaque forming units, PFU/mL, of the unirradiated control and N is the CFU/mL or PFU/mL for each sample. Dose response data was

fit linearly and the fluence-based inactivation rate constant, k_D (cm^2/mJ) was determined as follows:

$$\boldsymbol{log \frac{N_0}{N_t} = k_D F_\lambda} \quad [5]$$

where N_t is the CFU/mL at time, t, and F is the fluence at the given wavelength, λ, determined as described above. Data for *B. pumilus* spores also exhibited linear inactivation kinetics and was fit with the above equation; however, *B. pumilus* spore dose response showed tailing and there was therefore a constant term included in the equation above. Adenovirus data exhibited curvature and was therefore fit with a second order polynomial. All data was collected in triplicate and is presented with error bars representing one standard deviation.

6.3 RESULTS AND DISCUSSION

6.3.1 E. coli

Dose response results from the collimated beam trials with *E. coli* (Figure 6.2a) were similar for all five sources. The curves showed tailing at high doses, due, in part, to the starting concentration of *E. coli* and the dilutions used for the experiments. UVC LEDs at 260 nm, 280 nm and combined 260|280 nm as well as the LP UV and MP UV lamps attained over 3-log reduction of *E. coli* at 12 mJ/cm^2 or lower. The fluence-based inactivation rate constants, k_D, are given in Table 6.2. The k_D of 0.31 cm^2/mJ at 280 nm was very similar to that of 0.29 cm^2/mJ reported by Oguma (2013). In this study, the 280 nm LED was more effective than the 260 nm LED, which was unexpected given that 260 nm is closer than 280 nm to the relative peak of the UV action spectrum and the relative peak of the UV absorbance of a 0.8 mm layer of *E coli* on an agar surface (Gates, 1930). Bowker et al. (2011) reported a similar occurrence, that a 275 nm LED was more effective than a 255 nm LED. One possible explanation is that the 275 nm LED

(or 280 nm LED in this case) could have caused damage to repair enzymes (Kalisvaart, 2004). Another potential cause is that the proteins could be absorbing the photons and transferring the energy to the DNA. The results from the MP UV and LP UV inactivation of *E. coli* corresponded with a previous study where LP UV and MP UV *E. coli* inactivation rates were equal and 3-log inactivation was reached at 10-11 mJ/cm^2 (Guo et al., 2009).

The results for the UVC LED synergy experiment with *E. coli* are shown in Figure 6.2b. When the dose response results from the 260 nm and 280 nm LEDs are weighted by their respective average irradiance percentages and summed together, visually, they equal the dose response results of the 260|280 nm LEDs combined. Statistically, using a two-tailed paired t-test the results show that the differences are not statistically significant ($p > 0.05$) at all UV doses tested of 4 mJ/cm^2 ($p = 0.16$), 8 mJ/cm^2 ($p = 0.58$), 12 mJ/cm^2 ($p = 0.25$), and 16 mJ/cm^2 ($p = 0.16$). This indicates that there was no synergy from the two units acting together on *E. coli* at those doses.

The electrical energy per order, E_{EO} for *E. coli* inactivation of the three LED configurations tested are also given in Table 6.2 in comparison with the E_{EO} for MP UV and LP UV. The technology with the lowest E_{EO}, corresponding to the least amount of energy required per log reduction of *E. coli*, was the LP UV lamp, followed by the 280 nm LED, the MP UV lamp, the 260|280 nm LED combination and lastly the 260 nm LED.

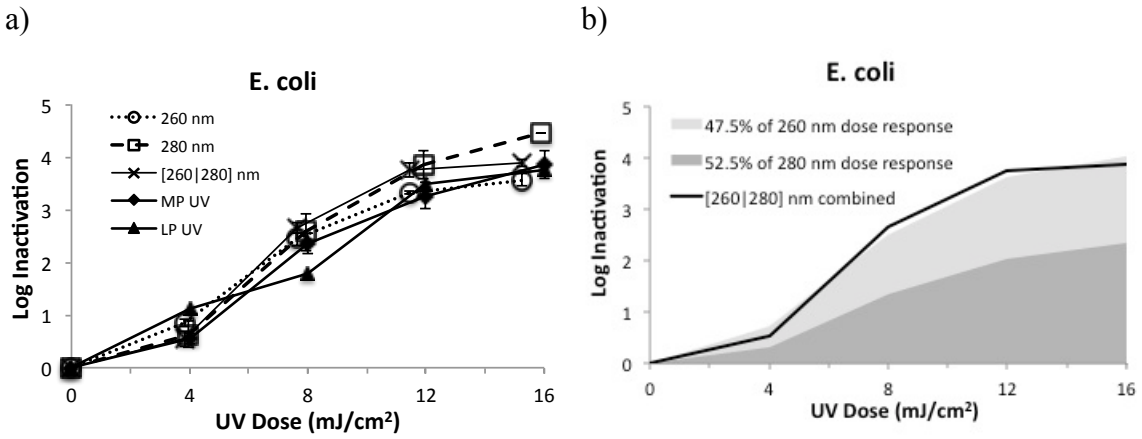

Figure 6.2. a) Dose response of *E. coli* to UV irradiation from UV LEDs emitting at 260 nm, 280 nm, 260/280 nm combined, compared with its dose response to MP and LP UV light. b) Dose response of a 260|280 nm combined LED unit on inactivating *E. coli* compared with the sum of its dose response from exposure to the LEDs separately.

Table 6.2. Inactivation rate constants and electrical energy per order (E_{EO}) of *E. coli* by the five UV sources.

UV Source	k_D (cm^2/mJ)	Germicidal Irradiance (mW/cm^2)	E_{EO} (Ws)
260 nm LED	0.29	0.132	1,031
280 nm LED	0.31	0.245	409
260|280 nm LED	0.32	0.349	589
MP UV Lamp	0.27	8.33	478
LP UV Lamp	0.27	8.82	60

6.3.2 MS2 Coliphage

Dose response results of MS2 coliphage (Figure 6.3.a) to the UVC LEDs and LP and MP UV lamps exhibited linear inactivation kinetics; the data was fit linearly yielding the fluence-based inactivation rate constants in Table 6.3. The 260 nm LEDs were more effective at inactivating MS2 than the 280 nm LEDs, which is expected given that the MS2 RNA has a relative peak UV absorbance near 260 nm and that the MS2 action spectrum also peaks near 260 nm (Rauth, 1965, Mamane-Gravetz et al., 2005). Both the RNA and the MS2 virus are more sensitive to UV light at 260 nm than at 280 nm (Strauss, 1963; Mamane-Gravetz et al, 2005).

The combination of 260|280 nm LEDs together was less effective against MS2 than the 260 nm LED and more effective than the 280 nm LED; which was also expected.

The dose response of MS2 coliphage to the 260 nm LED yielded an inactivation rate coefficient, k_D, of 0.072 cm^2/mJ, which corresponds to a 2-log dose at 27.8 mJ/cm^2. This was much lower than the response of MS2 to a 255 nm LED, in a past study, which displayed 2-log reduction at a dose of approximately 50 mJ/cm^2 (Bowker et al., 2011). However, these results agreed very well with the results from a recent study of MS2 inactivation by monochromatic 260 nm irradiation from a tunable laser, which achieved 2-log reduction at a UV dose in between 24 and 30 mJ/cm^2 (Beck et al., 2015. Chapter 2).

The dose response of MS2 coliphage to the 280 nm LED yielded a k_D of 0.052 cm^2/mJ, corresponding to a 2-log dose at 38.5 mJ/cm^2. This was lower than the response of MS2 to a 275 nm LED described previously, in which 2-log reduction occurred at a dose of approximately 55 mJ/cm^2 (Bowker et al., 2011). However, it agreed well with the results from the study of MS2 inactivation by a tunable laser emitting at 280 nm, which achieved 2-log reduction at a UV dose in between 38 and 53 mJ/cm^2. One factor accounting for a difference between this study and the previous LED study with MS2 are the differences in UV irradiation between, for example, 255 nm and 260 nm and between 275 nm and 280 nm. Another factor could be that the previous study treated the LEDs as monochromatic sources, determining the dose using average irradiance whereas this study treated the UVC LEDs as polychromatic sources and weighted the average irradiance by the absorbance of DNA, which slightly alters the dose applied.

The dose response of MS2 coliphage to MP UV irradiation was almost identical to the response from the combined 260|280 nm irradiation; both yielding a k_D of 0.061 cm^2/mJ, which corresponds to 2-log reduction at a UV dose of 32.8 mJ/cm^2. The k_D for MP UV was lower than

that reported of 0.122 cm^2/mJ (Hijnen et al., 2006; Malley et al., 2004), requiring a higher dose for 2-log inactivation than those previously shown of 18 mJ/cm^2 – 20 mJ/cm^2 (Malley et al., 2004; Beck et al., 2015 (Chapter 2)).

The results for the UVC LED synergy experiment with MS2 coliphage are shown in Figure 6.3b. When the dose response results from the 260 nm and 280 nm LEDs are weighted by their respective average irradiance percentages and summed together, visually, they equal the dose response results of the 260|280 nm LEDs combined. Statistically, using a two-tailed paired t-test the results show that differences were not statistically significant at 15 mJ/cm^2 ($p = 0.144$), 30 mJ/cm^2 ($p = 0.82$), and 60 mJ/cm^2 ($p = 0.64$). The results were statistically different at 45 mJ/cm^2 ($p = 0.03$), but with the sum of individual irradiations being slightly larger than the 260|280 nm irradiations together. This indicates that there was no synergy from the two units acting together on MS2 at those doses.

The technology with the lowest electrical energy per order, E_{EO}, corresponding to the lowest amount of energy required per log reduction of MS2 (Table 6.3) was the LP UV lamp, which was an order of magnitude more efficient than the other sources. Despite the enhanced energy efficiency of the UV LEDs, given the current state of the technology, the medium-pressure UV lamp was more energy efficient at inactivating MS2, followed by the 280 nm LED, the 260|280 nm LED, and the 260 nm LED.

a) b)

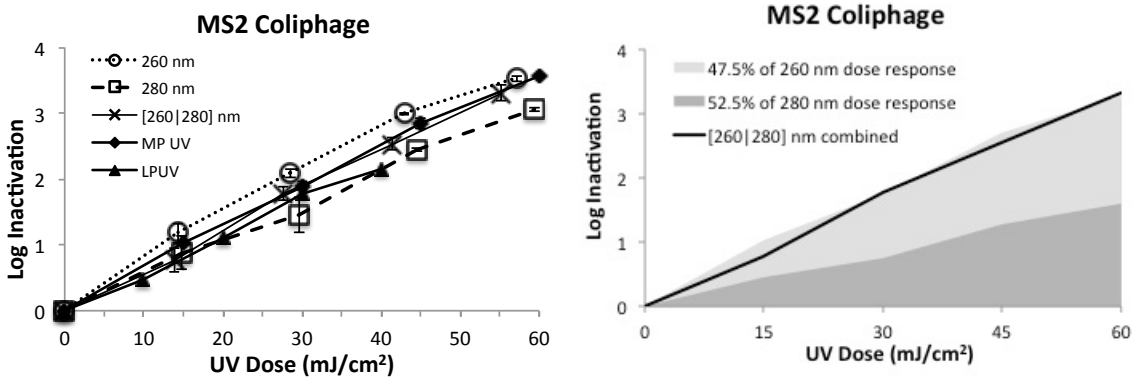

Figure 6.3. a) Dose response of MS2 coliphage to UV irradiation from UV LEDs emitting at 260 nm, 280 nm, 260/280 nm combined, compared with its dose response to MP and LP UV light. b) Dose response of a 260|280 nm combined LED unit on inactivating MS2 coliphage compared with the sum of its dose response from separate LED exposures.

Table 6.3. Inactivation rate constants and electrical energy per order (E_{EO}) of MS2 coliphage by the five UV sources.

UV Source	k_D (cm^2/mJ)	Germicidal Irradiance (mW/cm^2)	E_{EO} (Ws)
260 nm LED	0.072	0.141	3,884
280 nm LED	0.052	0.253	2,362
260|280 nm LED	0.061	0.374	2,881
MP UV Lamp	0.061	8.07	2,184
LP UV Lamp	0.057	8.71	289

6.3.3 Adenovirus

Dose response results of adenovirus 2 to the UVC LEDs emitting at 260 nm, 280 nm, and 260|280 nm combined (Figure 6.4a) showed 3.25- to 3.5-log reduction at UV doses between 85 and 90 mJ/cm^2 and over 4-log inactivation between 114 to 119 mJ/cm^2. This is a lower dose than that required for 3-log reduction in the literature. When irradiated with a tunable laser emitting at 260 nm, 103.4 mJ/cm^2 was required for 3-log inactivation and 137.9 for 4-log (Beck et al., 2014). At 280 nm, 93.8 and 125 mJ/cm^2 were required for 3- and 4-log reduction, respectively (Beck et al., 2014). The discrepancy could be due to the differences in the assay used between cell culture and the integrated cell culture PCR. They could also be a result of the light source.

The literature values in Beck et al. (2014) were produced by irradiating with a monochromatic (< 1 nm) UV light source whereas the LEDs have a full width at half maximum (FWHM) of approximately 10-12 nm. Past research has shown polychromatic irradiation to be more effective at inactivating a microorganism or virus than monochromatic light emitting at the weighted average wavelength (Wright et al., 2007; Mamane-Gravetz et al., 2005).

The most notable difference between the three LED curves, was the higher log reduction from the 280 nm LED at the highest dose tested. The dose response from the three trials was on the same order of magnitude for the first three doses, which were just below 30, 60, and 90 mJ/cm^2. However, at the highest dose tested, between 114 and 119 mJ/cm^2, the 280 nm LED caused significantly more damage, one full log reduction more, than the 260 and 260|280 nm LEDs combined. Although this was detected in all three replicate experiments, it warrants further research, as it is only one data point. The additional log inactivation detected from the 280 nm LED could be due to protein damage occurring at 280 nm from higher energy inputs. A previous study showed that protein damage was much higher at a dose of 300 mJ/cm^2 than at lower doses of 50 and 186 mJ/cm^2 (Eischeid and Linden, 2011). It was suggested that the change in kinetics of protein damage with increasing dose could be the result of structural changes occurring as the proteins are broken down (Rexroad, 2003).

Dose response results of adenovirus 2 to the MP and LP UV lamps are also given in Figure 6.4a. When exposed to MP UV, adenovirus 2 was inactivated by 2-log, 3-log, and 4-log at doses of 16, 26, and 38 mJ/cm^2 respectively. This agrees with a past study that showed approximately 4.3-log reduction of adenovirus 2 at a UV dose of 40 mJ/cm^2 (Linden et al., 2007). Another past study showed 2-log and 3-log reduction of adenovirus 2 by MP UV irradiation at doses of 19 mJ/cm^2 and 34 mJ/cm^2 respectively (Beck et al., 2014).

The dose response of adenovirus 2 to LP UV irradiation showed 2-log, 3-log, and 4-log at 37, 63, and 113 mJ/cm^2 respectively. These doses were lower than the literature, which showed approximately 1.6-log and 2.25-log at 40 mJ/cm^2 and 60 mJ/cm^2 respectively or 4-log reduction between 120 mJ/cm^2 and 168 mJ/cm^2 (Gerba et al., 2002; Linden et al., 2009; Shin et al., 2005; Thompson et al., 2003; Beck et al., 2014). Variations in log-reduction could be due to differences in assays used.

The results for the UVC LED synergy experiment with adenovirus 2 are shown in Figure 6.4b. When the dose response results from the 260 nm and 280 nm LEDs are weighted by their respective average irradiance percentages and summed together, they equal the dose response results of the 260|280 nm LEDs combined, showing no statistical significance at 60 mJ/cm^2 ($p = 0.46$), 90 mJ/cm^2 ($p = 0.39$), or 120 mJ/cm^2 ($p = 0.058$). At 30 mJ/cm^2, the difference was statistically significant ($p = 0.012$); however, it differed in the opposite direction, showing that the sum of the log inactivation proportions from 260 nm and 280 nm was greater than the inactivation from the those wavelengths combined with the 260|280 LED unit. This indicates that there is no synergy from the two LEDs acting together on adenovirus 2 at those doses.

The electrical energy required for 2-log reduction of adenovirus 2, $E_{EL,2}$, by the UV LEDs and mercury vapor lamps are given in Table 6.4. Again, the LP UV and then MP UV sources required the least amount of energy. This is due to the energy efficiency of LP UV lamps as well as the enhanced UV inactivation from the low-wavelengths (< 240 nm) of the MP UV lamp. Of the LEDs, the 280 nm LED required the least energy for 2-log reduction, followed by the 260|280 nm LED combination and the 260 nm LED unit.

a) b)

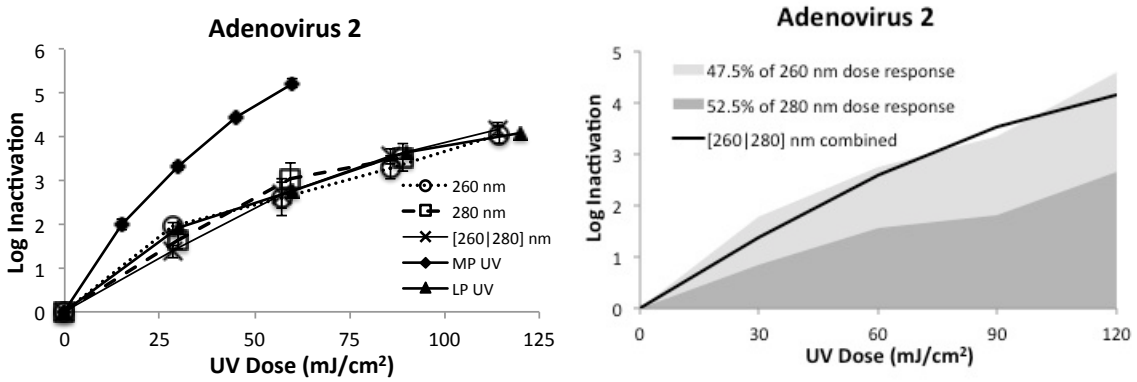

Figure 6.4. a) Dose response of adenovirus 2 to UV light from UV LEDs emitting at 260 nm, 280 nm, and 260/280 nm combined, compared with its dose response to MP and LP UV light. b) Dose response of a 260|280 nm combined LED unit on inactivating adenovirus 2 compared with the sum of the dose response from separate LED exposures.

Table 6.4. Dose response curves for inactivation of adenovirus 2 and electrical energy for 2-log reduction ($E_{EL,2}$) of the five UV sources.

UV Source	Log inactivation curve	Dose for 2-log reduction (mJ/cm^2)	Germicidal Irradiance (mW/cm^2)	$E_{EL,2}$ (Ws)
260 nm LED	$y = -0.000237x^2+0.0614x$	38.2	0.151	9,976
280 nm LED[a]	$y = -0.000316x^2+0.0682x$	35.0	0.254	4,281
260|280 nm LED	$y = -0.000164x^2+0.0554x$	41.1	0.385	7,016
MP UV Lamp	$y = -0.000855x^2+0.1381x$	16.1	7.49	2,310
LP UV Lamp	$y = -0.000246x^2+0.0632x$	36.9	8.88	596

6.3.4 Bacillus pumilus Spores

The dose response of *Bacillus pumilus* spores to the UVC LEDs and mercury vapor lamps (Figure 6.5a) exhibited a shoulder and was therefore fit linearly with lines not originating at the origin. The lines of best fit are given in Table 6.5 along with the UV dose required for 2-log reduction. *B. pumilus* spores exhibited almost identical inactivation kinetics for the 260 nm and the 260|280 nm UV irradiation, both of which were more effective than the 280 nm UV irradiation. This matches the action spectrum of *B. pumilus* spores, which shows a greater sensitivity to 260 nm and 270 nm irradiation than to 280 nm (Rochelle et al., 2010; Beck et al.,

2015 (Chapter 2)). The resistance of *Bacillus* spores varies greatly with the concentration of $MnSO_4$ used in the spore propagation medium and incubation time. This was especially evident with *B. subtilis* spores, but also has an effect on *B pumilus* spore data (Rochelle et al., 2010). Given the differences in propagation methods between this study and past studies, it's difficult to compare the *B pumilus* data with past results for inactivation at 260 nm and 280 nm.

When exposed to MP UV, *B. pumilus* spores were inactivated by 2-log, 3-log, and 4-log at doses of 102, 175, and 248 mJ/cm^2 respectively. These spores were less sensitive than those of a different strain reported in the literature from a similar propagation protocol (Rochelle et al., 2010). The dose response of *B. pumilus* spores to LP UV irradiation showed 2-log reduction at 189 mJ/cm^2 respectively. This agrees with the literature for different strains of *B pumilus* spores propagated with the same method (Rochelle et al., 2010).

The UVC LED synergy experiments with *B. pumilus* spores (Figure 6.5b) show no synergy. When the dose response results from the 260 nm and 280 nm LEDs are weighted by their respective irradiance percentages and summed together, they equal the dose response results of the 260|280 nm LEDs combined, showing no statistical significance at all doses tested, including 30 mJ/cm^2 ($p = 0.28$), 60 mJ/cm^2 ($p = 0.63$), 90 mJ/cm^2 ($p = 0.78$), 120 mJ/cm^2 ($p = 0.054$)..

The electrical energy required for 2-log reduction of *B pumilus* spores, $E_{EL,2}$, using the five UV sources (Table 6.5) again showed that the LP UV and MP UV lamps inactivated *B. pumilus* spores at the lowest energy cost. Of the UV LEDs, the 280 nm wavelength required the least energy per 2-log inactivation, followed by the 260|280 nm wavelength combination and the 260 nm wavelength.

a) b)

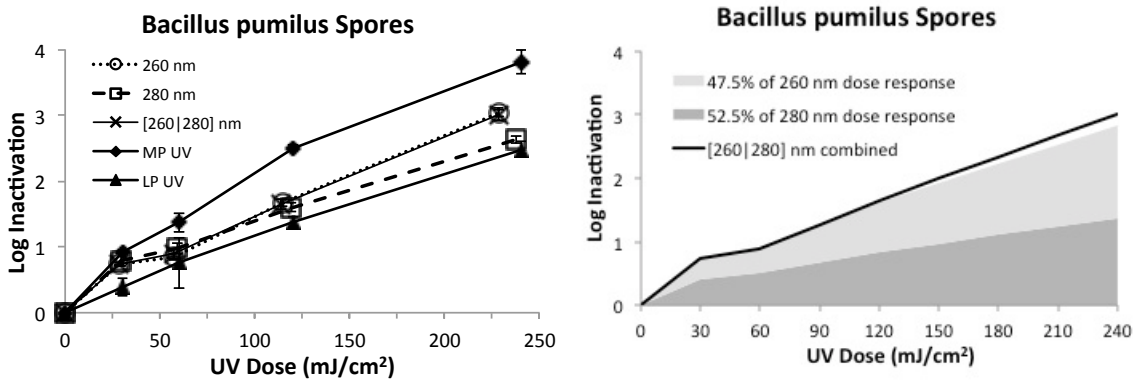

Figure 6.5. a) Dose response of *Bacillus pumilus* spores to UV light from UV LEDs emitting at 260 nm, 280 nm, and 260/280 nm combined, compared with its dose response to MP and LP UV light. b) Dose response of a 260|280 nm combined LED unit on inactivating *B. pumilus* spores compared with the sum of the dose response from separate LED exposures.

Table 6.5. Dose response curves for inactivation of *Bacillus pumilus* spores and electrical energy per 2-log reduction ($E_{EL,2}$) of the five UV sources.

UV Source	Log inactivation curve	Dose for 2-log reduction (mJ/cm^2)	Germicidal Irradiance (mW/cm^2)	$E_{EL,2}$ (Ws)
260 nm LED	y = 0.012x + 0.2867	143	0.138	40,864
280 nm LED	y = 0.009x + 0.4978	167	0.255	20,348
260|280 nm LED	y = 0.0118x + 0.3106	143	0.341	27,562
MP UV Lamp	y = 0.0137x + 0.6082	102	8.17	13,421
LP UV Lamp	y = 0.0102x + 0.0823	188	8.82	3,056

6.3.5 Synergistic Damage to the Viral DNA and RNA

The log reduction in amplification of the adenoviral genome fragment after exposure to 260 nm, 280 nm, and 260|280 nm UV LEDs is shown in Figure 6.6a. Genome damage from exposure to the UV LEDs, which have a bandpass of close to 10-13 nm, agreed well with the literature values for genome damage following exposure to a monochromatic laser (Beck et al., 2014). For example, the inactivation rate constant, k in cm^2/mJ, from the 260 nm LED was 0.045, compared to 0.045 from the tunable laser emitting at 260 nm. At 280 nm, the inactivation rate constant was 0.032, compared to 0.033 from the tunable laser. When both wavelengths

emitted together, the inactivation rate constant was slightly higher at 0.049. However, this caused no synergy as analyzed using the paired t-test at 30 mJ/cm^2 ($p = 0.18$), 60 mJ/cm^2 ($p = 0.07$), or 90 mJ/cm^2 ($p = 0.39$).

The log reduction in amplification of the MS2 coliphage genome after exposure to the UVC LEDs is shown in Figure 6.6b. The inactivation rate constant, k in cm^2/mJ, from the 260 nm LED was 0.061, compared to 0.069 from exposure to the tunable laser at 260 nm (Beck et al., in press). At 280 nm, the inactivation rate constant was 0.048, compared to 0.038 from the tunable laser (Beck et al., in press). The inactivation rate constant from the combined 260|280 nm emission was 0.0571. No synergy was detected in RNA damage, as analyzed using the paired t-test at 15 mJ/cm^2 ($p = 0.45$), 30 mJ/cm^2 ($p = 0.19$), or 45 mJ/cm^2 ($p = 0.81$).

a) Adenovirus DNA Damage

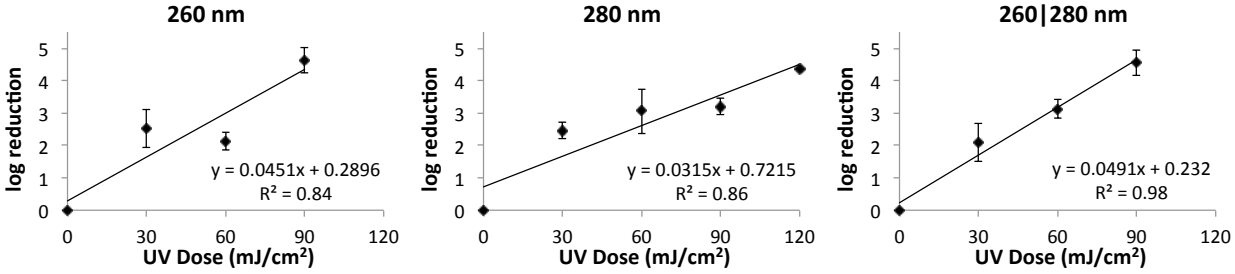

b) MS2 Coliphage RNA Damage

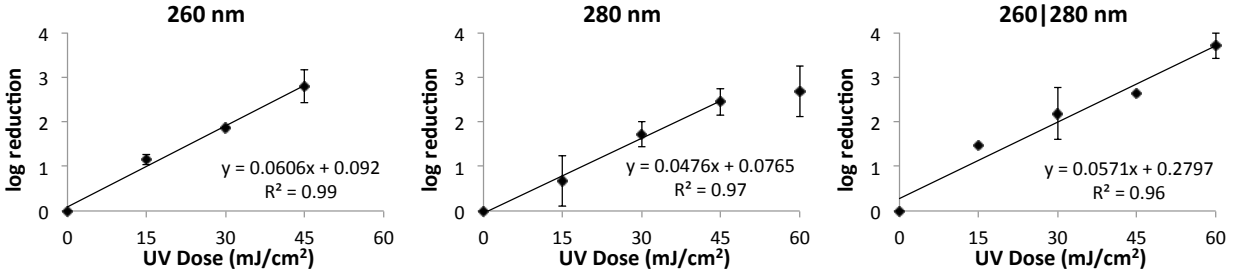

Figure 6.6. Dose response of a) adenovirus 2 DNA and b) MS2 coliphage RNA to UV light from a UV LED unit emitting at 260 nm, 280 nm, and 260/280 nm.

CHAPTER 7

CONCLUSIONS, IMPACTS, AND SUGGESTIONS FOR FUTURE RESEARCH

Recent advances in UV applications have revealed an opportunity and a need to fully understand the fundamentals of polychromatic UV inactivation; this research adds insight into those fundamentals. As introduced in section 1.6, the following hypotheses were tested:

1) **Weighting polychromatic UV dose calculations by their action spectra would be more accurate, i.e. yield dose response results that are more equivalent to the LP UV dose response, than weighting by DNA absorbance.**

The research discussed in Chapter 2 measured the action spectra of *Cryptosporidium parvum,* adenovirus 2, and coliphage MS2, T1UV, Q beta, T7, and T7m as well as *Bacillus pumilus* spores. The spectra for adenovirus and MS2 were used in place of DNA absorbance to calculate the UV dose for medium-pressure UV irradiation. When using the action spectra as opposed to DNA absorbance for weighting the dose calculation, the MP UV dose responses for adenovirus 2 and MS2 were less statistically significant than the dose responses of LP UV light. This confirms Hypothesis 1 for these two viruses.

2) **For MS2, loss of viral infectivity from polychromatic UV irradiation is due primarily to genomic damage.**

Chapter 3 presented data on the spectral sensitivity of the MS2 genome for comparison with the spectral sensitivity of the virus, measured by viral infectivity. The relative genome

sensitivity followed the same trend as the virus; the susceptibility of the MS2 RNA to UV irradiation was not statistically different than the susceptibility of the MS2 virus to UV irradiation at both low and high germicidal UV wavelengths. This indicates that inactivation of MS2 coliphage is due primarily to genomic damage, confirming Hypothesis 2.

3) For adenovirus, loss of infectivity from polychromatic UV irradiation is due to damage to other viral components, i.e. proteins, in addition to genomic damage.

Chapter 4 described damage to the adenoviral genome across the germicidal UV spectrum, comparing the spectral sensitivity of the DNA with the spectral sensitivity of the virus as measured by cell culture infectivity. In contrast to MS2, the adenovirus genome sensitivity differed significantly from the adenovirus sensitivity at wavelengths below 240 nm. This suggests that UV damage to a viral component other than DNA contributed to loss of infectivity at those wavelengths, confirming Hypothesis 3. This hypothesis was further tested in Chapter 5, in which SDS-PAGE was used to measure adenoviral protein damage across the germicidal UV spectrum. Protein damage at 220 nm was significantly greater than damage occurring at 254 nm, 260 nm, or 280 nm. This work proves insight into why medium-pressure UV irradiation has been shown to be more effective than 254 nm at inactivating adenovirus 2.

4) A UV LED system that combines 260 and 280 nm would be as effective as a polychromatic, medium-pressure mercury vapor lamp but at a much lower energy cost.

Chapter 6 described a novel UV light emitting diode (LED) system that incorporated LEDs emitting at 260 nm and 280 nm. The system was compared with MP UV and LP UV for inactivating *E. coli*, MS2 coliphage, adenovirus 2, and *Bacillus pumilus* spores. Although the

UVC LEDs were on par with the mercury vapor lamps at inactivating the microorganisms and viruses, an energy analysis of the required electrical energy per order of log reduction, E_{EO}, showed that the 260|280 nm combination of LEDs was not yet more energy efficient than the MP UV lamp. This disproved Hypothesis 4.

5) **A UV LED system combining 260 and 280 nm wavelengths would be more effective at inactivating bacterial and viral pathogens than the sum of efficacy from the 260 nm and 280 nm LEDs separately.**

Chapter 6 also discussed a test of dual wavelength synergy using the 260|280 nm UV LED in comparison with the sum of efficacy from the 260 and 280 nm LEDs separately. No synergy was detected in inactivating *E coli,* MS2 coliphage, adenovirus 2, and *Bacillus pumilus* spores. At the nucleic acid level, no synergy was detected in damaging MS2 RNA or adenoviral DNA as well. This research disproves Hypothesis 5.

The action spectra measured in this project, discussed in Chapter 2, are being used to validate MP UV disinfection systems to verify that they are capable of inactivating harmful pathogens to a mandated level. The data is first incorporated into Computational Fluid Dynamics models to integrate pathogen response with other variables such as lamp outputs, water qualities, quartz sleeves, and hydraulics. The outcome of these models helps develop validation matrices that will be used by utilities to understand the limitations of their UV disinfection systems. This information is currently being used to develop a protocol and guidance for validating polychromatic UV disinfection systems as a supplement to the USEPA's UV Disinfection Guidance Manual, to account for low wavelength emissions and pathogen response. Ultimately,

the research provides understanding of the impact of low UV wavelengths (200-240 nm) on pathogens found in drinking water with the goal of ensuring that UV disinfection systems in the United States are adequately protecting human health.

This research on UV-induced damage to nucleic acids and proteins at germicidal UV wavelength intervals provides insight into the mechanisms of polychromatic UV inactivation. Understanding the mechanisms involved across the deep UV spectrum helps explain why some viruses, including adenovirus, are more susceptible to polychromatic irradiation than monochromatic low-pressure UV, which could impact disinfection requirements. The DNA damage data clearly indicate that nucleic acid damage is not the only mechanism responsible for adenovirus inactivation from medium-pressure UV lamps. The protein damage measurements show the importance of the low UV wavelengths, below 240 nm, at damaging viral proteins, which ultimately enhances UV disinfection. This work also gives additional knowledge on which wavelengths may be less likely to be repaired. Future research would complement this study by further evaluating the spectral sensitivity of adenoviral proteins using mass spectrometry, specifically the fiber, penton base, hexon, and core proteins.

Finally, this wavelength-specific research will help predict the effects of emerging UV disinfection technology, such as deep UV LEDs, on viruses and bacteria. It makes the case for tailored wavelength units, which could combine a wavelength in the germicidal range, such as 254 or 260 nm, with a wavelength in the protein absorbance region, such as 220 or 230 nm, to optimize pathogen inactivation and minimize energy costs. A recent (2014) analysis on the economic viability of UV LEDs in developed countries predicts “water disinfection systems employing UV LEDs should start to appreciably penetrate the residential and industrial market within the next 5 years” (Ibrahim et al., 2014).

In addition to the impact of UV LEDs in developed countries, could be their impact in developing countries. The transformative impact of LEDs in the visible range was recognized this year with the award of the Nobel Prize in Physics to three Japanese scientists for developing the blue LED, the last puzzle piece remaining for producing white light, a long-lasting energy efficient alternative to fluorescent mercury lamps. The visible LEDs are widely popular in the developing world; photovoltaic-powered LED lights have been providing electricity to an estimated 28.5 million people, approximately 5% of Africans who otherwise lacked electricity.

This transformation could extend to UVC LEDs over time. Over the last ten years, small mercury-based UV systems have become available, including commercially available household systems and the low-cost, locally manufactured UV-Tube system. UV disinfection has been incorporated in water treatment systems in a number of developing countries including Mexico, Sri Lanka, and India (Brownell et al. 2008). UV disinfection would be a viable alternative to chemical disinfection in communities where people have a heightened sensitivity to the taste of chlorine. Recently-developed photovoltaic (PV) powered UVC LED disinfection systems (Lui et al., 2014) are a proof of concept for UVC LED disinfection that would become more practical once the technology becomes more affordable.

Another area with potential for UVC LED disinfection is in water reuse and wastewater treatment. In a region like Southeast Asia, for example, approximately 80% of wastewater is discharged, untreated, into canals and rivers, contaminating local water supplies. UV LEDs emitting in the germicidal range could be incorporated into decentralized water treatment systems (DEWATS), for disinfecting effluent or supernatant from septic tanks, membrane bioreactors, or solid/liquid separators in fecal sludge management trucks. UVC LEDs have been evaluated for their efficacy at inactivating fecal bioindicators found in urban wastewaters

(Chevremont et al., 2012). A pilot-scale proof-of-concept incorporating PV-powered UV LED disinfection for post-biological treatment of sewage effluent was developed and tested in Hong Kong (Close et al., 2006). These lab-based and pilot scale studies could be scaled up and adopted and applied at a practical level to contribute to addressing sanitation issues in the region.

Many barriers exist to widespread practical application of UV LEDs for water and wastewater disinfection, however. The biggest barriers to practical application are their high costs and low efficiency. Prices of UVC LEDs have dropped from $100/mW in 2012 to $10/mW in 2014. UVC LED manufacturers based in the United States, Japan, Taiwan, and South Korea are working to improve efficiencies and durability of their chips while reducing cost; however UV LED efficiencies currently remain below 20% (Peters, 2012). This results in high heat, which affects the efficiency of the LEDs and must be dissipated. After improving the efficiency of the UVC LED technology, the biggest barrier will be scaling it up to a large scale. This requires mass-production of LED substrates and wafers that are currently fabricated in small sizes. Once efficiency and manufacturing hurdles are addressed, technology adoption will increase and UVC LEDs will have a larger share of the water and wastewater disinfection market. The biggest room for practical application is in the design of novel disinfection technologies that, rather than duplicate mercury disinfection products, take advantage of the unique characteristics of the LEDs, primarily their small size. The biggest area for future research is further evaluation of the mechanisms of UVC LEDs disinfection at various wavelengths for inactivating microorganisms and viruses.

Given the rapid research and development in UV LED technology, broad potential exists for its use in the waste and wastewater treatment industry. Potential impacts of polychromatic

UV disinfection from these and other sources are enormous. As such, it is an exciting time to contribute to their research and development and I'm grateful for the opportunity.

REFERENCES

Adams, R.L.P., J.T. Knowler, and D.P. Leader, *The biochemistry of the nucleic acids*. 10th ed. 1986, London ; New York: Chapman and Hall. xviii, 526.

Aitken, A., Learmonth, M.P., 2002. Protein Determination by UV Absorption. *The Protein Protocols Handbook.* 3-6.

APHA. 2005. *Standard Methods for the Examination of Water and Wastewater*. 21st ed, Washington D.C.

Ayala-Torres, S.; Chen, Y.M.; Svoboda, T.; Rosenblatt, J.; Van Houten, B. 2000. Analysis of gene-specific DNA damage and repair using quantitative polymerase chain reaction. Methods-a Companion to Methods in Enzymology, 22 (2), 135-147.

Battigelli, D. A., Sobsey, M. D., & Lobe, D. C. 1993. The Inactivation of Hepatitis a Virus and Other Model Viruses by Uv Irradiation. *Wat. Sci. Technol*. 27(3-4): 339-342.

Beck, S.E., Rodriguez, R.A., Linden, K.G., Hargy, T.M., Larason, T.C., Wright, H.B., 2014. Wavelength dependent UV inactivation and DNA damage of adenovirus as measured by cell culture infectivity and long range quantitative PCR. *Environ. Sci. Technol*. 48(1): 591-598.

Beck, S.E., Wright, H.B., Hargy, T.M., Larason, T.C., Linden, K.G. 2015. Action Spectra for Validation of Pathogen Disinfection in Medium-Pressure Ultraviolet (UV) Systems. *Wat. Res*. 70: 27-37.

Besaratinia, A.; Yoon, J.I., Schroeder, C., Bradforth, S.E., Cockburn, M., Pfeifer, G.P. 2011. Wavelength dependence of ultraviolet radiation-induced DNA damage as determined by laser irradiation suggests that cyclobutane pyrimidine dimers are the principal DNA lesions produced by terrestrial sunlight. *Faseb J.* 25(9): 3079-3091.

Bohrerova, Z., Linden, K.G. 2006. Assessment of DNA damage and repair in Mycobacterium terrae after exposure to UV irradiation. *J. Appl. Microbiol.* 101(5): 995-1001.

Bolton, J.R., Stefan, M.I. 2002. Fundamental photochemical approach to the concepts of fluence (UV dose) and electrical energy efficiency in photochemical degradation reactions. *Res. Chem. Intermed.* 28: 857–870.

Bolton, J.R., Linden, K.G. 2003. Standardization of methods for fluence (UV dose) determination in bench-scale UV experiments. *J. Environ. Eng*. 129(3): 209-215.

Bounty, S., Rodriguez, R.A., Linden, K.G. 2012. Inactivation of adenovirus using low-dose UV/H2O2 advanced oxidation. *Wat. Res.* 46(19): 6273-6278.

Bowker, C.A.S., Shatalov, M., Ducoste. J. 2011. Microbial UV fluence-response assesment using a novel UV-LED collimated beam system. *Wat. Res.* 45: 2011-2019.

Blatchley III, E.R., & Peel, M.M. 2001. *Disinfection, Sterilization and Preservation*. New York: Lippincott Williams and Wilkins.

Cabaj, A., Sommer, R., Pribil, W., Haider, T. 2001. What means "dose" in UV-disinfection with medium pressure lamps? *Ozone-Sci. Eng.* 23(3): 239-244.

Cabaj, A., Sommer, R., Pribil, W., Haider, T. 2002. The spectral UV sensitivity of microorganisms used in biodosimetry. *Wat. Sci. Technol.*, 2(3): 175-181.

Campbell, A.T., Robertson, L.J., Snowball, M.R., Smith, H.V. 1995. Inactivation of oocysts of cryptosporidium parvum by ultraviolet irradiation. *Wat. Res.*, 29(11): 2583-2586.

Campbell, A.T., Wallis, P. 2002. The effect of UV irradiation on human-derived Giardia lamblia cysts. *Wat. Res.*, 36(4): 963-969.

Cashdollar, J.L., Brinkman, N.E., Griffin, S.M., McMinn, B.R., Rhodes, E.R. Varughese, E.A., Grimm, A.C., Parshionikar, S.U., Wymer, L., Fout, G.S. 2013. Development and evaluation of EPA method 1615 for detection of enteroviruses and noroviruses in water. *Appl. Environ. Microbiol*. 79: 215-223.

Chang, J.C.H., Ossoff, S.F., Lobe,D.C., Dorfman, M.H., Dumais, C.M., Qualls, R.G., Johnson, J.D. 1985. UV Inactivation of Pathogenic and Indicator Microorganisms. *Appl. and Environ. Microbiol*. 49(6): 1361-1365.

Chatterley, C., Linden, K.G. 2010. "Demonstration and evaluation of germicidal UV-LEDs for point-of-use water disinfection." *J. Wat.Health* 8(3): 479-486.

Chen, R.Z.; Craik, S.A.; Bolton, J.R. 2009. Comparison of the action spectra and relative DNA absorbance spectra of microorganisms: Information important for the determination of germicidal fluence (UV dose) in an ultraviolet disinfection of water. *Wat. Res*. 43(20): 5087-5096.

Cheng, S., Chen, Y.M., Monfrote, J.A., Higuchi, R., Vanhouten, B. 1995. Template Integrity Is Essential for Pcr Amplification of 20-Kb to 30-Kb Sequences from Genomic DNA. *Pcr-Methods and Appl*. 4(5): 294-298.

Chevremont, A.C., Farnet, A.M., Coulomb, B., Boudenne, J.L. 2012. Effect of coupled UV-A and UV-C LEDs on both microbiological and chemical pollution of urban wastewaters. *Sci. Total Environ.* 426: 304-10.

Close, J., Ip, J. and Lam, K.H. 2006. Water recycling with PV-Powered UV LED Disinfection. *Renewable Energy*. 31: 1657-1664.

Coohill, T.P., 1991. Action Spectra Again? *J. Photochem. and Photobiol*. 54(5): 859-870.

Crabtree, K.D., Gerba, C.P., Rose, J.B., Haas, C.N. 1997. Waterborne adenovirus: a risk assessment. *Wat. Sci.Technol.* 35(11): 1–6.

Crawford, M.H., Banas, M.A., Ross, M.P., Ruby, D.S., Nelson, J.S., Boucher, R., Allerman, A.A. 2005. Final LDRD report: ultraviolet water purification systems for rural environments and mobile applications. *Sandia Report*; 2005. Doi: 10.2172/876370.

Cromeans, T.L., Lu, X.Y., Erdman, D.D., Humphrey, C.D., Hill, V.R. 2008. Development of plaque assays for adenoviruses 40 and 41. *J. Virol. Methods*. 151(1):140-145.

Crook, M.J., Jefferson, B., Autin, O., MacAdam, J. Nocker, A. 2014. Comparison of ultraviolet light emitting diodes with traditional UV for greywater disinfection. *J. Wat. Reuse and Desalination*. 5(1): 17-27.

Davidson, J.N., *The Biochemistry of Nucleic Acids*. 8th ed Academic Press: 1976.

Detsch, R.M., Dudley Byran, F., Coohill, T.P. 1980. The Wavelength Dependence of Herpes Simplex Virus Inactivation by Ultraviolet Radiation. *Photochem. Photobiol.* 32 (2):173-176.

Draper, N., Smith, H. 1998. *Chapter 14: Dummy Variables, in Applied Regression Analysis* John Wiley and Sons: New York.

Dunn, J.J., Studier, F.W. 1983. Complete Nucleotide-Sequence of Bacteriophage-T7 DNA and the Locations of T7 Genetic Elements. *J. Mol. Biol.* 166(4): 477-535.

Eischeid, A.C.; Meyer, J.N.; Linden, K.G. 2009. UV Disinfection of Adenoviruses: Molecular Indications of DNA Damage Efficiency. *Appl. Environ. Microbiol*. 75 (1): 23-28.

Eischeid, A. C., Linden, K. G., 2011. Molecular Indications of Protein Damage in Adenoviruses after UV Disinfection. *Appl. Environ. Microbiol.* 77(3): 1145-1147.

Fallon, K.S., Hargy, T.M., Mackey, E.D., Wright, H.B., Clancy, J.L., 2007. Development and characterization of nonpathogenic surrogates for UV reactor validation. *J. Amer. Water Works Assoc.* 99(3): 73-82.

Fayer, R., Morgan, U., Upton, S. 2000. Epidemiology of Cryptosporidium: transmission, detection, and identification. *Intl J. Parasitol.*, 30: 1305-1322.

Furusawa, Y., Suzuki, K., Sasaki, M. 1990. Biological and Physical Dosimeters for Monitoring Solar Uv-B Light. *J. Radiation Res.* 31(2): 189-206.

Gates, F.L. 1930. A study of the bactericidal action of ultra violet light III. The absorption of ultra violet light by bacteria. *J. Gen. Physiol*. 14(1): 31-42.

Gerba, C.P.; Gramos, D.M.; Nwachuku, N. 2002. Comparative inactivation of enteroviruses and adenovirus 2 by UV light. *Appl. Environ. Microbiol.* 68(10): 5167-5169.

Gerrity, D., Ruy, H., Crittenden, J., Abbaszadegan, M. 2008. UV Inactivation of Adenovirus Type 4 measured by integrated cell culture qPCR. *J. Environ. Sci. Health*, Part A: Toxic/ Hazardous Substances and Environ. Eng. 43(14): 1628-38.

Gibson, C.J., Haas, C.N., Rose, J.B. 1998. Risk assessment of waterborne protozoa: current status and future trends. *Parasitology*, 117: S205-S212.

Guo, M.T., Hu, Y.Y., Bolton, J.R., El-Din, M.G. 2009. Comparison of low- and medium-pressure ultraviolet lamps: Photoreactivation of Escherichia coli and total coliforms in secondary effluents of municipal wastewater treatment plants. *Water Res.* 43(3): 815-821.

Guo, H.L., Chu, X.N., Hu, J.Y. 2010. Effect of Host Cells on Low- and Medium-Pressure UV Inactivation of Adenoviruses. *Appl. Environ. Microbiol*. 76(21): 7068-7075.

Harm, W. 1980. *Biological effects of ultraviolet radiation.* Cambridge University Press: New York, 216.

Hegedus, M., Modos, K., Ronto, G., AFekete, A. 2003. Validation of Phage T7 Biological Dosimeter by Quantitative Polymerase Chain Reaction Using Short and Long Segments of Phage T7 DNA. *Photochem. Photobiol*. 78(3): 213-219.

Hijnen, W.A., Beerendonk, E.F., Medema, G.J. 2006. Inactivation credit of UV radiation for viruses, bacteria, and protozoan (oo)cysts in water: a review. *Wat. Res.* 40(1): 3-22.

Hijnen, W.A.M.; Medema, G.J. 2010. *Elimination of Microorganisms by Water Treatment Processes*; IWA Publishing: London, UK.

Ibrahim, M.A.S., MacAdam, J., Autin, O., Jefferson, B. 2014. Evaluating the impact of LED bulb development on the economic viability of ultraviolet technology for disinfection. *Environ. Technol.* 35:4. 400-406.

Ito, T., Kada, T., Okada, S., Hieda, K., Kobayashi, K., Maezawa, H., Ito, A. 1984. Synchrotron System for Monochromatic Uv Irradiation (Greater-Than 140 Nm) of Biological-Material. *Radiation Res.* 98(1): 65-73.

Jagger, J., 1967. *Introduction to research in ultra-violet photobiology*. Prentice-Hall: Englewood Cliffs, N.J., 164.

Johnson, A.M., Rochelle, P.A., DiGiovanni, G.D., 2010. Detection of Infectious Cryptosporidium in Conventionally Treated Drinking Water (WRF Final Report. Denver, CO).

Jones, M. S., Harrach, B., Ganac, R. D., Gozum, M. M. A., dela Cruz, W. P., Riedel, B., Pan, C., Delwart, E. L., & Schnurr, D. P. 2007. New adenovirus species found in a patient presenting with gastroenteritis. *J. Virol.* 81(11): 5978-5984.

Jothikumar, N., Cromeans, T.L., Hill, V.R., Lu, X.Y., Sobsey, M.D., Erdman, D.D. 2005. Quantitative real-time PCR assays for detection of human adenoviruses and identification of serotypes 40 and 41. *Appl. Environ. Microbiol.* 71(6): 3131-3136.

Kalisvaart, B.F. 2001. Photobiological effects of polychromatic medium pressure UV lamps. *Wat. Sci. Technol*. 43(4): 191-197.

King, N., Lake, R., Campbell, D. 2011. Source Attribution of Nontyphoid Salmonellosis in New Zealand Using Outbreak Surveillance Data. *J. Food Protection*, 74(3): 438-445.

Kirkwood, C. D., Bogdanovic-Sakran, N., Barnes, G., & Bishop, R. 2004. *Rotavirus Serotype G9P[8] and Acute Gastroenteritis Outbreak in Children, Northern Australia. Emerging Infectious Diseases.*

Kuhn, H.J., Braslavsky, S.E., Schmidt, R. 2004. Chemical actinometry. *Pure and Applied Chemistry*, 76(12): 2105-2146.

Kukkula, M.; Arstila, P.; Klossner, M.L.; Maunula, L.; Bonsdorff, C.H.; Jaatinen, P. 1997. Waterborne outbreak of viral gastroenteritis. Scandinavian. *J. of Infect. Dis*. 29(4): 415-418.

Kuluncsics, Z.; Perdiz, D.; Brulay, E.; Muel, B.; Sage, E. 1999. Wavelength dependence of ultraviolet-induced DNA damage distribution: involvement of direct or indirect mechanisms and possible artefacts. *J. Photochem. and Photobiol B-Biol.* 49(1): 71-80.

Lakretz, A.; Ron, E.Z.; Mamane, H. 2010. Biofouling control in water by various UVC wavelengths and doses. *Biofouling*. 26(3): 257-267.

Lee, S.H.; Kim, S.J. 2002. Detection of infectious enteroviruses and adenoviruses in tap water in urban areas in Korea. *Wat. Res.* 36(1): 248-256.

Lin, T.Y., Lo, Y.H., Tseng, P.W., Chang, S.F., Lin, Y.T., Chen, T.S. 2012. A T3 and T7 Recombinant Phage Acquires Efficient Adsorption and a Broader Host Range. Plos One. 7 (2): e30954. doi:10.1371/journal.pone.0030954.

Linden, K.G.; Darby, J.L. 1997. Estimating effective germicidal dose from medium pressure UV lamps. *J. Environ. Eng*. 123(11): 1142-1149.

Linden, K.G., Thurston, J., Schaefer, R., Malley, J.P. 2007. Enhanced UV inactivation of adenoviruses under polychromatic UV lamps. *Appl. Environ. Microbiol*. 73(23): 7571-7574.

Linden, K.G., Shin, G., Sobsey, M.D., 2001. Comparative effectiveness of UV wavelengths for the inactivation of Cryptosporidium parvum oocysts in water. *Water. Sci. Technol*. 43(12): 171-174.

Linden, K.G., Shin, G.A., Lee, J.K., Scheible, K., Shen, C.Y., Posy, P. 2009. Demonstrating 4-log adenovirus inactivation in a medium-pressure UV disinfection reactor. *J. Amer. Water Works Assoc.* 101 (4): 90-99.

Liu, G.Y., Roser, D., Corkish, R., Ashbolt, N., Jagals, P., Stuetz, R. 2014. Photovoltaic powered ultraviolet and visible light emitting diodes for sustainable point-of-use disinfection of drinking waters. *Sci. Total Environ*. 493: 185-196.

Mackenzie, W.R., Hoxie, N.J., Proctor, M.E., Gradus, M.S., Blair, K.A., Peterson, D.E., Kazmierczak, J.J. Addiss, D.G., Fox, K.R., Rose, J.B., Davis, J.P. 1994. A Massive Outbreak in Milwaukee of Cryptosporidium Infection Transmitted through the Public Water-Supply *New England J. Medicine*, 331: 161-167.

Mackey, E.D., Hargy, T.M., Wright, H.B., Malley, J.P., Cushing, R.S. 2002. Comparing cryptosporidium and MS-2 bioassays-implications for UV reactor validation. *J. Am. Water Works Assoc,* 2002. 94(2): 62-69.

Maezawa, H., Ito, T., Hieda, K., Kobayashi, K. Ito, A., Mori, T., Suzuki, K. 1984. Action Spectra for Inactivation of Dry Phage-T1 after Monochromatic (150-254 Nm) Synchrotron Irradiation in the Presence and Absence of Photoreactivation and Dark Repair. *Radiation Res.* 98(2): 227-233.

Maizel, J.V. Jr., White, D.0., and Scharff, M.D. 1968. The polypeptides of adenovirus. 1. Evidence for multiple protein components in the virion and a comparison of types 2, 7A, and 12. *Virology*. 36: 115-125.

Malley, J.P., Ballester, N.A., Margolin, A.B., Linden, K., Mofidi, A., Bolton, J.R., Crozes, G., Laine, J.M., Janex, M.L. 2004. Inactivation of pathogens with innovative UV technologies, American Research Foundation and American Water Works Association.

Mamane-Gravetz, H., Linden, K.G., Cabaj, A., Sommer, R. 2005. Spectral sensitivity of Bacillus subtilis spores and MS2 Coliphage for validation testing of ultraviolet reactors for water disinfection. *Environ. Sci. & Technol.* 39(20): 7845-7852.

Marshall, M.M., Naumovitz, D., Ortega, Y., Sterling, C.R. 1997. Waterborne protozoan pathogens. *Clinical Microbiol. Reviews*, 10(1): 67-85.

McCuin, R.M., Clancy, J.L., 2003. Modifications to USEPA methods 1622 and 1623 for detection of Cryptosporidium oocysts and Giardia cysts in water. *Appl. Environ. Microbiol*. 69(1): 267-274.

McMinn, B.R., Cashdollar, J.L., Grimm, A.C., Fout, G.S. 2012. Evaluation of the celite secondary concentration procedure and an alternate elution buffer for the recovery of enteric adenoviruses 40 and 41. *J. Virolog. Methods*. 179(2) 423-428.

Meng, Q.S., Gerba, C.P. 1996. Comparative inactivation of enteric adenoviruses, poliovirus and coliphages by ultraviolet irradiation. *Wat. Res.* 30(11): 2665-2668.

Miller, R.L., Plagemann,P.G.W. 1974. Effect of Ultraviolet Light on Mengovirus: Formation of Uracil Dimers, Instability and Degradation of Capsid, and Covalent Linkage of Protein to Viral RNA. *J. Virol*. 13(3): 729-739.

Mofidi, A.A., Meyer, E.A., Wallis, P.M., Chou, C.I., Meyer, B P., Ramalingam, S., Coffey, B.M. 2002. The effect of UV light on the inactivation of Giardia lamblia and Giardia muris cysts as determined by animal infectivity assay (P-2951-01). *Wat. Res.* 36(8): 2098-2108.

Munakata, N., Hieda, K., Kobayashi, K., Ito, A., Ito, T. 1986. Action Spectra in Ultraviolet Wavelengths (150-250 Nm) for Inactivation and Mutagenesis of Bacillus-Subtilis Spores Obtained with Synchrotron Radiation. *Photochem. Photobiol*. 44(3): 385-390.

Nermut, M. V. 1979. Structural elements in adenovirus cores: evidence for a "core shell" and linear structures in "relaxed" cores. *Arch. Virol*. 62: 101–116.

Ogorzaly, L. and C. Gantzer, 2006. Development of real-time RT-PCR methods for specific detection of F-specific RNA bacteriophage genogroups: Application to urban raw wastewater. *J. Virological Methods*. 138(1-2): 131-139.

Oguma, K., Kita, R., Sakai, H., Murakami, M., Takizawa, S. 2013. Application of UV light emitting diodes to batch and flow-through water disinfection systems. *Desalination*. 328: 24-30.

ONORM. 2003. Plants for the disinfection of water using radiation - Requirements and testing. Part 2: Medium pressure mercury lamp plants. Vienna, Austria: Österreichisches Normungsinstitut.

Pace, C. N., Vajdos, F., Fee, L., Grimsley, G., Gray, T. 1995. How to Measure and Predict the Molar Absorption Coefficient of a Protein. *Prot. Sci*. 4: 2411–2423.

Park, G.W., Linden, K.G., Sobsey, M.D. 2011. Inactivation of murine norovirus, feline calicivirus and echovirus 12 as surrogates for human norovirus (NoV) and coliphage (F+) MS2 by ultraviolet light (254 nm) and the effect of cell association on UV inactivation. *Letters in Appl. Microbiol.* 52(2): 162-167.

Peabody, D.S. 1993. The RNA binding site of bacteriophage MS2 coat protein. *The EMBO Journal*. 12(2): 595-600.

Pecson, B.M., Ackermann, M., Kohn, T. 2011. Framework for Using Quantitative PCR as a Nonculture Based Method To Estimate Virus Infectivity. *Environ. Sci. Technol*. 45(6): 2257-2263.

Peters, L., 2012. UV LEDs ramp up the quiet side of the market. *LED Design and Manufacturing.* www.ledsmagazine.com.

Petit-Frere, C.; Clingen, P.H., Arlett, C.F., Green, M.H.L. 1995. Inhibition of RNA and DNA synthesis in UV-irradiated normal human fibroblasts is correlated with pyrimidine (6-4) pyrimidone photoproducts formation. *Mutation Res*. 354: 87-94.

Rauth, A., 1965. The physical state of viral nucleic acid and the sensitivity of viruses to ultraviolet light. *Biophys. J.* 5, 257-273.

Rexroad, J., Wietoff, C.M., Green, A.P., Kierstead, T.D., Scott, M.O., Middaugh, C.R., 2003. Structural ability of adenovirus type 5. *J. Pharm. Sci.* 92: 665-678.

Rice, E.W., Hoff, J.C. 1981. Inactivation of Giardia-Lamblia Cysts by Ultraviolet-Irradiation. *Appl. Environ. Microbiol.*, 42(3): 546-547.

Rochelle, P.A., Marshall, M.M., Mead, J.R., Johnson, A.M., Korich, D.G., Rosen, J.S., De Leon, R. 2002. Comparison of in vitro cell culture and a mouse assay for measuring infectivity of Cryptosporidium parvum. *Appl. Environ. Microbiol.* 68(8): 3809-3817.

Rochelle, P.A., Blatchley III, E.R., Chan, P., Scheible, O.K., Shen, C.Y., 2010. Challenge Organisms for Inactivation of Viruses by Ultraviolet Treatment. Final Report. Water Research Foundation and US EPA, Denver, CO.

Rodriguez, R.A., Bounty, S., Linden, K. 2013. Long-Range Quantitative PCR for Determining Inactivation of Adenovirus 2 by Ultraviolet Light. *J. Appl Microbiol*. 114(6): 1854-1865.

Ronto, G., Gaspar, S., Berces, A. 1992. Phages T7 in biological UV dose measurement. J. *Photochem. Photobiol. B-Biol*. 12: 285-294.

Ronto, G., Gaspar, S., Grof, P., Berces, A., Gugolya, Z. 1994. Ultraviolet Dosimetry in Outdoor Measurements Based on Bacteriophage-T7 as a Biosensor. *Photochem. Photobiol.* 59(2): 209-214.

Rosenstein. B.S., Mitchell, D.L. 1987. Action spectrum for the induction of pyrimidine (6-4) pyrimidone photoproducts and cyclobutane pyrimidine dimers in normal human skin fibroblasts. *Photochem. Photobiol*. 45: 775-780.

Russell, K.L., Hawksworth, A.W., Ryan, M.A.K., Strickler, J., Irvine, M., Hansen, C.J., Gray, G.C., Gaydos, J.C. 2006. Vaccine-preventable adenoviral respiratory illness in US military recruits, 1999-2004. *Vaccine*. 24(15): 2835-2842.

Russell, W.C. 2009. Adenoviruses: Update on structure and function. *J. Gen. Virol*. 90: 1-20.

Rux, J.R., Burnett, R.M. 1999. Adenovirus capsid proteins, pp. 5–16. In P. Seth (ed.), *Adenoviruses: basic biology to gene therapy*. R. G. Landes Company, Austin, TX.

Saidel, L.J., Goldfar, A.R., Waldman, S. 1952. The absorption spectra of amino acids in the region two hundred to two hundred and thirty millimicrons. *J. Biol. Chem*. 197: 285-291.

Salone, B., Martina, Y., Piersanti, S., Cundari, E., Cherubine, G., Franqueville, L., Failla, C., Boulanger, P., Saggio, I. 2003. Integrin a3B1 is an alternative cellular receptor for adenovirus serotype 5. *J. Virol.* 77(24): 13448-13454.

San Martín, C. 2012 Latest Insights on Adenovirus Structure and Assembly. *Viruses*. 4(12): 847–877.

Seth, P., 1999. Adenoviruses: Basic Biology to Gene Therapy; R.G. Landes Company: Austin. 31-38.

Setlow, P. 2001. Resistance of spores of Bacillus species to ultraviolet light. *Environ. Mol. Mutagen*. 38 (2-3), 97-104.

Setlow, P. 2006. Spores of Bacillus subtilis: Their resistance to and killing by radiation, heat and chemicals." *J. Appl. Microbiol*. 101(3): 514-25.

Sharpless, C.M. Linden, K.G. (2005) Interpreting collimated beam ultraviolet photolysis rate data in terms of electrical efficiency of treatment. *J. Environ. Eng. Sci*. 4:S19-26.

Shiba, T., Suzuki, Y. 1981. Localization of A protein in the RNA-A protein complex of RNA phage MS2. *Biochim Biophys Acta*. 654(2): 249-55.

Shin, G.A., Linden, K.G., Arrowood, M.J., Sobsey, M.D. 2001. Low-pressure UV inactivation and DNA repair potential of Cryptosporidium parvum oocysts. *Appl. Environ. Microbiol.*, 67(7): 3029-3032.

Shin, G., Linden, K.G., Sobsey, M.D. 2005. Low pressure ultraviolet inactivation of pathogenic enteric viruses and bacteriophages. *J. Environ. Eng. Sci.* 4: S7-S11.

Shin, G.A., Lee, J.K., Linden, K.G. 2009. Enhanced Effectiveness of Medium-Pressure Ultraviolet Lamps on Human Adenovirus 2 and its Possible Mechanism. *Water. Sci. Technol.*. 260(4): 851.

Shin, G. A., Linden, K. G., & Faubert, G. 2009. Inactivation of Giardia lamblia cysts by polychromatic UV. *Letters in Appl. Microbiol.*, 48(6): 790-792.

Simonet, J. and C. Gantzer, *Inactivation of poliovirus 1 and F-specific RNA phages and degradation of their genomes by UV irradiation at 254 nanometers. Appl. Environ. Microbiol.* 2006. 72(12): 7671-7677.

Simonian, M.H., Smith, J.A. 2006. Spectrophotometric and colorimetric determination of protein concentration. *Curr. Protoc. Mol. Biol*. Chapter 10: Unit 10.1A.

Skaza, A.T., Beskovnik, L., Cretnik, T.Z. 2011. Outbreak of rotavirus gastroenteritis in a nursing home, Slovenia, December 2010. *Eurosurveillance*, 16(14).

Slifko, T.R., Huffman, D.E., Dussert, B., Owens, J.H., Jakubowski, W., Haas, C.N., & Rose, J.B. 2002. Comparison of tissue culture and animal models for assessment of Cryptospridium parvum infection. *Experimental Parasitol.* 101(2-3): 97-106.

Smith, K.C., 1963. Photochemical Reactions of Thymine, Uracil, Uridine, Cystosine and Bromouracil in Frozen Solution and in Dried Films. *Photochem.Photobiol.*. 2(4): 503-517.

Smith, C.A., Baeten, J., Taylor, J. 1998. The Ability of a Variety of Polymerases to Synthesize Past Site-specific cis-syn, trans-syn-II, (6-4), and Dewar Photoproducts of Thymidylyl-(3'-5')-thymidine. *J. Biol. Chem*. 273(34): 21933-21940.

Sommer, R., Cabaj, A. 1993. Evaluation of the Efficiency of a Uv Plant for Drinking-Water Disinfection. *Wat. Sci. Technol.* 27(3-4): 357-362.

Sommer, R., Haider, T., Cabaj, A., Pribil, W., Lhotsky, M. 1998. Time dose reciprocity in UV disinfection of water. *Wat. Sci. Technol.* 38(12): 145-150.

Stefan, M.; Odegaard, C.; Petri, B.; Rowntree, M.; Sealey, L. 2007. Development, Characterization, and Application of a UV-Sensitive Bacteriophage for UV Reactor Challenges. in IUVA Congress. Los Angeles, CA.

Strauss, J. H.; Sinsheimer, R. L. 1963**.** Purification and properties of bacteriophage MS2 and of its ribonucleic acid. *J. Mol. Biol*., 7: 43-54.

Sutherland, J.C., 2002. Biological effects of polychromatic light*. Photochem. Photobiol*., 2002. 76(2): p. 164-170.

Thompson, S.S.; Jackson, J.L.; Suva-Castillo, M.; Yanko, W.A.; El Jack, Z.; Kuo, J.; Chen, C.L.; Williams, F.P.; Schnurr, D.P. 2003. Detection of infectious human adenoviruses in tertiary-treated and ultraviolet-disinfected wastewater. *Wat. Environ. Res.* 75(2): 163-170.

USEPA. 1984. National primary drinking water regulations; giardia lamblia, viruses, and legionella, maximum contaminant levels, and turbidity and heterotrophic bacteria (surface water treatment rule), final rule, 43.

USEPA, 1996. Informative Collection Manual Microbial Manual, O.o.R.a. Development, Editor.

USEPA. 1999. Wastewater Technology Fact Sheet: Ultraviolet Disinfection.

USEPA, 2003. Ultraviolet Disinfection Guidance Manual - Draft Version, U.E.P. Agency, Editor, Washington, D.C.

USEPA,2006a, Long term 2 enhanced surface water treatment rule, U.S.E.P.A. (Ed.), Editor: Washington, D.C.

USEPA, 2006b, National Primary Drinking Water Regulations: Ground Water Rule, Final Rule, U.E.P. Agency, Editor, Washington D.C.

USEPA. 2006c. Ultraviolet Disinfection Guidance Manual for the Final Long Term 2 Enhanced Surface Water Treatment Rule. In O. o. G. a. D. Water (Ed.). Washington, D.C.

Valegard, K., Murray, J.B., Stonehouse, N.J., van den Worm, S., Stockley, P.G., Liljas, L. 1997. The three-dimensional structures of two complexes between recombinant MS2 capsids and RNA operator fragments reveal sequence-specific protein-RNA interactions. *J. Mol Biol.* 270: 724-38.

van Houten, B.; Cheng, S.; Chen, Y.M. 2000. Measuring gene-specific nucleotide excision repair in human cells using quantitative amplification of long targets from nanogram quantities of DNA. *Mutation Res-DNA Repair*. 460(2): 81-94.

van Oostrum, J., Burnett, R.M. 1985. Molecular Composition of the Adenovirus Type 2 Virion. *J. Virol*. 439-448.
van Regenmortel, M.H.V., Fauquet, C.M., Bishop, D.H.L., Carstens, E.B., Estes, M.K., Lemon, S.M., Maniloff, J., Mayo, M.A., McGeoch, D.J., Pringle, C.R., Wickner, R.B. 2000. Virus taxonomy. Seventh Report of the International Committee on Taxonomy of Viruses. San Diego: Academic Press.

Vellinga, J., Van der Heijdt, S., Hoeben, R.C. 2005. The adenovirus capsid: major progress in minor proteins. *J. Gen. Virol*. 86: 1581-88.

Vilhunen, S. M.; Sarkka, H.; Sillanpaa, M. 2009. Ultraviolet light-emitting diodes in water disinfection. *Environ. Sci. Pollu. Res*. 16: 439-442.

Vilhunen, S.M.S. 2010. Recent developments in photochemical and chemical AOPs in water treatment: a mini-review. *Review of Environ. Sci. Biotechnol.* 9: 323-330.

Wang, T., MacGregor, S.J., Anderson, J.G., Woolsey, G.A. 2005. Pulsed ultra-violet inactivation spectrum of Escherichia coli. *Wat. Res.* 39(13): 2921-2925.

Ward, H. M. 1892. Experiments on the action of light on Bacillus anthracis. Proc. Royal Soc. London, 52: 393-400.

Wellinger, R.E. Thoma, F. 1996. Taq DNA polymerase blockage at pyrimidine dimers. *Nucleic Acids Res.,* 24(8): 1578-1579.

Wickham, T.J., Mathias, P., Cheresh, D.A., Nemerow, G.R. 1993. Integrins alpha v beta 3 and alpha v beta 5 promote adenovirus internalization but not virus attachment. *Cell*. 73(2): 309-19.

Wigginton, K.R., Menin, L., Sigstam, T., Gannon, G., Cascella, M., Hamidane, H.B., Tsybin, Y.O., Waridel, P., Kohn, T. 2012. UV Radiation Induces Genome-Mediated, Site-Specific Cleavage in Viral Proteins. *Chem BioChem* 13: 837-845.

Wright, H., Mackey, E.D., Gaithuma, D., Fonseca, C., Baumberger, L., Dzurny, T., Clancy, J.L., Hargy, T.M., Fallon, K., Cabaj, A., Schmalweisser, A., Beierman, A., & Gribbin, C. 2007. Optimization of UV Disinfection. Denver, CO: Water Research Foundation.

Wright, H., Heath, M., Bandy, J. 2009. Conference presentation. "Yikes! What the UVDGM Does Not Address on UV Disinfection." IOA/IUVA World Congress, Paris, France.

Wurtele, M.A., Kolbe, T., Lipisz, M., Kulberg, A., Weyers, M., Kneissl, M., Jekel, M. 2011. Application of GaN-based ultraviolet-C light emitting diodes – UV LEDs – for water disinfection. *Wat. Res*. 45: 1481-1489.

Wurtmann, E.J. and S.L. Wolin, RNA under attack: Cellular handling of RNA damage. *Crit Rev Biochem Mol Biol*., 2009. 44(1): 34-49.

Xiao, L.H., & Ryan, U.M. 2004. Cryptosporidiosis: an update in molecular epidemiology. *Current Opinion in Infectious Diseases.* 17(5): 483-490.

Yates, M.V., Malley, J., Rochelle, P., Hoffman, R. 2006. Effect of adenovirus resistance on UV disinfection requirements: A report on the state of adenovirus science. *J. Amer. Water Works Assoc.* 98(6): 93-106.

APPENDIX A: ACTION SPECTRA DETAILED IN LITERATURE

The following compilation of action spectra detailed in the literature are also described in Chapter 2.

a.

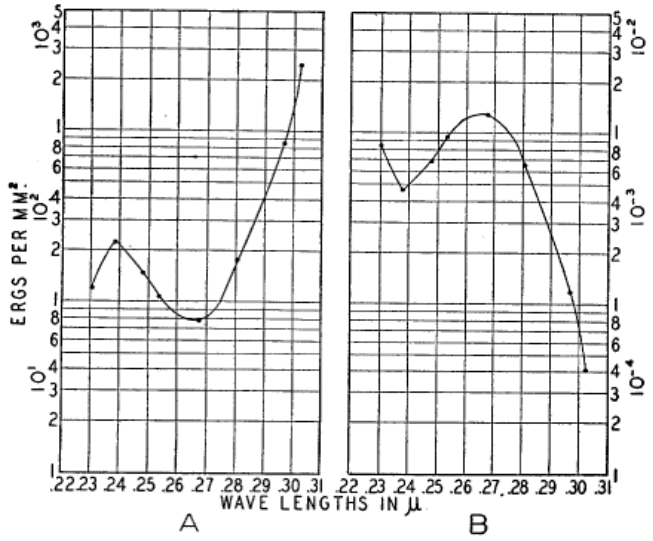

TEXT-FIG. 3. A. Curve of incident energies involved in the destruction of 50 per cent of *B. coli*.
B. Curve of the reciprocals of 3A.

b.

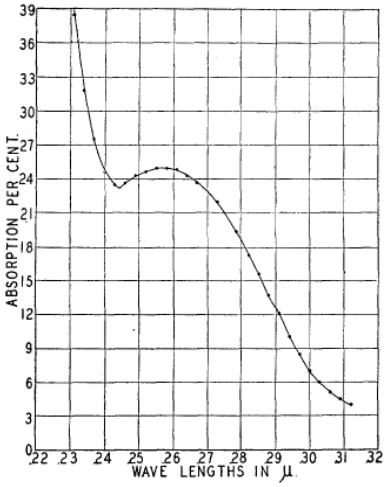

TEXT-FIG. 5. The coefficients of absorption of ultra violet light by a layer of *B. coli* 0.8 μ thick.

A.1. E. COLI. Gates made a direct correlation between (a.) the bactericidal action of *B. coli (E. coli)* and (b.) its absorbance of UV light (Gates, 1930).

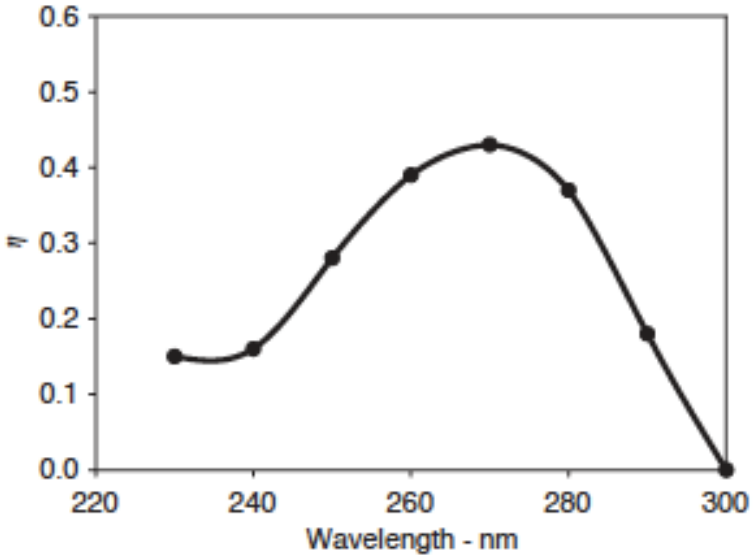

Fig. 5. Germicidal efficiency $\eta[\log_{10}(N/N_0)$ per mJ/cm^2] for *E. coli* as a function of wavelength.

A.2. E. COLI. Bactericidal action of *E. coli* in response to pulsed-UV light emitted from a xenon flashlamp with monochromator (8 nm bandwidth) (Wang, MacGregor, Anderson, & Woolsey, 2005).

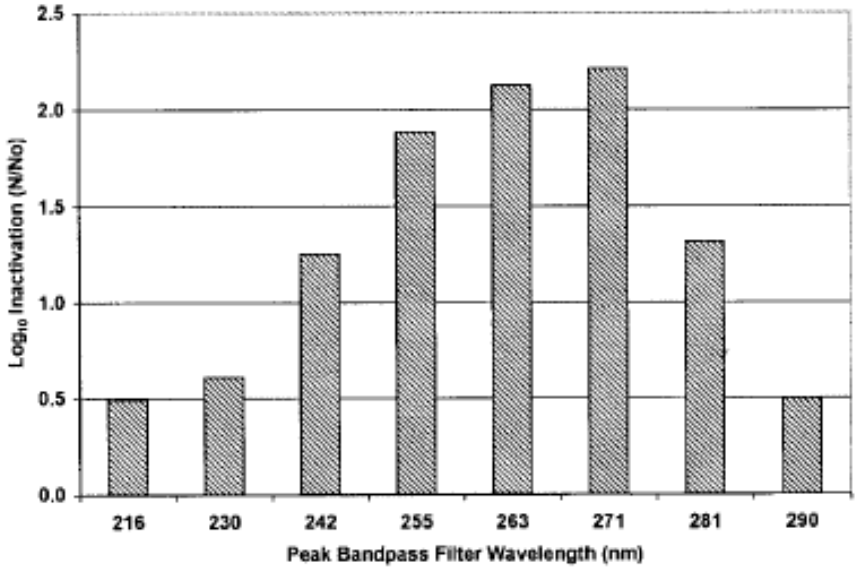

Figure 1 Relative germicidal effectiveness of UV wavelengths for inactivation of oocysts by 2 mJ/cm^2

A.3. CRYPTOSPORIDIUM. Action spectrum of *C parvum* oocysts using obtained using MP UV light with bandpass filters of 9-11 nm bandwidth (Linden, Shin, & Sobsey, 2001).

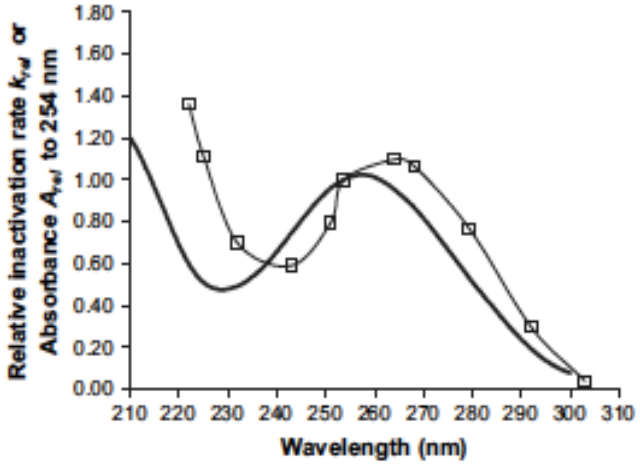

Fig. 5 – Comparison of the absorbance spectra of *S. typhimurium* LT2 DNA and the action spectra of *S. typhimurium* LT2: ——— absorption spectrum of DNA isolated from *S. typhimurium* LT2; —□— action spectrum of *S. typhimurium* LT2.

A.4. SALMONELLA. The action spectrum of *S. typhimurium* closely matched the absorption of its DNA at wavelengths above 240 nm. The action spectrum was measured with MP UV light and bandpass filters of 3-13 nm bandwidth (Chen et al., 2009).

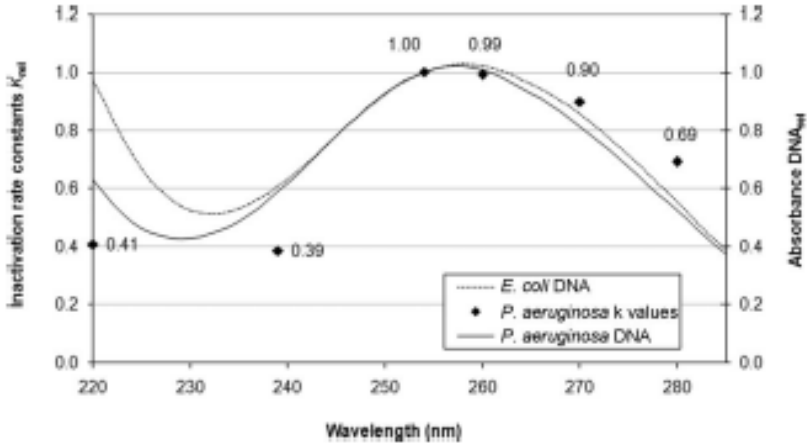

Figure 3. Action spectrum of *P. aeruginosa* PAO1 in comparison to its DNA absorbance and to the DNA absorbance of *E. coli* (all values are normalized to 254 nm).

A.5. PSEUDOMONAS. The action spectrum of *P. aeruginosa* (obtained with bandpass filters at 20-27 nm bandwidths) closely matched the absorption of its DNA at germicidal wavelengths of 254-270 nm (Lakretz, Ron, & Mamane, 2010).

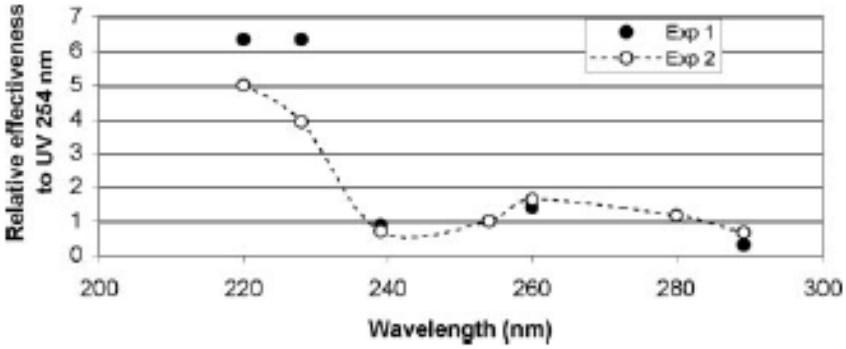

FIG. 3. Action spectrum for the inactivation of Ad2 with UV light. Data are from two experiments, each performed in duplicate, and represent the effectiveness for a 3-log inactivation relative to the response at 254 nm. Significant differences were found between the relative effectiveness of the 220 and 228-nm wavelengths compared to all the others and between the 260-nm and both the 239- and 289-nm wavelengths, based on the Tukey HSD test. In experiment 1, the 280- and 289-nm wavelengths were also significantly different.

A.6. ADENOVIRUS. The action spectrum of Adenovirus type 2 showed much higher UV inactivation at lower wavelengths of 220 and 228 compared to germicidal wavelengths (Linden, Thurston, Schaefer, & Malley, 2007).

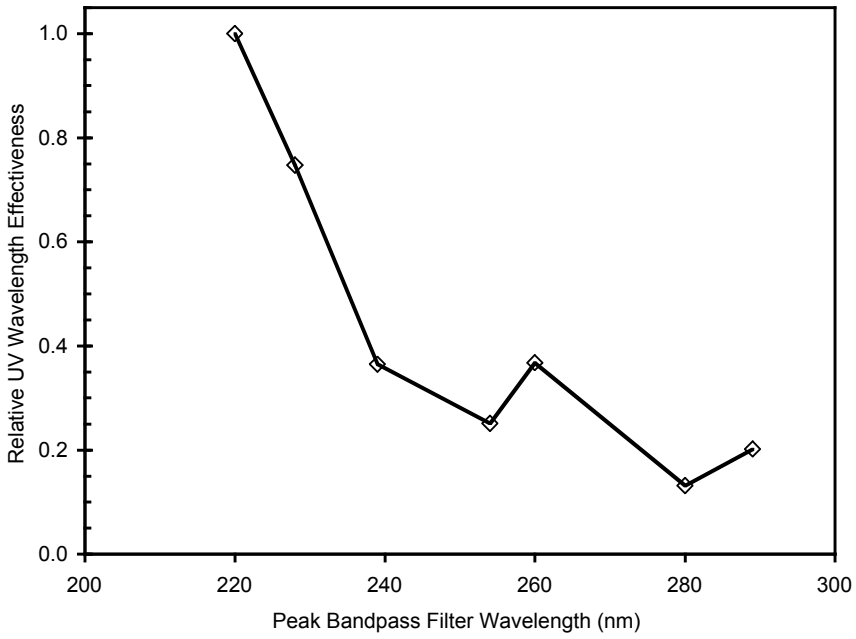

A.7. ROTAVIRUS. Action spectrum of Rotavirus obtained using medium-pressure UV light with bandpass filters (Malley et al., 2004).

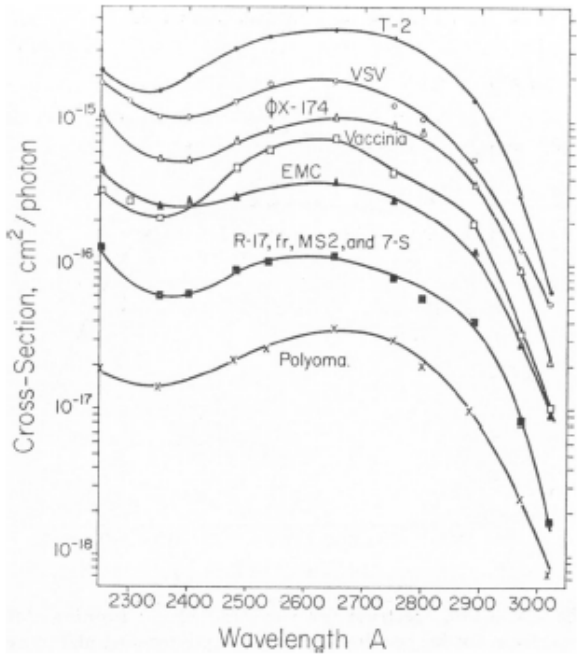

FIGURE 2 The UV action spectra for viral plaque-forming ability for ten of the viruses studied. The spectra for MS2, fd, R-17, and 7-S bacteriophages were identical within experimental error.

A.8. MS2. Action spectra for MS2 and several other bacteriophage and animal viruses developed with a monochromator emitting at 1.2 nm bandwidths (Rauth, 1965).

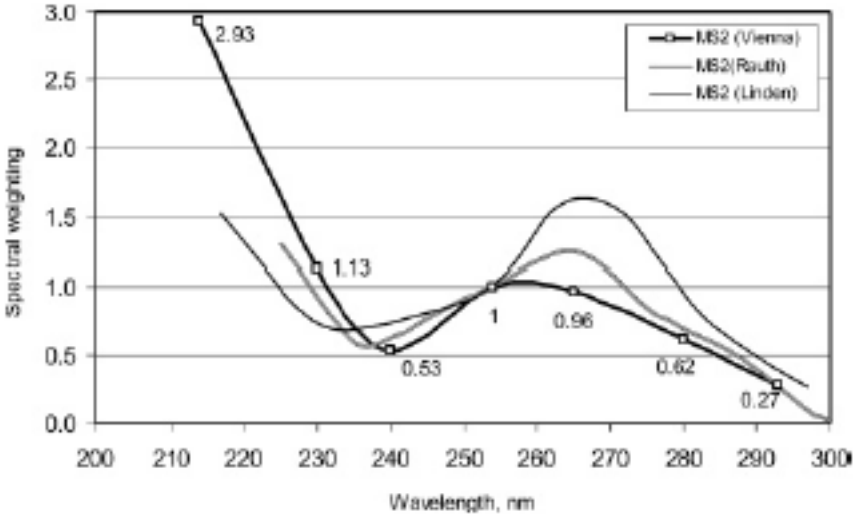

FIGURE 5. Comparative spectral sensitivity of MS2 as measured by different researchers, relative to the data obtained at 254 nm. MS2 (Rauth) from Rauth (*6*). MS2 (Linden) from Linden et al. (*29*). MS2 (Vienna) from current research study.

A.9. MS2. Variation of MS2 action spectra from 3 different research studies (Mamane-Gravetz, Linden, Cabaj, & Sommer, 2005).

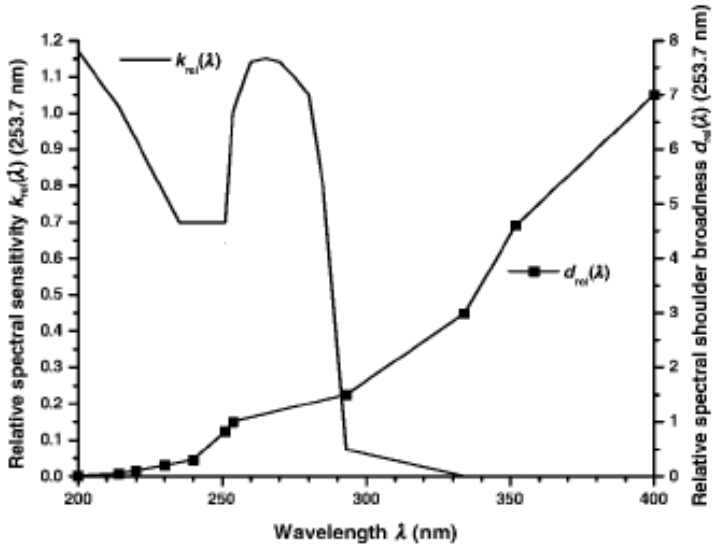

Figure 4 Relative spectral sensitivity functions $k_{rel}(\lambda)$ and $d_{rel}(\lambda)$ for spores of *Bacillus subtilis* ATCC 6633 in aqueous suspension. The values were normalized to 253.7 nm in using the following absolute values $k(253.7) = 0.00612$ m^2/J and $d(253.7) = 0.79$

A.10. BACILLUS SUBTILIS. The action spectrum of *B. subtilis,* obtained with medium-pressure light and bandpass filters yielding bandwidths of 20 nm, was adopted by the Australian National Standards Institute. (Cabaj, Sommer, Pribil, & Haider, 2002)

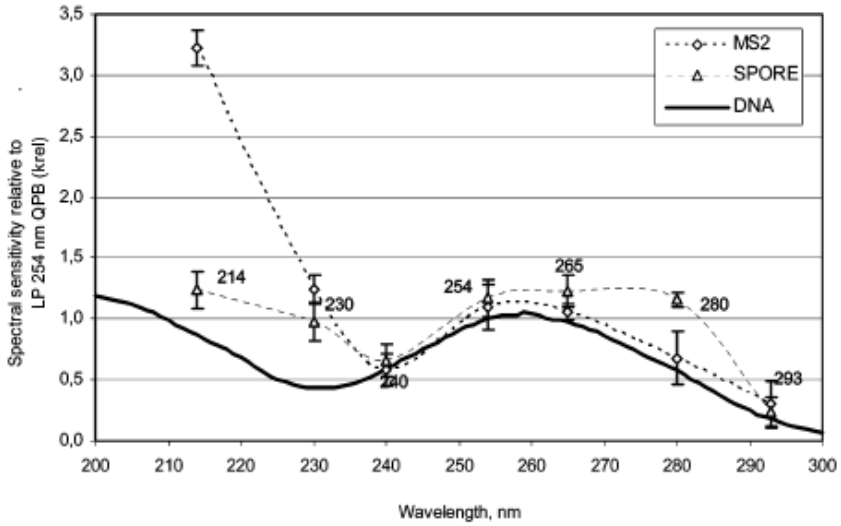

FIGURE 3. Spectral sensitivity of S6633 spores and MS2, as produced using the monochromator, relative to LP 254 nm QPB for spores and MS2, respectively, and DNA relative to 254 nm of DNA. Error bars represent 95% CI for mean sensitivity coefficient.

A.11. BACILLUS SUBTILIS AND MS2. Spectral sensitivity of *B. subtilis* and MS2 obtained with a monochromator and a maximum bandwidth of 10 nm (Mamane-Gravetz et al., 2005).

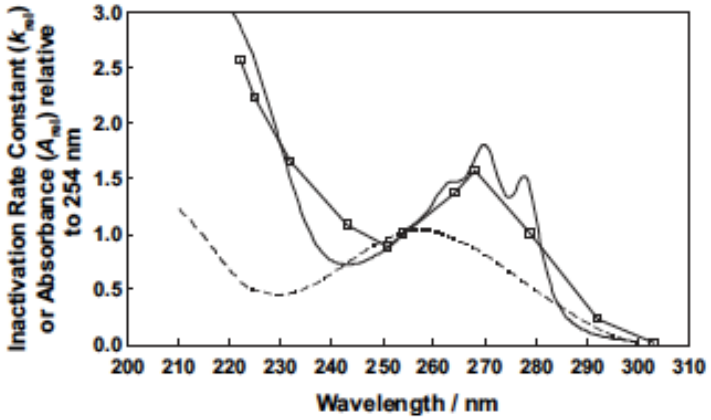

Fig. 2 – Comparison of the absorbance spectrum of DNA purified from *B. subtilis* spores, the absorbance spectrum of decoated *B. subtilis* spores and the spore action spectrum: ——— absorbance spectrum of decoated spores; ---------- absorption spectrum of DNA isolated from spores; —□— action spectrum of *B. subtilis* spores.

A.12. BACILLUS SUBTILIS. Action spectrum of *B. subtilis* determined with bandpass filters (3-13 nm bandwidth) compared to absorbance spectrum of *B. subtilis* spores (Chen, Craik, & Bolton, 2009).

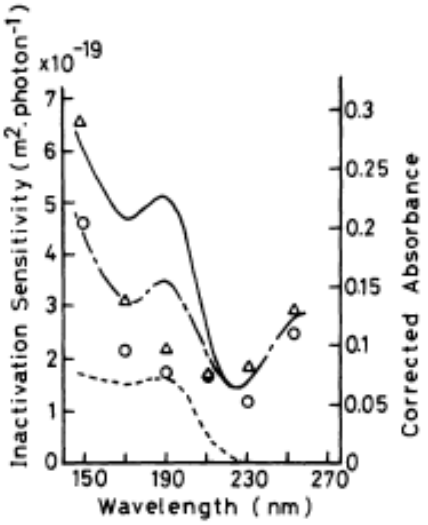

FIG. 4. Comparison of the inactivation sensitivity of dry phage on B_{s-1} cells exposed to uv radiation (○, △) with the absorption spectra of phage DNA (— - —), head-coat protein (- - -), and whole phage head (——). The magnitude of absorption is represented by the corrected absorbance described in text. The corrected absorbance was drawn to scale as the absorption curve of DNA fits the experimental points of inactivation sensitivity at 254 nm.

A.13. T1 COLIPHAGE. Action spectrum of dry T1 bacteriophage in the vacuum UV and far UV regions, produced through synchrotron radiation with bandwidths of 8.7 nm (Maezawa et al., 1984).

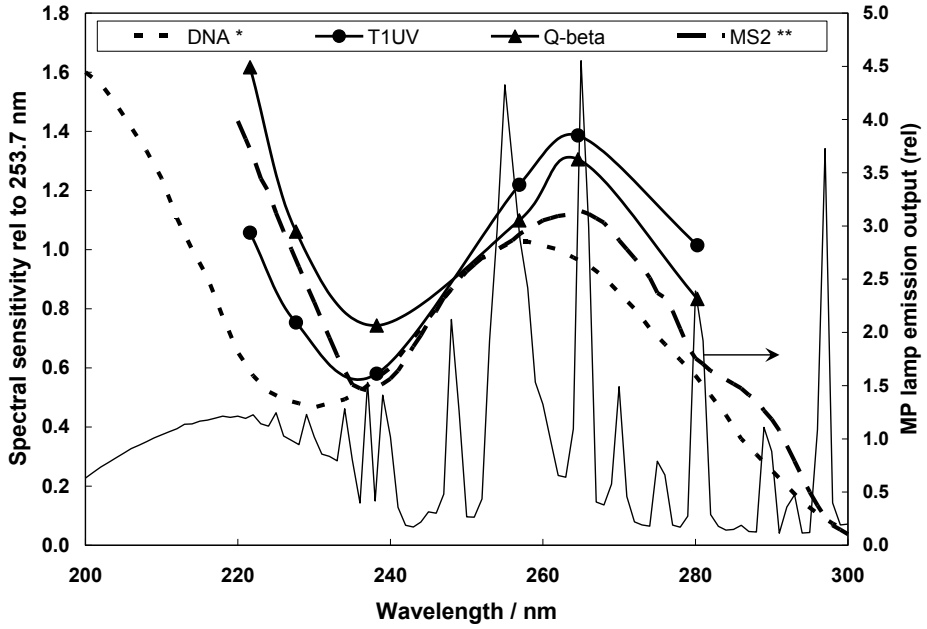

A.14. T1UV and Q-BETA. Action spectrum for isolated organism, T1UV, and Q-beta determined with MP UV and bandpass filters (9- 11 nm bandwidths). Both bacteriophage exhibited similar action as MS2 (Stefan, Odegaard, Petri, Rowntree, & Sealey, 2007).

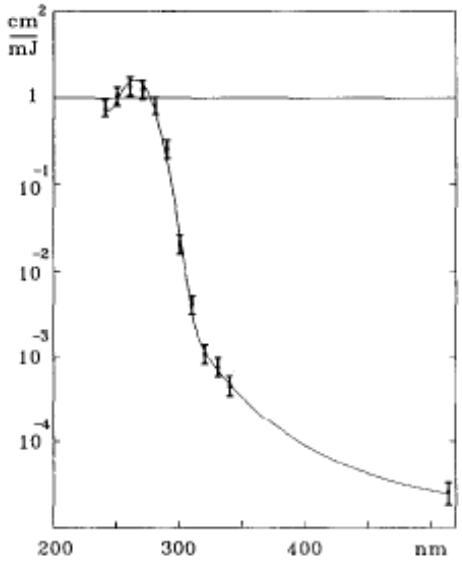

Fig. 1. Action spectrum of phage T7 inactivation determined in the range 240–340 nm at every 10 nm and at 514 nm. The bars represent the experimental errors. The curve fitted to the experimental points is given by eqn. (3).

A.15. T7. Action spectrum of T7 coliphage determined with a xenon lamp and monochromator (4 nm dispersion) (Ronto, Gaspar, & Berces, 1992).

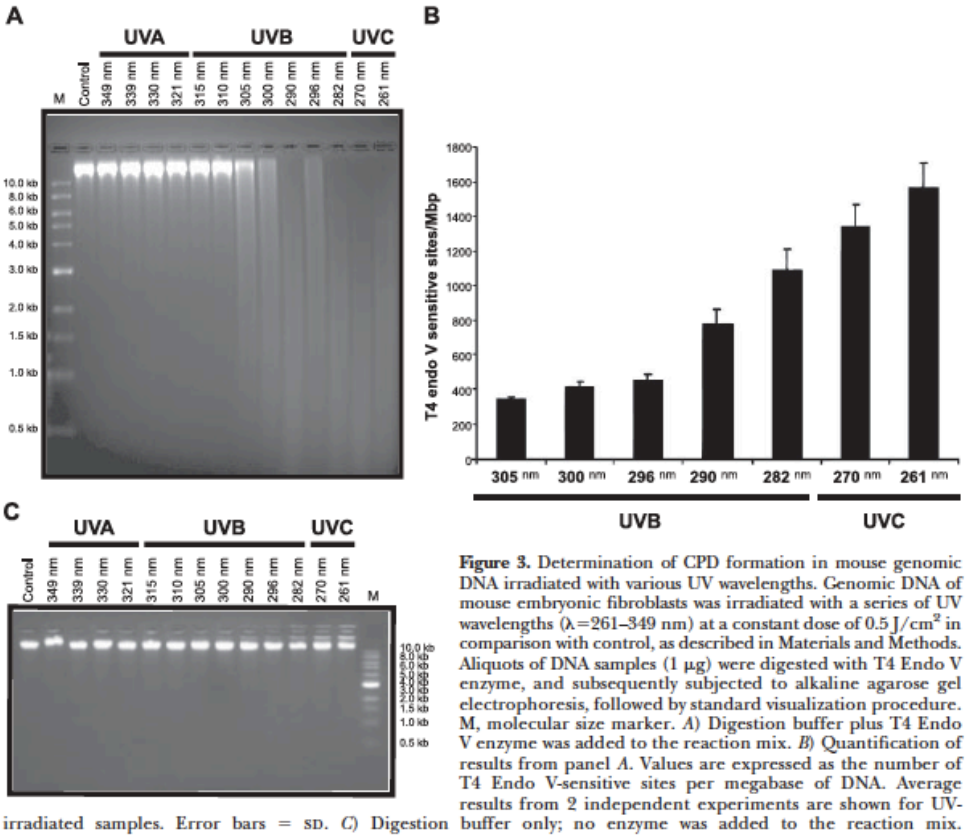

Figure 3. Determination of CPD formation in mouse genomic DNA irradiated with various UV wavelengths. Genomic DNA of mouse embryonic fibroblasts was irradiated with a series of UV wavelengths (λ=261–349 nm) at a constant dose of 0.5 J/cm^2 in comparison with control, as described in Materials and Methods. Aliquots of DNA samples (1 μg) were digested with T4 Endo V enzyme, and subsequently subjected to alkaline agarose gel electrophoresis, followed by standard visualization procedure. M, molecular size marker. *A*) Digestion buffer plus T4 Endo V enzyme was added to the reaction mix. *B*) Quantification of results from panel *A*. Values are expressed as the number of T4 Endo V-sensitive sites per megabase of DNA. Average results from 2 independent experiments are shown for UV-irradiated samples. Error bars = SD. *C*) Digestion buffer only; no enzyme was added to the reaction mix.

A.16. Correlation between cyclobutane pyramidine dimer formation and UV wavelength from a Ti:sapphire laser (Besaratinia et al., 2011).

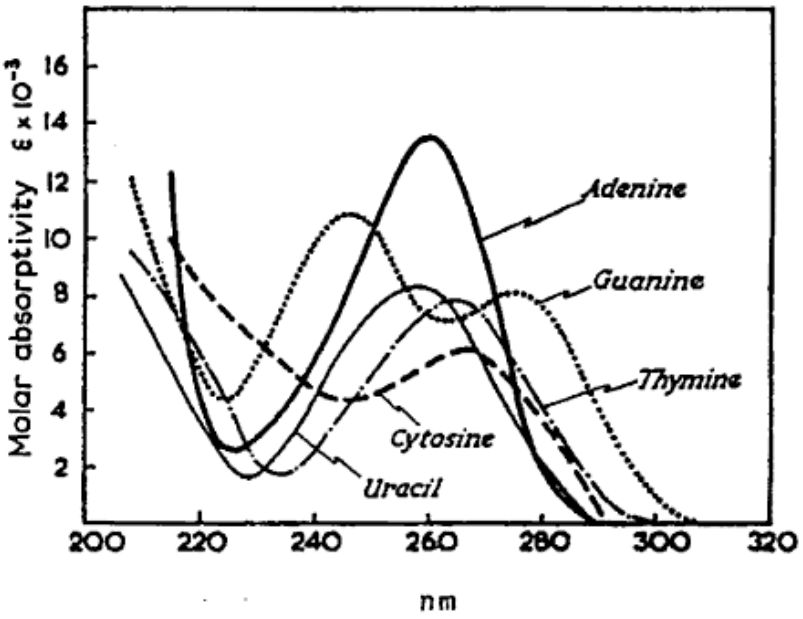

FIG. 41.1. Absorption spectra of purine and pyrimidine bases in aqueous solution at pH = 7. (From Davidson JN. *The biochemistry of nucleic acids*, 5th ed. London: Metheun, 1965, with permission.)

A.17. Absorption spectra of nucleotide bases forming DNA and RNA, which may show a direct correlation to the spectral sensitivity of an organism or virus (Blatchley III & Peel, 2001).

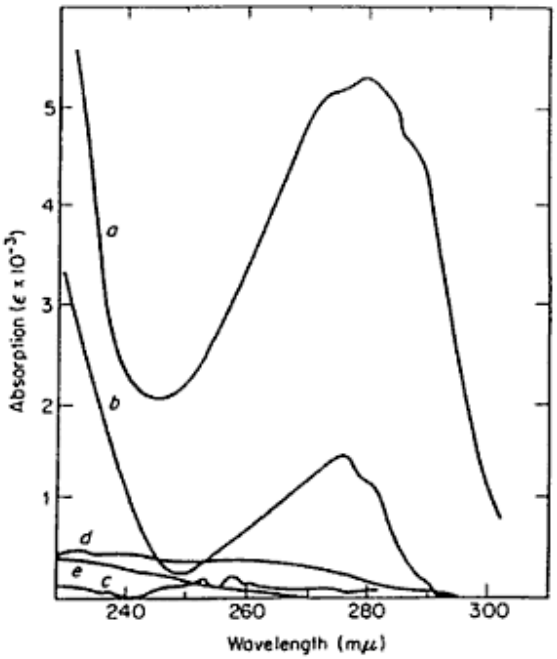

FIG. 41.2. Absorption spectra for aqueous solutions of amino acids at pH = 7: *(a)* tryptophan, *(b)* tyrosine, *(c)* phenylalanine, *(d)* cystine, *(e)* cysteine. (From McLaren AD, Shugar D. *Photochemistry of proteins and nucleic acids*. Long Island City, NY: Pergamon Press, 1964., with permission.)

A.18. Absorption spectra for amino acids (Blatchley III & Peel, 2001).

APPENDIX B: SUPPLEMENTARY INFORMATION ABOUT NIST TRANSPORTABLE TUNABLE LASER IRRADIANCE FACILITY

The fundamental component of the NIST tunable UV irradiance laser system is an EKSPLA NT242-SH/SFG 1 kHz pulsed laser (EKSPLA, Vilnius, Lithuania), tunable over 210 nm to 2600 nm. Once the laser beam leaves the EKSPLA laser it enters a light-tight enclosure through a computer-controlled shutter that determines the dose to the water samples. The beam, which is approximately 2.5 mm in diameter, is then reflected off two dielectric mirrors, which filter out visible light co-aligned with the laser beam when the laser is set to wavelengths shorter than 300 nm. The beam then travels through a beam splitter and an etched fused silica diffuser (RPC Photonics, Rochester, NY). The beam splitter sends a small portion of the UV light to a silicon photodiode, which was used monitor the irradiance level during sample exposure. The diffuser is specifically engineered to modify the laser beam from a collimated oval shape (1.5 mm by 10 mm) to a uniform diverging beam (10° half-angle) to irradiate the water samples. Neutral density filters could be added to the optical path between the shutter and first mirror to reduce the irradiance level at the water sample. The UV standard detector is placed at the water sample location to measure the irradiance at each wavelength of interest. The NIST tunable UV irradiance laser system optical configuration is shown in Figure B.1.

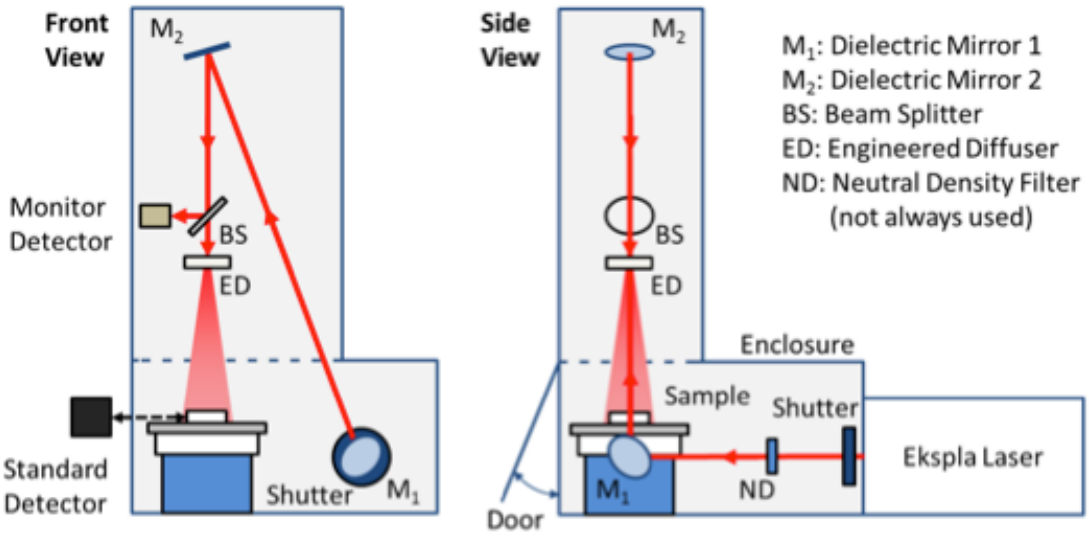

Figure B.1. The NIST tunable UV irradiance laser system optical configuration for 240 nm to 300 nm. The Standard Detector is substituted for the Sample to measure the irradiance at each wavleength of interest.

The dielectric mirrors, labeled M_1 and M_2 in Figure B.1, were highly reflective from 240 nm to 300 nm. For 210 nm to 230 nm ,the dielectric mirrors were replaced by aluminum mirrors and a fused silica prism and slit were added to filter out the visible light. This configuration is shown in Figure B.2.

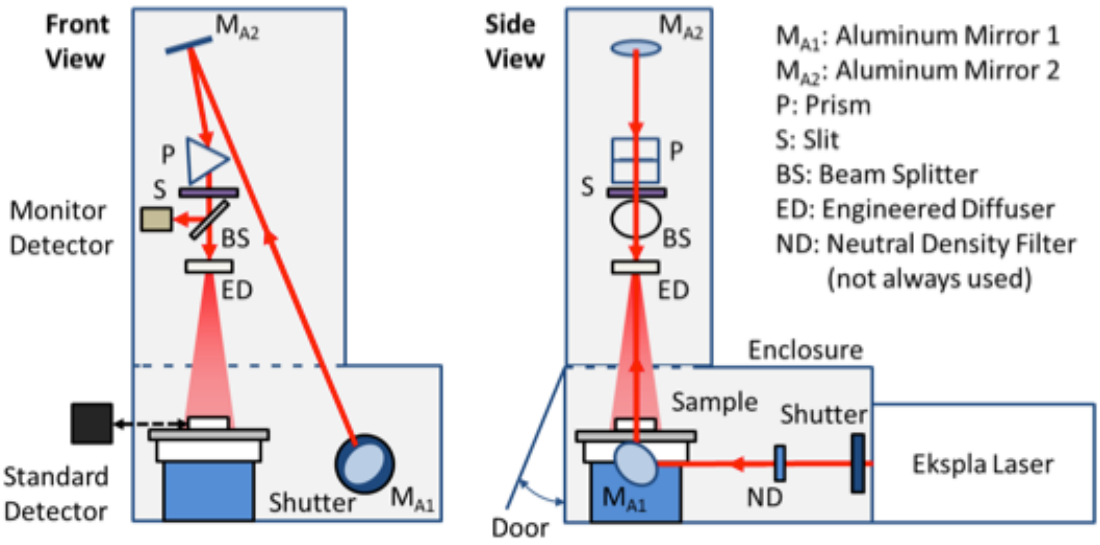

Figure B.2. The NIST tunable UV irradiance laser system's optical configuration for 210 nm to 230 nm. The dielectric mirrors were replaced by aluminum mirrors and a prism and slit were added.

The spectral filtering of the laser beam by the dielectric mirrors or prism and slit was required because the visible light co-aligned with the laser beam but at double the selected UV laser wavelength (see, for example, the 420 nm peak in Figure B.3). An Instrument Systems CAS 140CT array spectrometer (Instrument Systems, Munich, Germany) was used to measure the laser system spectra at the water sample position from 200 nm to 600 nm. Figure B.3 shows the calibrated counts normalized to the peak wavelength for the laser system spectra at each of the UV wavelengths of interest confirming the visible light in the beam was reduced to an acceptable level.

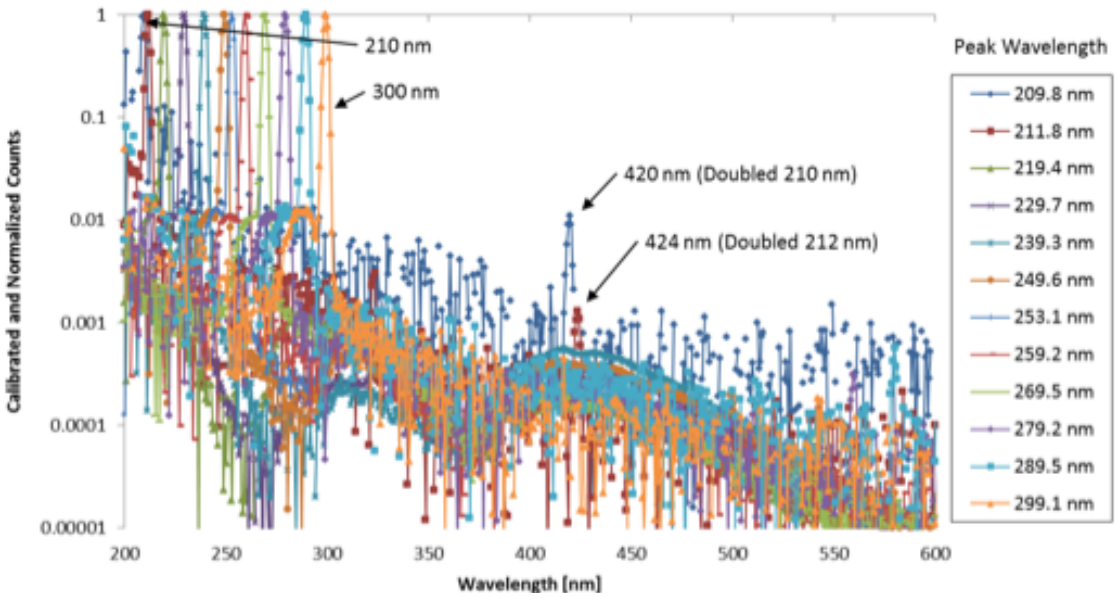

Figure B.3. Plot of the calibrated counts normalized to the peak wavelength for the laser system spectra at the water sample position from 200 nm to 600 nm for each of the UV wavelengths of interest. The visible light has been reduced to an acceptable level.

The UV standard detector consisted of an International Radiation Detectors (now Opto Diode Corp.) SXUV100 10 mm x 10 mm windowless silicon photodiode, known to be stable with UV exposure (Shaw, 2005), and a precision 8 mm diameter electroformed aperture in a cylindrical aluminum housing. The photodiode output was measured with a Keithley 6517

electrometer. The spectral irradiance responsivity [A/(μW/cm^2)] of the UV standard detector was calibrated at NIST in the UV Spectral Responsivity Facility (Larason and Houston, 2008).

The uniformity of the UV irradiance at the water sample was determined by calculating the ratio of the average of the incident irradiance over the area of the Petri dish to the irradiance at the center of the dish, or petri factor (Bolton and Linden, 2003), each time the wavelength was changed before exposing any water samples. The irradiance was measured by a radiometer (model 1400A) and detector (SED 240) with a 1 mm aperture in front of the detector. Measurements were taken at 5 mm steps along two orthogonal axes across the beam diameter at the water surface plane. All petri factors were within the range of 0.94 to 1.05. The fluorescence from typical card stock paper was used as a qualitative measure of the beam uniformity. A digital image of the paper fluorescence from a camera mounted above the water sample and irradiance uniformity normalized to the beam center at 253.7 nm is shown in Figure B.4.

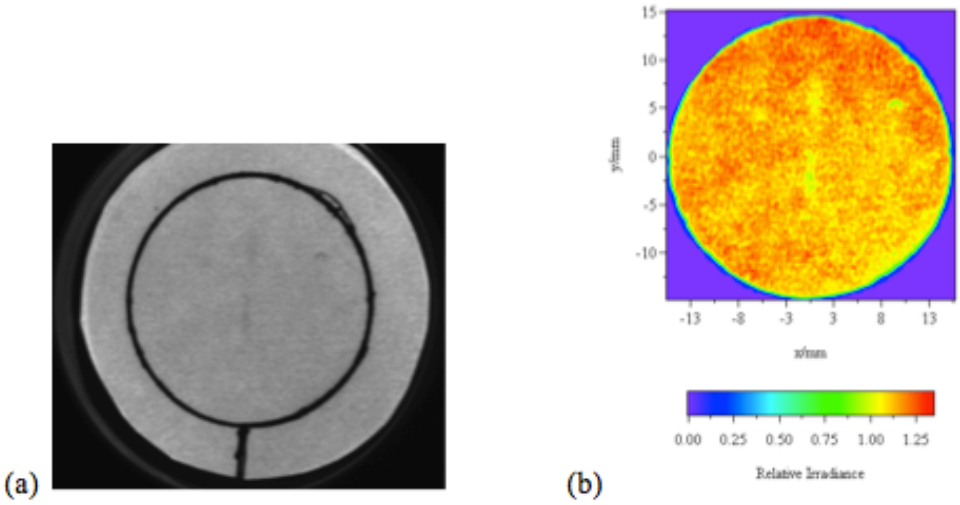

Figure B.4. Example of the irradiance uniformity at 253.7 nm. A photograph (a) from the camera mounted above the water sample imaging the fluorescence from typical card stock paper. The dark circle marks the area of the water sample Petri dish. A plot (b) of the relative irradiance uniformity normalized to the beam center.

Statistical Analysis for Determining Action Spectra

Figure B.5 illustrates the mapping approach for determining action spectra with the UV dose-response of MS2 phage measured at 220 and 253.7 nm. A constant was determined as the value that mapped the UV dose response at 220 nm onto the UV dose response at 253.7 nm, minimizing the sum of the squares of the differences between the measured log inactivation and that predicted using the quadratic function for a given UV dose. In this example, an action spectrum constant of 2.37 maps the UV dose-response at 220 nm onto that at 253.7 nm.

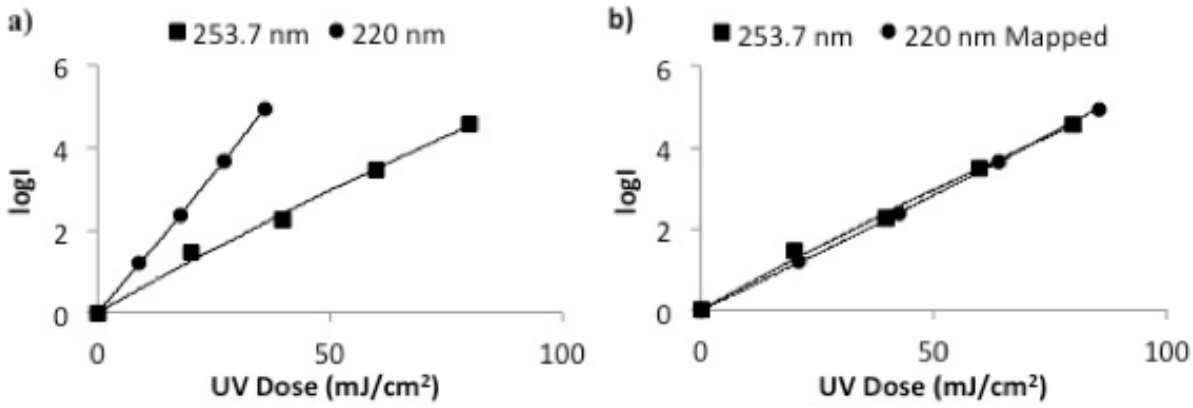

Figure B.5. The dose response of MS2 coliphage to 253.7 nm and 220 nm light, a) originally and b) after the dose response from 220 nm was mapped to the dose response from 253.7 nm.

References

Bolton, J.R., Linden, K.G. 2003. Standardization of Methods for Fluence (UV Dose) Determination in Bench-Scale UV Experiments. J. Environ. Eng. 129(3) 209-215.

Larason, T.C., Houston, J.M. 2008. Spectroradiometric Detector Measurements: Ultraviolet, Visible, and Near-Infrared Detectors for Spectral Power, NIST Special Publication 250-41. Gaithersburg, MD USA: National Institute of Standards and Technology.

Shaw, P.S., Gupta, R., Lykke, K.R. 2005. Stability of photodiodes under irradiation with a 157 nm pulsed excimer laser. Applied Optics. 44(2), 197-207.

APPENDIX C: ADDITIONAL ACTION SPECTRA DATA

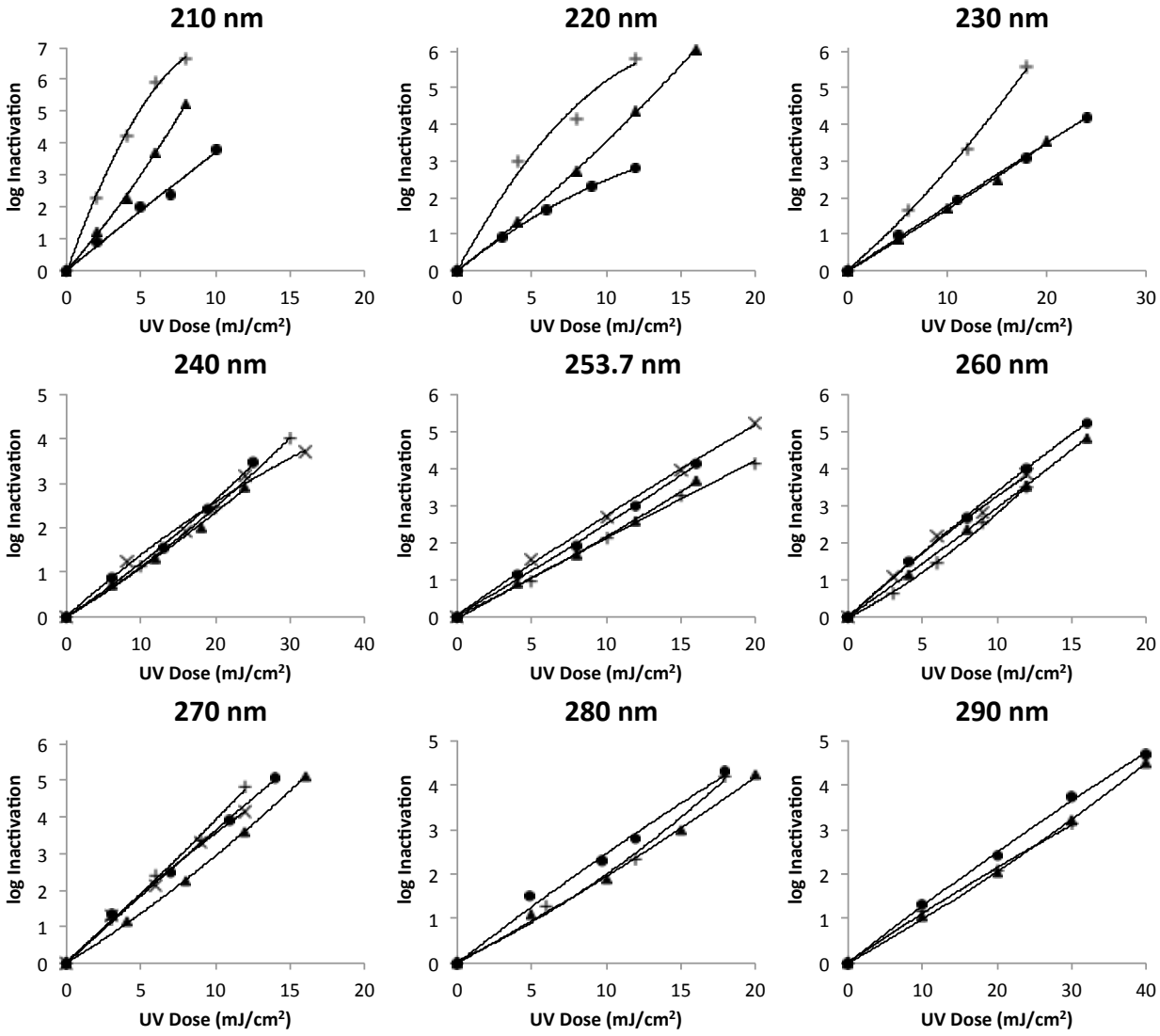

Figure C.1. Dose response of T1UV Coliphage to wavelength-specific UV irradiaiton from the tunable laser. Note different x- and y-axis values. Symbols represent data from four separate trials: R1 (●) and R2 (▲) from one laboratory and R3 (+) and R4 (×) from two additional laboratories. Average standard deviation from replicate platings = 5.5 pfu/mL.

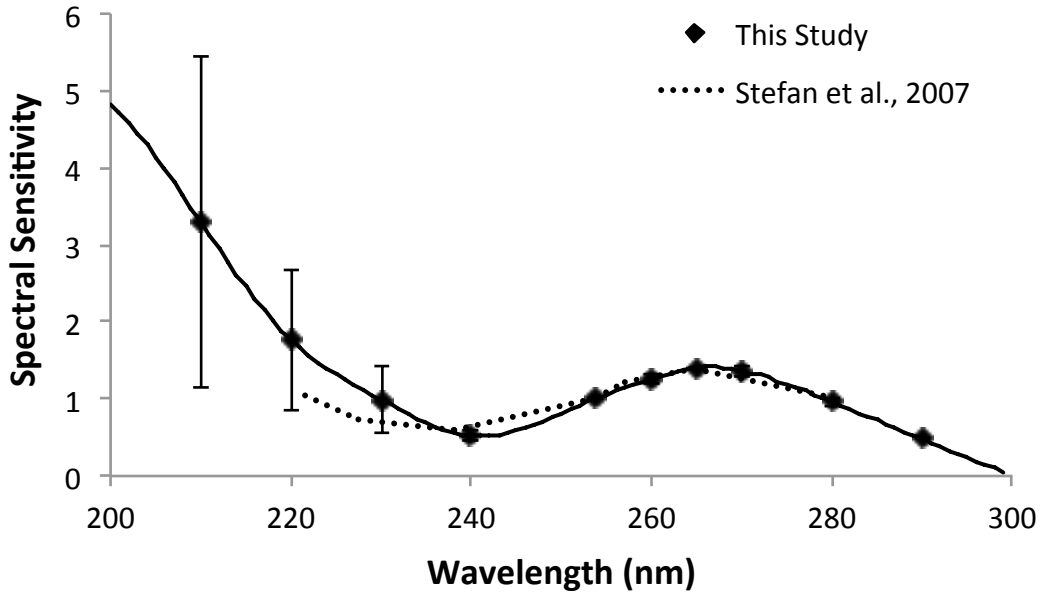

Figure C.2. Relative spectral sensitivity of T1UV Coliphage to UV irradiation compared to a past study (Stefan, Odegaard et al. 2007). Error bars represent 1 standard deviation from the mean sensitivity value. n = 4 for 240 nm, 253.7 nm, 260 nm, and 270 nm and n = 3 for all other wavelengths tested.

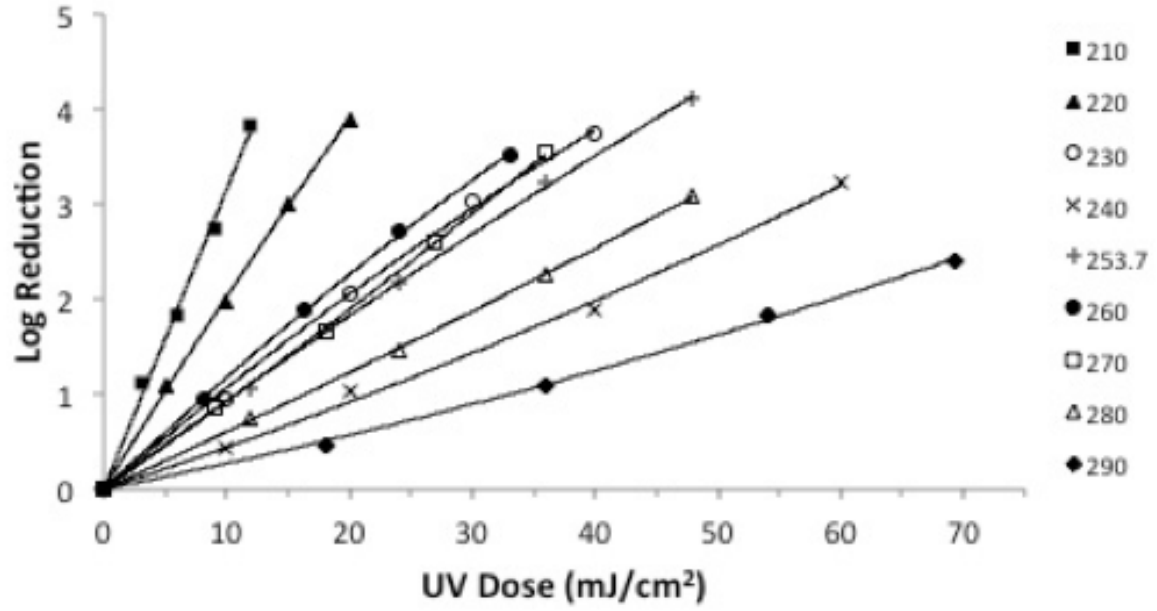

Figure C.3. Dose response of Q Beta Coliphage to wavelength-specific UV irradiation from the tunable laser. Average standard deviation from triplicate platings = 8.9 pfu/mL.

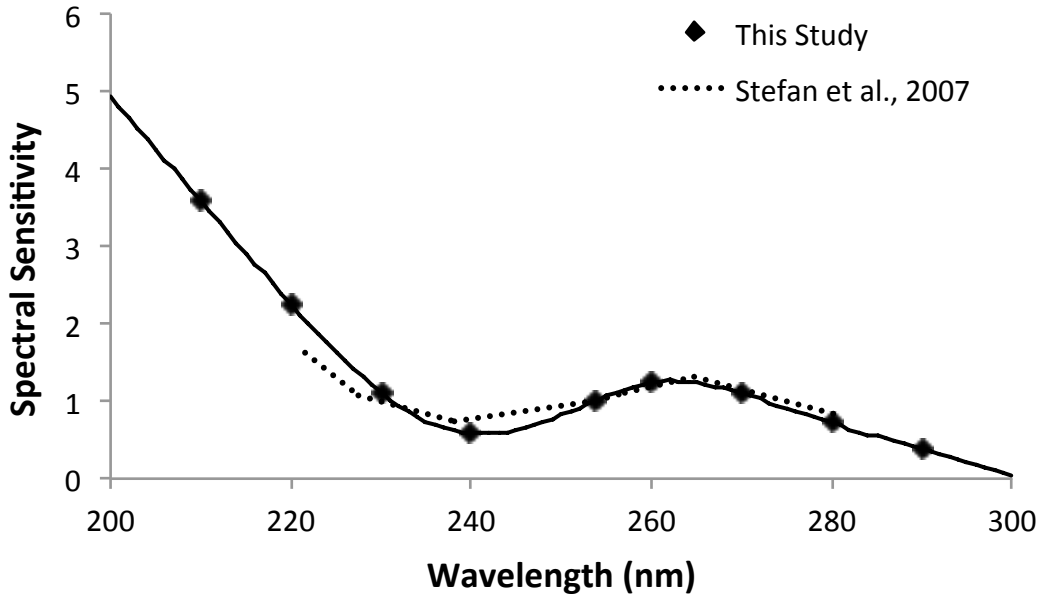

Figure C.4. Relative spectral sensitivity of Q Beta Coliphage to UV irradiation compared to a past study (Stefan, Odegaard et al. 2007). n = 1.

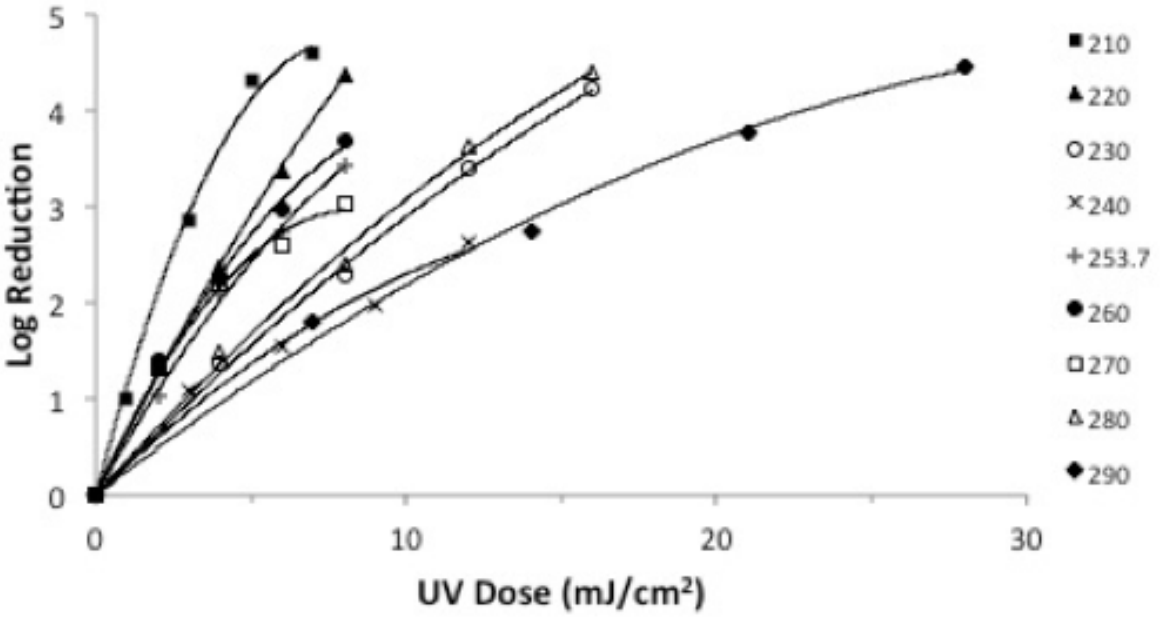

Figure C.5. Dose response of T7m Coliphage to wavelength-specific UV irradiation from the tunable laser. Average standard deviation from triplicate platings = 8.4 pfu/mL.

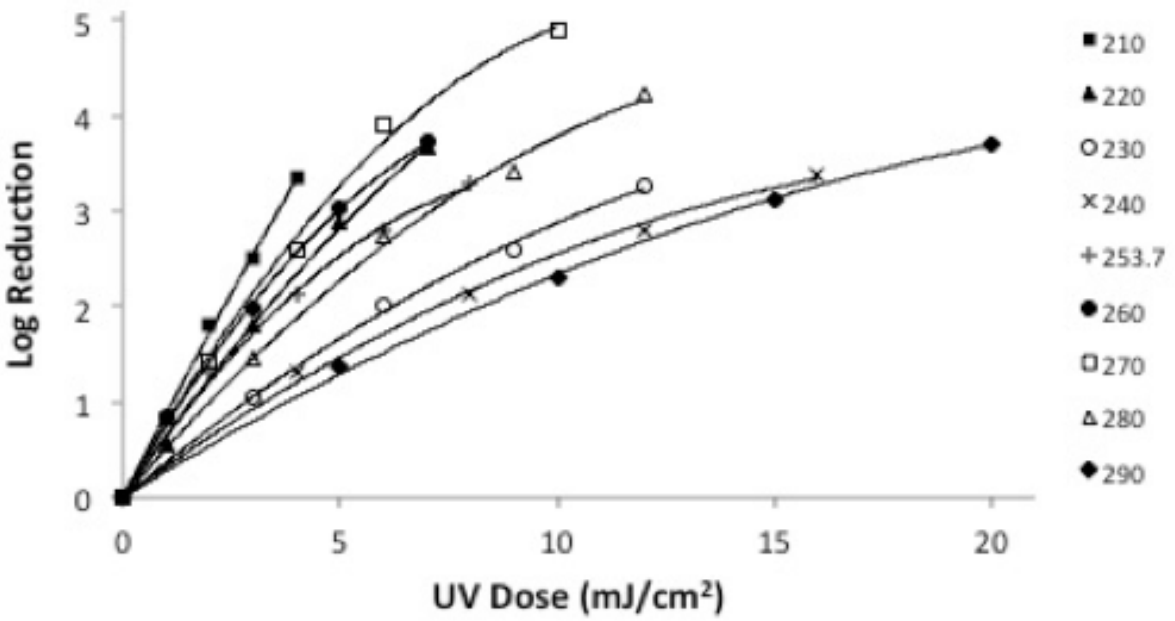

Figure C.6. Dose response of T7 Coliphage to wavelength-specific UV irradiation from the tunable laser. Average standard deviation from triplicate platings = 6.6 pfu/mL.

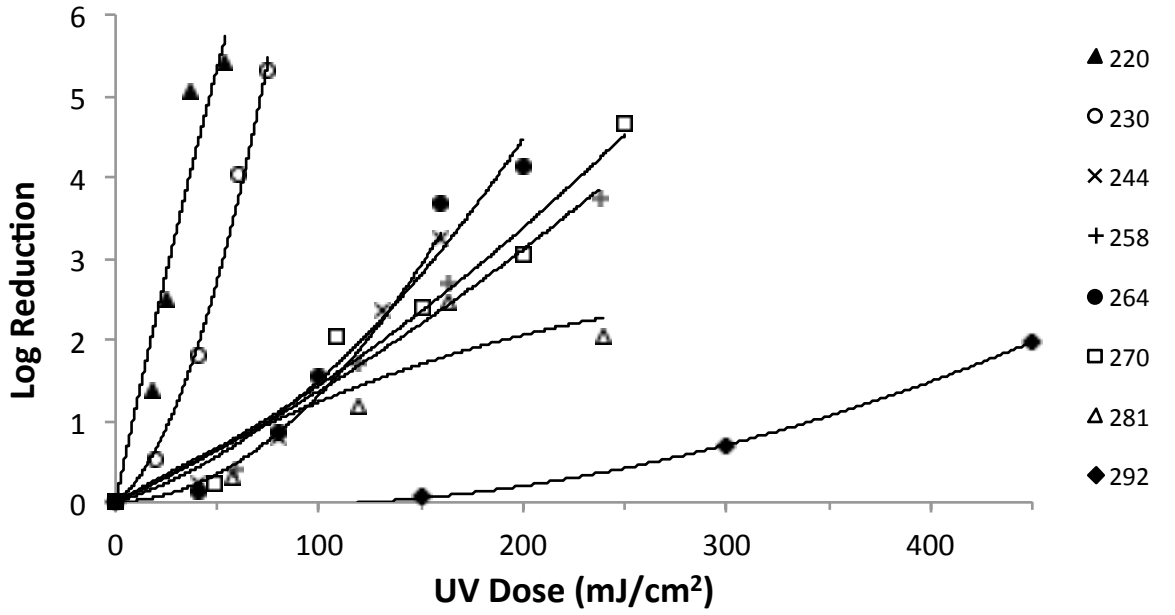

Figure C.7. Dose response of *Bacillus pumilus* to UV irradiation from a medium-pressure UV lamp with bandpass filters. Average standard deviation from triplicate platings = 11.5 CFU/mL.

Table C.1 Action Spectra

Wavelength (nm)	MS2	T1UV	T7	QB	T7m	Cryptosporidium	B. pumilus
200	5.41021	4.83667	2.37651	4.91522	2.90274	0.945018	
201	5.25438	4.71654	2.31311	4.78531	2.82437	0.926916	
202	5.10027	4.58578	2.25155	4.65431	2.74591	0.912577	
203	4.94769	4.44557	2.19162	4.52236	2.66739	0.901582	
204	4.79644	4.2971	2.13313	4.38958	2.5888	0.893514	
205	4.64634	4.14154	2.07586	4.25607	2.51016	0.887955	
206	4.4972	3.98009	2.01961	4.12197	2.43147	0.884486	
207	4.34881	3.8139	1.96418	3.98738	2.35274	0.882689	
208	4.201	3.64418	1.90936	3.85244	2.27399	0.882147	
209	4.05357	3.4721	1.85495	3.71726	2.19522	0.882441	
210	3.90633	3.29883	1.80075	3.58196	2.11644	0.883153	
211	3.75909	3.12557	1.74654	3.44665	2.03766	0.883865	
212	3.61166	2.95348	1.69213	3.31147	1.95889	0.884158	
213	3.46385	2.78376	1.63731	3.17653	1.88014	0.883616	
214	3.31547	2.61758	1.58188	3.04195	1.80142	0.881819	
215	3.16632	2.45612	1.52563	2.90784	1.72273	0.87835	
216	3.01622	2.30056	1.46836	2.77433	1.64408	0.872791	
217	2.86497	2.15209	1.40987	2.64155	1.5655	0.864723	
218	2.71239	2.01188	1.34994	2.5096	1.48697	0.853729	
219	2.55828	1.88112	1.28838	2.37861	1.40852	0.839389	
220	2.40246	1.76099	1.22498	2.24869	1.33014	0.821287	9.07127
221	2.24501	1.65224	1.15972	2.12005	1.25196	0.799213	8.77305
222	2.08719	1.55401	1.0933	1.99314	1.17444	0.773792	8.41689
223	1.93053	1.46499	1.02658	1.86853	1.09818	0.745859	8.01336
224	1.77657	1.38387	0.960442	1.74676	1.02375	0.716248	7.57308
225	1.62685	1.30937	0.895767	1.62837	0.951729	0.685794	7.10664
226	1.48289	1.24018	0.833427	1.51392	0.882705	0.65533	6.62463
227	1.34624	1.17501	0.774299	1.40394	0.817255	0.62569	6.13765
228	1.21843	1.11256	0.719257	1.29898	0.75596	0.59771	5.65631
229	1.10099	1.05153	0.669177	1.1996	0.699401	0.572224	5.1912
230	0.995463	0.990613	0.624935	1.10634	0.648159	0.550065	4.75291
231	0.903014	0.928945	0.587221	1.0197	0.602735	0.53191	4.34992
232	0.82334	0.867341	0.555979	0.939971	0.563312	0.517804	3.98218
233	0.75577	0.807045	0.530969	0.867425	0.529995	0.507632	3.64752
234	0.699634	0.749298	0.51195	0.802312	0.502889	0.501282	3.34377
235	0.654261	0.695345	0.49868	0.744887	0.482098	0.498639	3.06876
236	0.618981	0.646426	0.490919	0.695406	0.467726	0.49959	2.82031
237	0.593123	0.603786	0.488425	0.654126	0.459878	0.504021	2.59625
238	0.576017	0.568666	0.490959	0.621302	0.458659	0.511819	2.39441
239	0.566991	0.54231	0.498278	0.597189	0.464172	0.52287	2.21261
240	0.565375	0.525959	0.510142	0.582044	0.476522	0.537061	2.04869
241	0.570524	0.520482	0.526308	0.575962	0.495663	0.554282	1.90048
242	0.581891	0.525247	0.54653	0.578396	0.520942	0.574444	1.76579
243	0.598955	0.539244	0.570558	0.588641	0.551554	0.597461	1.64247
244	0.621195	0.561468	0.598143	0.60599	0.586697	0.62325	1.52833
245	0.648088	0.59091	0.629038	0.629737	0.625566	0.651724	1.4218
246	0.679115	0.626562	0.662992	0.659175	0.667358	0.6828	1.32368

247	0.713754	0.667418	0.699758	0.693599	0.711269	0.716391	1.23534
248	0.751483	0.71247	0.739086	0.732302	0.756495	0.752414	1.15819
249	0.791781	0.76071	0.780728	0.774577	0.802232	0.790782	1.09361
250	0.834127	0.81113	0.824436	0.819719	0.847677	0.831412	1.04299
251	0.877999	0.862723	0.86996	0.867022	0.892025	0.874218	1.00771
252	0.922877	0.914482	0.917051	0.915778	0.934474	0.919116	0.989173
253	0.968238	0.965399	0.965461	0.965281	0.974218	0.966019	0.98876
254	1.01356	1.01447	1.01494	1.01482	1.01046	1.01484	1.00784
255	1.05805	1.06113	1.06515	1.06345	1.04253	1.06481	1.04587
256	1.10045	1.10556	1.1156	1.10979	1.07003	1.11406	1.09913
257	1.13949	1.148	1.16578	1.15243	1.09255	1.16059	1.16354
258	1.17386	1.18869	1.21519	1.18997	1.1097	1.20242	1.23506
259	1.20228	1.22788	1.26333	1.22099	1.12111	1.23756	1.30949
260	1.22346	1.26582	1.30968	1.24408	1.12636	1.26401	1.38204
261	1.23645	1.30243	1.35367	1.25821	1.12526	1.28032	1.4478
262	1.2417	1.33637	1.39441	1.2638	1.11836	1.28713	1.50183
263	1.24002	1.36598	1.43095	1.26163	1.1064	1.28562	1.53921
264	1.2322	1.3896	1.46232	1.25251	1.09013	1.27697	1.55503
265	1.21904	1.40556	1.48756	1.23724	1.07028	1.26235	1.5461
266	1.20135	1.41262	1.50571	1.21659	1.0476	1.24294	1.5163
267	1.17991	1.41125	1.51581	1.19137	1.02283	1.21992	1.47126
268	1.15553	1.40231	1.5169	1.16237	0.99671	1.19446	1.41659
269	1.12901	1.38668	1.50802	1.13038	0.969982	1.16775	1.35794
270	1.10115	1.36524	1.48821	1.0962	0.943388	1.14094	1.30091
271	1.0726	1.33879	1.45695	1.06053	0.917522	1.11498	1.25004
272	1.04343	1.3079	1.41546	1.0237	0.892393	1.08978	1.20542
273	1.01355	1.27308	1.36541	0.985943	0.86786	1.06501	1.16606
274	0.982893	1.23482	1.30846	0.9475	0.843784	1.04034	1.13096
275	0.95137	1.19362	1.24627	0.908607	0.820025	1.01544	1.09911
276	0.918904	1.14998	1.18051	0.869503	0.796444	0.989967	1.06951
277	0.885416	1.10441	1.11285	0.830425	0.772901	0.963603	1.04117
278	0.850824	1.05741	1.04494	0.79161	0.749257	0.936012	1.01308
279	0.81505	1.00947	0.978454	0.753295	0.725372	0.906864	0.984245
280	0.778013	0.961095	0.915052	0.715719	0.701106	0.875826	0.953658
281	0.739668	0.912705	0.856042	0.679063	0.676351	0.842665	0.920321
282	0.700116	0.864376	0.801306	0.643285	0.651129	0.807536	0.883457
283	0.659489	0.8161	0.750369	0.608287	0.62549	0.770694	0.843183
284	0.617921	0.767872	0.702756	0.573972	0.599487	0.732392	0.799841
285	0.575549	0.719684	0.657992	0.540243	0.573172	0.692883	0.75377
286	0.532505	0.67153	0.615603	0.507001	0.546597	0.652421	0.705313
287	0.488923	0.623402	0.575113	0.47415	0.519814	0.61126	0.65481
288	0.444939	0.575295	0.536048	0.441591	0.492875	0.569652	0.602602
289	0.400687	0.527201	0.497932	0.409227	0.465831	0.527852	0.54903
290	0.3563	0.479114	0.460292	0.376961	0.438736	0.486113	0.494436
291	0.311913	0.431028	0.422651	0.344695	0.411641	0.44464	0.439159
292	0.26766	0.382934	0.384536	0.312332	0.384598	0.403451	0.383541
293	0.223676	0.334827	0.345471	0.279773	0.357658	0.362513	0.327924
294	0.180095	0.286699	0.304981	0.246922	0.330875	0.321796	0.272647
295	0.137051	0.238545	0.262592	0.21368	0.3043	0.281267	0.218052
296	0.094678	0.190357	0.217828	0.179951	0.277985	0.240895	0.164481
297	0.053111	0.142129	0.170215	0.145636	0.251982	0.200649	0.112273

298	0.012484	0.093853	0.119278	0.110638	0.226343	0.160498	0.0617697
299	5.41021	4.83667	0.064542	0.07486	0.201121	0.120409	0.0133125
300	5.25438	4.71654	0.005532	0.038203	0.176367	0.080352	0